THE DEVELOPMENT AND EVALUATION OF THE CAL/AIR FORCE DYNAMIC WIND-TUNNEL TESTING SYSTEM

PART I — DESCRIPTION AND DYNAMIC TESTS OF AN F-80 MODEL

IRVING C. STATLER
ORREN B. TUFTS
WALTER J. HIRTREITER

CORNELL AERONAUTICAL LABORATORY, INC.

FOREWORD

The research and development effort documented in this report was performed for the Air Force Flight Dynamics Laboratory (AFFDL), Research and Technology Division, Wright-Patterson Air Force Base, Ohio, by the Applied Mechanics Department of the Cornell Aeronautical Laboratory, Inc. (CAL), Buffalo, New York. This work was done under Air Force Contract AF 33(616)-8034.

Over the years that the dynamic testing system has been in development, there have been several project engineers from AFFDL, each of whom has, during the period of his assignment, contributed substantially to this program. Initially this individual was Mr. George Xenakis, later Mr. Max Davis, and most recently Mr. Jerry Jenkins. Most particularly, however, the authors gratefully acknowledge the contributions of Mr. Charles B. Westbrook whose technical competence, enthusiastic interest, undiminishing confidence, and continuing support over all the years were, in very large measure, responsible for the success of the program.

At CAL, Dr. Irving C. Statler, Head of the Applied Mechanics Department, was the principal investigator and project engineering responsibilities were shared by Principal Engineers, Mr. Orren B. Tufts in the mechanical aspects and Mr. Walter J. Hirtreiter in the electronics. Much credit is due Mr. George Jackson, Engineering Assistant in the Applied Mechanics Department, whose outstanding performance was a very large factor in achieving the objectives of this effort.

A special acknowledgment is made to Unico Controls, Inc. for their ingenuity, competence and cooperation in the development of two of the most critical elements of the system — the angular accelerometer and the phase and amplitude analyzers.

The manuscript was released by the authors September 1966 for publication as an AFFDL Technical Report.

This technical report has been reviewed and is approved.

C. B. Westbrook

C. B. WESTBROOK
Chief, Control Criteria Branch
Flight Control Division
Flight Dynamics Laboratory

ABSTRACT

This report reviews the development and evaluation of a new capability for dynamic testing in wind tunnels. The Cornell Aeronautical Laboratory (CAL) system provides a unique mounting through which a model can be forced precisely in any desired planar sinusoidal motion.

The versatility and overall accuracy of the CAL/Air Force dynamic testing system was demonstrated during a series of wind-tunnel tests. These tests permitted, for the first time, a measurement of the separate components of the rotary damping moment. The moment due to rate of change of angle of attack was measured by oscillating the model in pure plunging motion. The moment due to pitch rate was measured during pitching motion. The sum of these is compared with the total rotary damping moment as measured in rotation. Comparisons of data taken at two frequencies and four Mach numbers indicate that the components are accurate to within plus or minus ten percent of the total rotary damping moment. The results are compared with theory, flight test data, and other wind-tunnel measurements on the same and similar models.

Future applications of this equipment are reviewed, particularly with regard to its use as a research tool to support basic investigations for the development of theoretical or semiempirical methods for predicting dynamic stability characteristics of aircraft at transonic speeds. Recommendations for modifications and improvements to the system are presented and discussed.

TABLE OF CONTENTS

ILLUSTRATIONS

ILLUSTRATIONS (Cont'd)

ILLUSTRATIONS (Cont'd)

ILLUSTRATIONS (Cont'd)

TABLES

SYMBOLS

$\underline{\textcircled{A}}$	is the readout indication of the angular acceleration $\underline{\textcircled{A}} = \ddot{\theta} + k\underline{\textcircled{L}}$, rad/sec.^{2}
b	is used to correct for the effects of crosstalk, k, and the c. g. location error, $x_{c.g.}$ (see Figure 19)
C_{L_α}	is the slope of the lift-coefficient curve. (Dynamically it is given by the magnitude of the component of $\underline{\textcircled{F}}$ normal to $\tau\underline{\textcircled{A}}/2\pi j$ divided by $qS(\tau/2\pi)^2\lvert\underline{\textcircled{A}}\rvert$ in rotation or by the magnitude of the component of $\underline{\textcircled{F}}$ normal to $\underline{\textcircled{L}}/U$ divided by $qS(\tau/2\pi)(\lvert\underline{\textcircled{L}}\rvert/U)$ in plunging.)
C_{m_α}	is the slope of the moment-coefficient curve. (Dynamically it is given by the magnitude of the component of $\underline{\textcircled{M}}$ normal to $\tau\underline{\textcircled{A}}/2\pi j$ divided by $qSc(\tau/2\pi)^2\lvert\underline{\textcircled{A}}\rvert$ in rotation or by the magnitude of the component of $\underline{\textcircled{M}}$ normal to $\underline{\textcircled{L}}/U$ divided by $qSc(\tau/2\pi)(\lvert\underline{\textcircled{L}}\rvert/U)$ in plunging.)
$C_{L_{\dot{\alpha}}}$	is the derivative of the lift coefficient with respect to rate of change of angle of attack, 1/rad/sec.
$C_{m_{\dot{\alpha}}}$	is the derivative of the moment coefficient with respect to rate of change of angle of attack, 1/rad/sec.
$C_{L_{\dot{\theta}}}$	is the derivative of the lift coefficient with respect to pitching velocity, 1/rad/sec.
$C_{m_{\dot{\theta}}}$	is the derivative of the moment coefficient with respect to pitching velocity, 1/rad/sec.
c	is the mean aerodynamic chord, ft. (0.672 ft. for the F-80 model)
$c.g.$	is the center of gravity
D	is the operator d/dt
$\underline{\textcircled{F}}$	is the aerodynamic normal force, lb. (positive up)
$\underline{F_B}$	is the reactive force of the model on the normal-force strain beams, lb. (positive up)
F_α	is the derivative of the lift with respect to angle of attack, lb/rad.
$F_{\dot{\alpha}}$	is the derivative of the lift with respect to rate of change of angle of attack, lb/rad/sec.
$F_{\dot{\theta}}$	is the derivative of the lift with respect to pitch rate, lb/rad/sec.

SYMBOLS (Cont'd)

f is the frequency of oscillation, cps, $f = \frac{1}{\tau}$.

GC is the gain code denoting the combination of gains on the four channels of phase and amplitude analyzers

g is the acceleration due to gravity, $g = 32.2$ ft/sec.^{2}

I is the pitching moment of inertia of the mass m about its c. g., lb. ft. sec.^{2}

I^* is used to cancel the moment due to inertial reaction (see Figure 19)

j is a quantity $\sqrt{-1}$ which, when multiplied by a vector, rotates the vector by $+\frac{\pi}{2}$.

k is the crosstalk sensitivity of the angular accelerometer, $\frac{\text{rad/sec}^2}{\text{ft/sec}^2}$

$\underline{(L)}$ is the readout indication of the linear acceleration, $\underline{(L)} = \underline{\ddot{z}}$, ft/sec.^{2}

l_t is the distance from the c. g. to the 1/4 chord of the horizontal tail, ft.

l_B is the distance between the sensitive axes of the forward and aft strain beams, ft.

$\frac{1}{l_B^*}$ is used to cancel the force due to the moment component sensed by the forward strain beams (see Figure 19)

$\underline{(M)}$ is the aerodynamic pitching moment, ft. lb. (positive for model nose up)

$\underline{M_B}$ is the reactive moment of the model on the aft strain beam, ft. lb. (positive for model nose up)

M_α is the derivative of the moment with respect to angle of attack, ft. lb/rad.

$M_{\dot{\alpha}}$ is the derivative of the moment with respect to rate of change of angle of attack, ft. lb/rad/sec.

$M_{\dot{\alpha}_g}$ is the derivative of the moment with respect to rate of change of gust velocity, ft. lb/rad/sec.

$M_{\dot{\theta}}$ is the derivative of the moment with respect to pitch rate, ft. lb/rad/sec.

$\underline{M}_{T0}$ is the pitching moment due to the drag load on the horizontal tail during model motions with no wind

M is the Mach number

m is the mass of the model plus metric part of the balance (including the linear and angular accelerometers), lb. sec.^{2}/ft.

m^* is used to cancel the normal force due to inertial reaction (see Figure 19)

q is the dynamic pressure, lb/ft.^{2}

S is the wing area, ft.^{2} (2.37 ft.^{2} for the F-80 model)

U is the free stream velocity, fps

$\underline{w}_g$ is the vertical velocity of a gust, fps (positive up)

$x_{c.g.}$ is the longitudinal displacement of the sensitive axis of the forward strain beams from the center of gravity of the mass m, ft. (positive aft)

$\underline{\dot{z}}$ is the translational (vertical) velocity of the c. g., fps (positive down), $\underline{\dot{z}} = (\tau/2\pi)\underline{\ddot{z}}$

$\underline{\ddot{z}}$ is the translational (vertical) acceleration of the c. g., ft/sec.^{2} (positive down)

$\underline{\alpha}$ is the oscillatory angle of attack, rad. (positive nose up relative to tangent to flight path)

$\underline{\theta}$ is the oscillating rotational angle about the c. g., rad. (positive nose up relative to horizontal), $\underline{\theta} = -(\tau/2\pi)^2\underline{\ddot{\theta}}$

$\underline{\dot{\theta}}$ is the angular velocity of the model about its c. g. rad/sec. (positive for model nose up), $\underline{\dot{\theta}} = (\tau/2\pi)\underline{\ddot{\theta}}$

$\underline{\ddot{\theta}}$ is the angular acceleration of the model about its c. g. rad/sec.^{2} (positive for model nose up)

τ is the oscillation period, sec.

$\phi_{④}$ is the phase angle between the angular-accelerometer readout and the oscillator drive motion

SYMBOLS (Cont'd)

$\phi_{(F)}$	is the phase angle between the normal-force readout and the oscillator drive motion
$\phi_{(L)}$	is the phase angle between the linear-accelerometer readout and the oscillator drive motion
$\phi_{(M)}$	is the phase angle between the pitching moment readout and the oscillator drive motion
ω	is the frequency of oscillation, rad/sec., $\omega = 2\pi f$

NOTE: An underscored symbol denotes a vector.

SECTION 1

INTRODUCTION

The diversity of operation of present-day aircraft introduces new problems to the prediction of flight stability and handling characteristics. The supersonic transport with its thin, highly swept wings is substantially different from a maneuverable reentry vehicle with a blunt lifting body and, perhaps, no wings at all. The low-altitude, high-speed attack bomber looks very little like the coming generation of advanced VTOL and STOL aircraft. These various configurations have one cardinal feature in common, however; all are manned aircraft that must have good handling qualities.

Unusual configurations introduce unusual control problems. This has been demonstrated by the CAL/Air Force Variable-Stability T-33 shown in Figure 1. For example, the chart presented in Figure 2 is derived from pilot evaluations of many different configurations which can be simulated with the T-33 aircraft. [1]* It shows how the stability characteristics — that is, the frequency and the damping — of the longitudinal short-period mode influence the pilot's opinion of the vehicle's handling qualities. An aircraft's handling qualities are determined by its dynamic stability characteristics.

The designer who must know the dynamic stability characteristics of a new aircraft configuration when it flies at high subsonic and transonic speeds faces a dilemma, however. Available theories for predicting the required aerodynamic characteristics in this speed range are totally inadequate. The difficulties are associated with the large changes in pressure and distribution of pressure with formation, growth, and position of shock waves on aerodynamic surfaces. Even when idealized to an inviscid fluid undergoing isentropic processes, transonic flow presents certain unique mathematical difficulties.

The last ten years have seen fundamental advances in theoretical analysis of unsteady transonic flows. There are, currently, however, no proven methods for predicting the unsteady aerodynamic loads at transonic speeds and, particularly, at the low reduced frequencies typical of aircraft rigid-body dynamics. To aid in the development of such a theory and to advance the technical understanding of unsteady transonic flow in general, there exists a requirement for wind-tunnel tests of unsteady aerodynamics in the transonic speed range. In recognition of this need, Cornell Aeronautical Laboratory (CAL), under sponsorship of the U. S. Air Force Flight Dynamics Laboratory, Control Criteria Branch, undertook the development of a unique oscillatory mounting system by means of which

---

* Numbers in brackets indicate References.

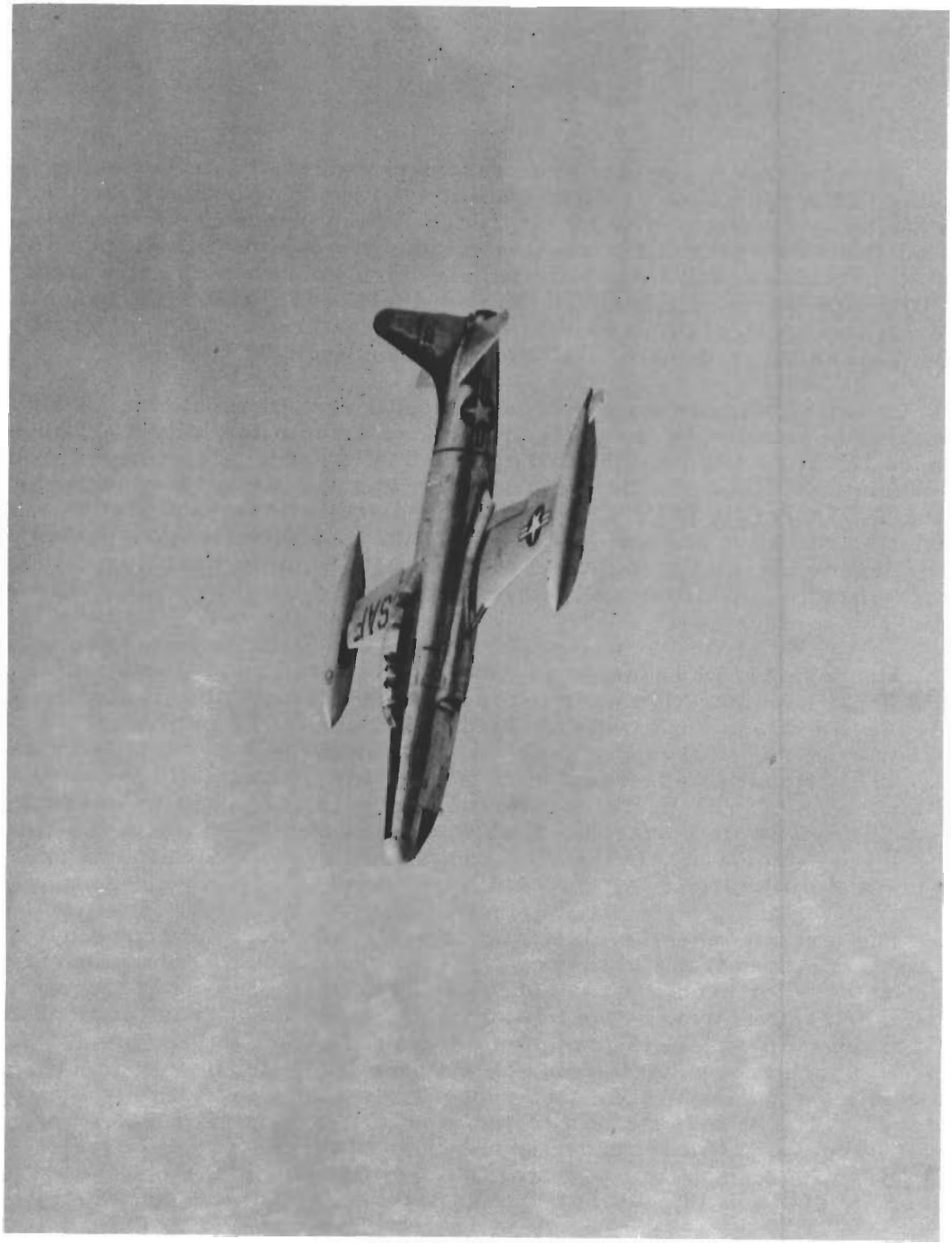

Figure 1 CAL/AIR FORCE VARIABLE STABILITY T-33 AIRCRAFT

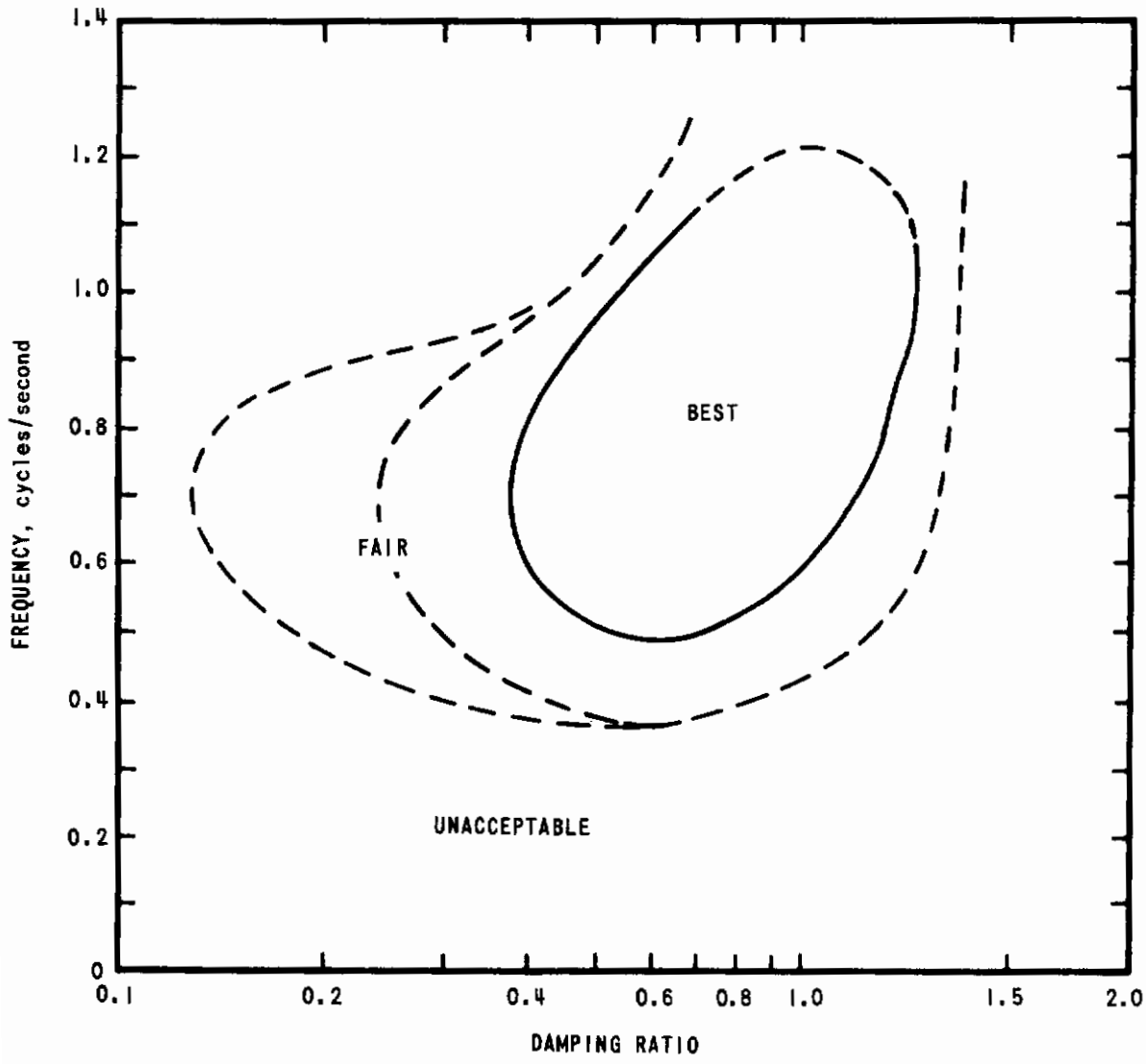

Figure 2 PILOT RATINGS OF LONGITUDINAL SHORT-PERIOD CHARACTERISTICS

a model in a wind tunnel can be forced precisely in any desired planar sinusoidal motion. Longitudinal short-period dynamic testing was chosen for the initial evaluation program to limit the equipment and experimentation necessary for obtaining useful and correlative results. The methods and equipment are, nevertheless, applicable to lateral-directional dynamic testing by rotating the model by 90° on its support. Although reference is made throughout this report to the longitudinal measurements, it is to be understood that comparable lateral tests (at small angles of attack) are also possible. It might even be possible to incorporate a roll degree of freedom in the system, but the measurement of rolling derivatives can be accomplished more simply by use of a separate roll oscillator or a continuous roll balance.

The dynamic characteristics of aircraft and the measurement of aerodynamic stability derivatives were first investigated in the early years of the 20th century by such pioneers of aeronautics as Bryan, Lanchester, Bairstow, and Hunsaker. A brief review of the early techniques for measuring the rotary forces and moments, given by B. Melville Jones in Reference 2, is indicated in Figure 3. Recent literature on dynamic wind-tunnel testing [3-16] shows that some of the basic techniques developed in those first years of aviation are still used today. These recent reports contain descriptions of current oscillators, instrumentation, and model-building practices. They represent curved flow or nonoscillatory testing techniques, free-oscillation methods, resonant excitation systems, a variety of inexorable forcing techniques, and two new "free-flight" approaches [12, 13] but, generally, they are limited to considerations of the measurement of <u>total</u> damping.

The unique capabilities provided by the CAL/Air Force Dynamic Wind-Tunnel Testing System result from the ability to force the model inexorably in <u>any</u> desired planar sinusoidal motion. For example, three basic motions can be achieved to study loncitudinal dynamics. These are

(1) A pure rotational motion about the model's center of gravity.

Both the angle of attack and the pitch angle vary continuously, as in the flight path shown in Figure 4(a). The vertical velocity of the c.g. is zero and the angle of attack equals the rotational angle. Dynamic measurements can be made of the lift and pitching moment due to angle of attack ($F_\alpha \alpha$ and $M_\alpha \alpha$) and also of the total rotary (dynamic) forces, the sum of contributions due to rate of change of angle of attack and the rate of rotation $\left[(F_{\dot\alpha} + F_{\dot\theta})\dot{\underline{\theta}}\right.$ and $\left.(M_{\dot\alpha} + M_{\dot\theta})\dot{\underline{\theta}}\right]$.

(2) A pure plunging motion.

The angle of attack varies continuously but is due only to the vertical translational velocity, since there is no significant rotation about the model's center of gravity, as in the flight path shown in Figure 4(b). Dynamic measurements can again be made of the lift and moment due to angle of attack as in rotation but, more important,

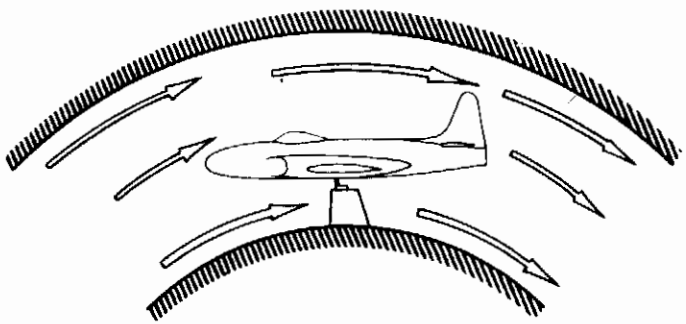

CURVED AIRFLOW

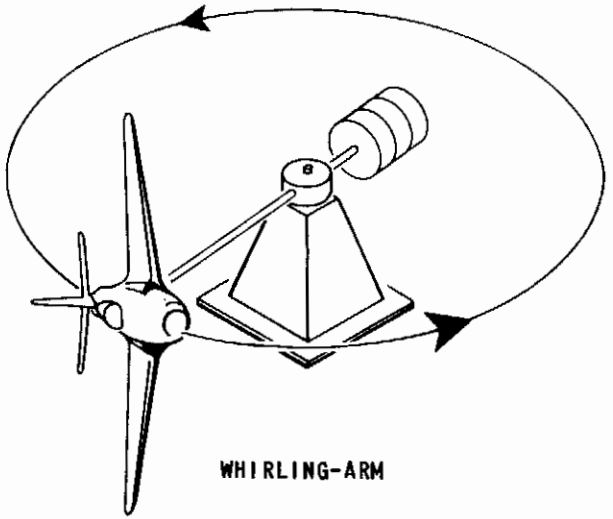

WHIRLING-ARM

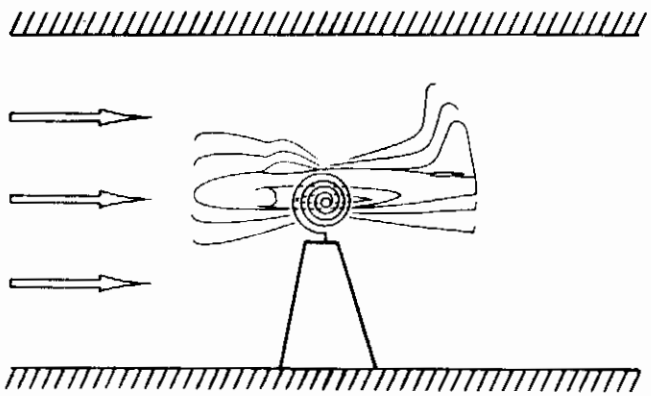

FREE-OSCILLATION

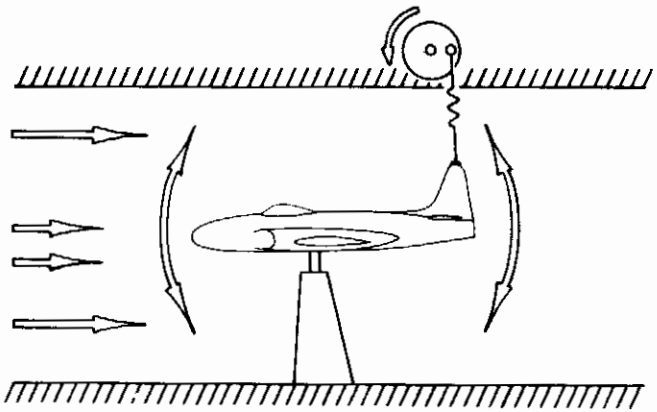

FORCING THROUGH A SPRING

Figure 3 DYNAMIC TESTING TECHNIQUES

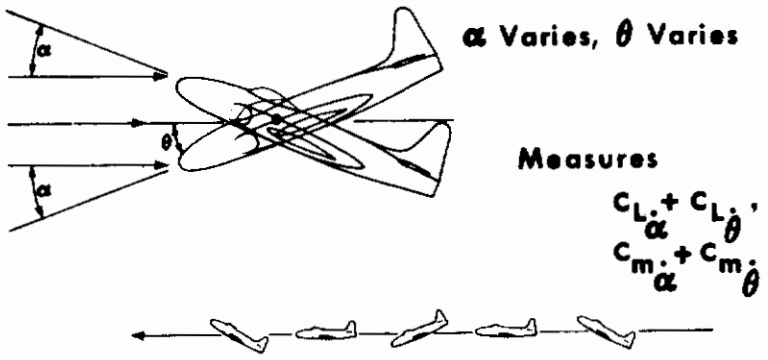

(a) PURE ROTATION

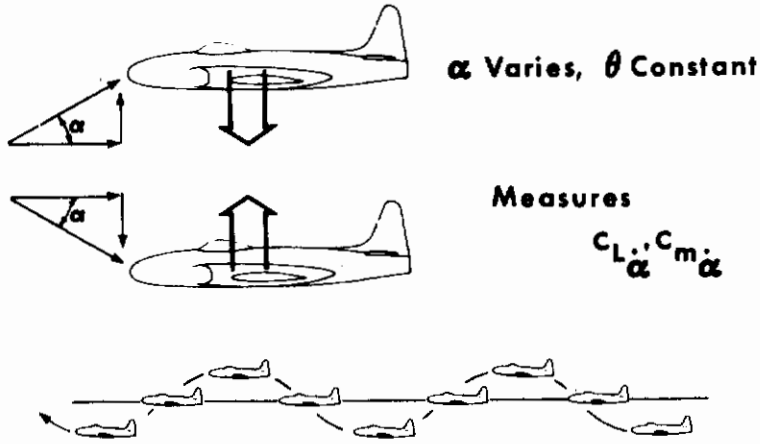

(b) PURE PLUNGE

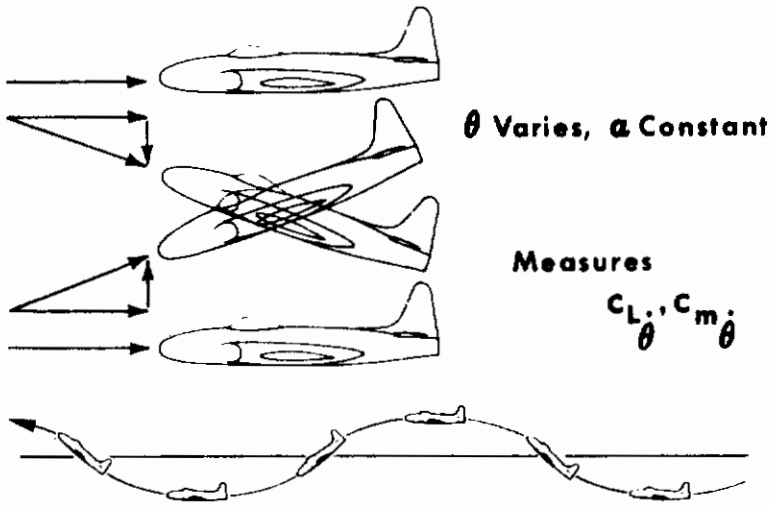

(c) PURE PITCH

Figure 4 LONGITUDINAL MOTIONS OF THE MODEL

the lift and moment due to rate of change of angle of attack alone (i.e., $F_{\dot{\alpha}}\dot{\underline{\alpha}}$ and $M_{\dot{\alpha}}\dot{\underline{\alpha}}$) can be evaluated.

(3) A pure pitching motion.

This is the particular combination of rotational and vertical translational motion such that the angle of attack remains constant, as shown in the flight path of Figure 4(c). In general, the effective oscillatory angle of attack of the model is the vector sum of the oscillating rotational angle about the c.g., $\underline{\theta}$, and the angle of attack due to the translational velocity of the c.g., $\dot{\underline{z}}/U$; i.e., $\underline{\alpha} = \underline{\theta} + \dot{\underline{z}}/U$. If the oscillating rotational angle is equal in amplitude and opposite in phase to the angle of attack due to the plunging motion, then the net angle of attack is maintained constant. This is called pure pitching, and this motion permits measuring the lift and moment due only to rotational (or pitch) rate (i.e., $F_{\dot{\theta}}\dot{\underline{\theta}}$ and $M_{\dot{\theta}}\dot{\underline{\theta}}$).

Similar considerations pertain to directional-lateral dynamics when the model is rotated by 90° on the balance support.

SECTION 2

WHY DERIVATIVE SEPARATION?

It is a well-accepted fact that the damping of the longitudinal short-period oscillations of an airplane can be evaluated satisfactorily if the sum of the damping derivatives, ($M_{\dot{\alpha}} + M_{\dot{\theta}}$), is known, although the separate values of the components, $M_{\dot{\alpha}}$ and $M_{\dot{\theta}}$, are unknown. Furthermore, the damping of the longitudinal oscillations of conventional, straight-wing, tailed aircraft at low speeds, as predicted on the basis of quasi-steady theory, agrees quite well with results using unsteady aerodynamics. This can perhaps be expected when the horizontal tail constitutes the major contributor to these fundamentally unsteady effects — that is, when the moment due to a pitching velocity is due almost entirely to the tail and when the classical "time-lag" of the downwash is an adequate explanation for the moment due to rate of change of angle of attack. Unsteady flow effects, however, might significantly influence the longitudinal damping of less conventional configurations at high subsonic and transonic speeds. It becomes important, therefore, to learn more about the variations with Mach number and configuration of the individual pieces that comprise the total effective damping. Since, at present, there is no suitable theory for unsteady flow effects at transonic speeds, such knowledge will depend, for some time to come, on good experimental data.

It appears, furthermore, from the little evidence available, that even more accurate evaluations of $M_{\dot{\alpha}}$ and $M_{\dot{\theta}}$ are required to predict the damping at high subsonic and transonic speeds than are necessary at low subsonic speeds. The reason for this is indicated by the moment-vector diagrams for the two speed ranges, as shown in Figure 5. Conventional nomenclature is used in this figure. The cases considered are for damped oscillations per unit vertical acceleration, $\ddot{z}$. Thus, the phase angle between the vectors representing a variable and its derivative is greater than 90°. In the relatively highly damped, low subsonic case of Figure 5(a), the vectors associated with $M_{\dot{\alpha}}$ and $M_{\dot{\theta}}$ are additive. At high subsonic or transonic speeds, $M_{\dot{\alpha}}$ can change sign causing the same terms to have the small difference shown in Figure 5(b). Hence, errors in $M_{\dot{\alpha}}$ and $M_{\dot{\theta}}$ result in larger percentage errors in the predicted total damping for this high-speed range. This sign reversal of $M_{\dot{\alpha}}$, furthermore, cannot be predicted from simple quasi-steady theory but is, rather, a nonstationary flow effect.

The separate importance of the derivatives $M_{\dot{\alpha}}$ and $M_{\dot{\theta}}$ also enters in evaluating an aircraft's response to a gust input using linearized, small-disturbance theory. Consider, for example, the motion of an airplane in response to a vertical gust with velocity w_g (positive up). Neglecting speed change as usual, and omitting the small $F_{\dot{\alpha}}$, $F_{\dot{\alpha}_g}$, and $F_{\dot{\theta}}$ terms, the equations of motion

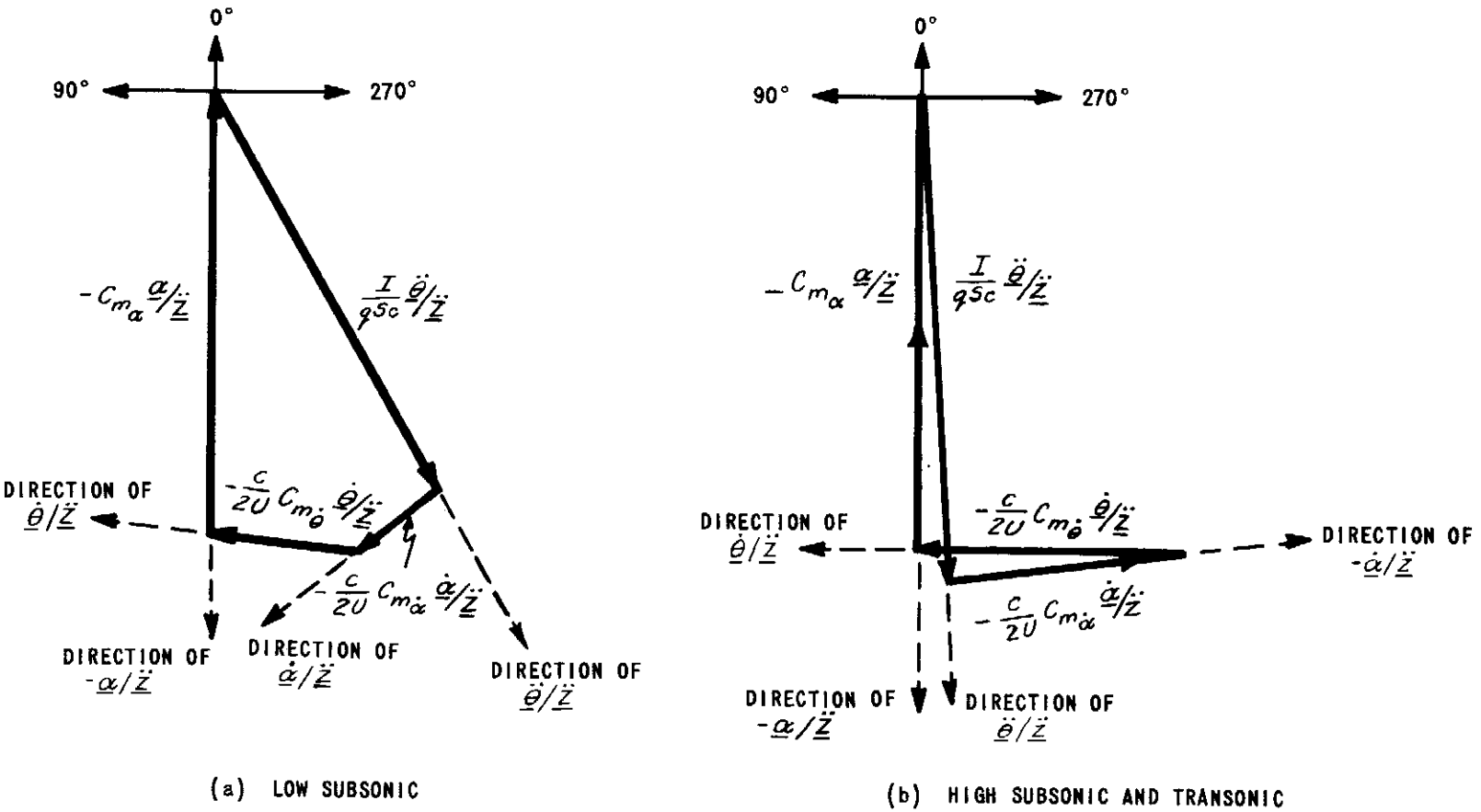

Figure 5 TYPICAL SOLUTIONS OF THE PITCHING MOMENT EQUATION

can be solved for the normal acceleration and the pitch rate as follows:

$$\underline{\ddot{z}} = \frac{\frac{F_\alpha D}{m} + \frac{F_\alpha}{m}\left[-\frac{M_{\dot\alpha} + M_{\dot\theta}}{I} - \frac{M_{\dot\alpha_g}}{I}\right]}{D^2 + \left(-\frac{F_\alpha}{mU} + \frac{M_{\dot\alpha} + M_{\dot\theta}}{I}\right)D + \left(-\frac{M_\alpha}{I} + \frac{F_\alpha M_{\dot\theta}}{mUI}\right)}\left(\frac{\underline{w}_g}{U}\right)$$

$$\underline{\dot\theta} = \frac{\left(\frac{M_{\dot\alpha_g}}{I}\right)D^2 + \left(\frac{M_\alpha}{I} - \frac{F_\alpha M_{\dot\alpha_g}}{mUI} + \frac{F_\alpha M_{\dot\alpha}}{mUI}\right)D}{D^2 + \left(-\frac{F_\alpha}{mU} + \frac{M_{\dot\alpha} + M_{\dot\theta}}{I}\right)D + \left(-\frac{M_\alpha}{I} + \frac{F_\alpha M_{\dot\theta}}{mUI}\right)}\left(\frac{\underline{w}}{U}\right)$$

The moment due to the time rate of change of angle of attack and the moment due to time rate of change of gust input have been introduced separately. If the wave length of the gust is much greater than the tail length, then $M_{\dot\alpha_g} \cong M_{\dot\alpha}$ so that $M_{\dot\theta}$ occurs separately in the transfer function for $\underline{\ddot{z}}/(\underline{w}_g/U)$ while $M_{\dot\alpha_g}$ appears alone in $\underline{\dot\theta}/(\underline{w}_g/U)$. However, if the wave length of the gust is not large with respect to the tail length, then $M_{\dot\alpha_g} \neq M_{\dot\alpha}$. In this case, $M_{\dot\alpha}$ and $M_{\dot\theta}$ appear as a sum in the numerator of the transfer function for $\underline{\ddot{z}}/(\underline{w}_g/U)$ while $M_{\dot\alpha}$ and $M_{\dot\alpha_g}$ appear separately in $\underline{\dot\theta}/(\underline{w}_g/U)$.

Other dynamic testing techniques have been used successfully to measure the <u>total</u> rotary moments, that is, the <u>sum</u> of the contributions due to the rate of change of angle of attack and the contributions due to rate of rotation, just as in the particular case of pure rotational motion on CAL's system. Instances have been pointed out, however, in which the application of test data to calculations requires the rotary damping derivatives in some way other than their combined form. Further, and perhaps most important, measurements of the individual derivatives provide the additional knowledge needed to aid the development of theory. Previous attempts to measure the <u>individual</u> components have had only limited success, however. The CAL/Air Force Dynamic Wind-Tunnel Testing System makes such measurements practical for the first time.

SECTION 3

THE DYNAMIC TESTING SYSTEM

The basic components of the dynamic testing system are represented in Figure 6. The mechanical oscillator can be adjusted by an operator so that the model is forced into a desired planar sinusoidal motion. The motion is measured by linear and angular accelerometers in the model while forces and moments are measured by a strain-beam balance system between the model and the sting support. Signals from these transducers are passed through a signal processing system which provides DC outputs proportional to the amplitudes and phases of the components of the force, moment, and accelerations at the oscillator frequency. This information, the oscillator frequency, and tunnel-test conditions are displayed visually in the dynamic testing control room and are recorded automatically and simultaneously in digital form. (The control room for the dynamic testing system is shown in Figure 7.)

The dynamic balance and mechanical oscillator system was designed for use with CAL's 8-Ft. Transonic Variable-Density Wind Tunnel which is particularly well suited to the requirements of the system. Over a Mach number range of 0.50 to 1.20, dynamic pressures can be held constant in a range of 200 through 600 lbs/sq.ft., or Reynolds number per foot of reference length can be held constant at values of 1×10^6 through 3.5×10^6. Impact temperatures are held between 120°F. and 155°F., even for the supersonic speeds. This tunnel's 8 x 8-ft. test section has "perforated" walls which permit complete performance measurements on models through the transonic speed range. A chart of tunnel operating conditions is shown in Figure 8.

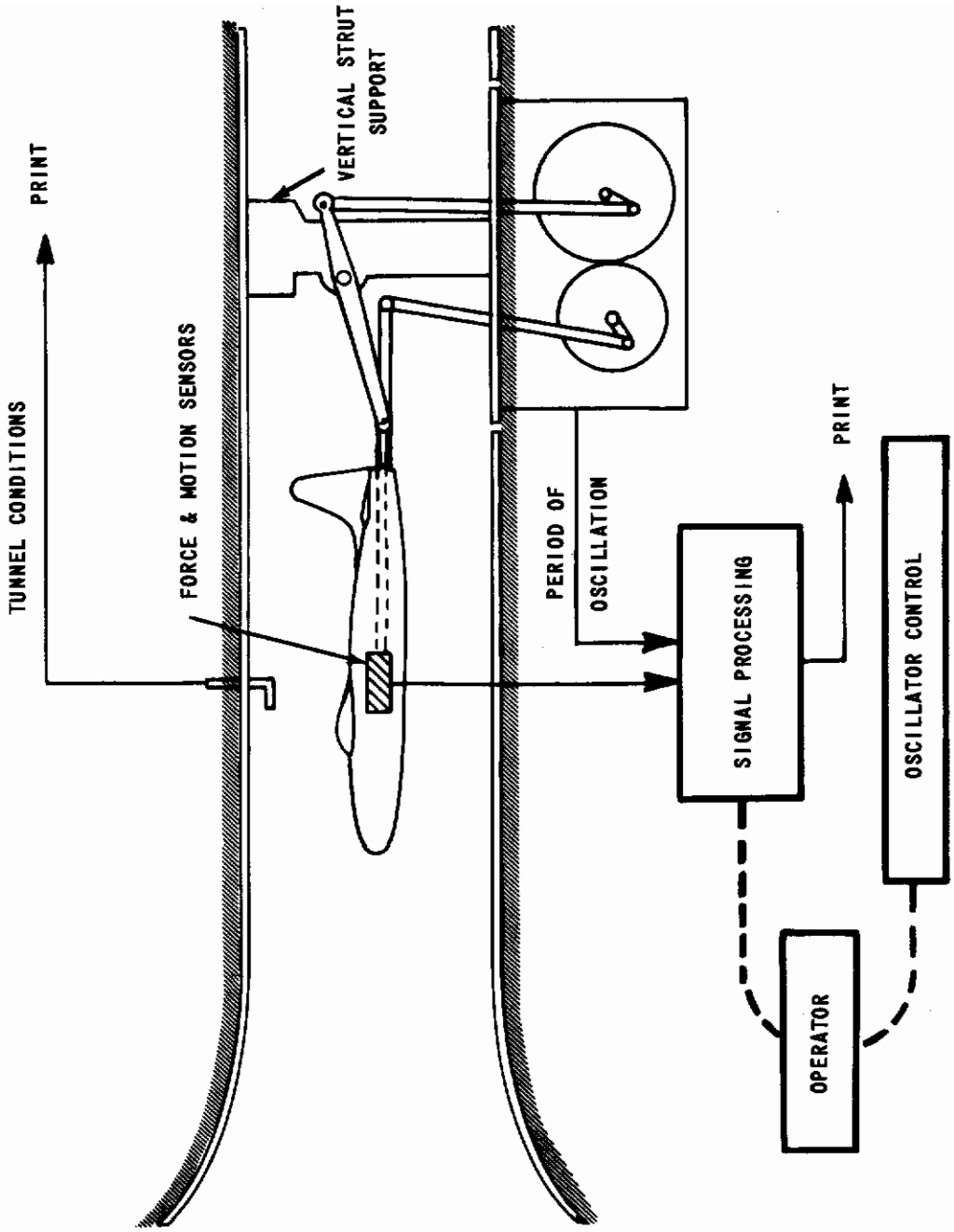

Figure 6 BASIC ELEMENTS OF THE DYNAMIC TESTING SYSTEM

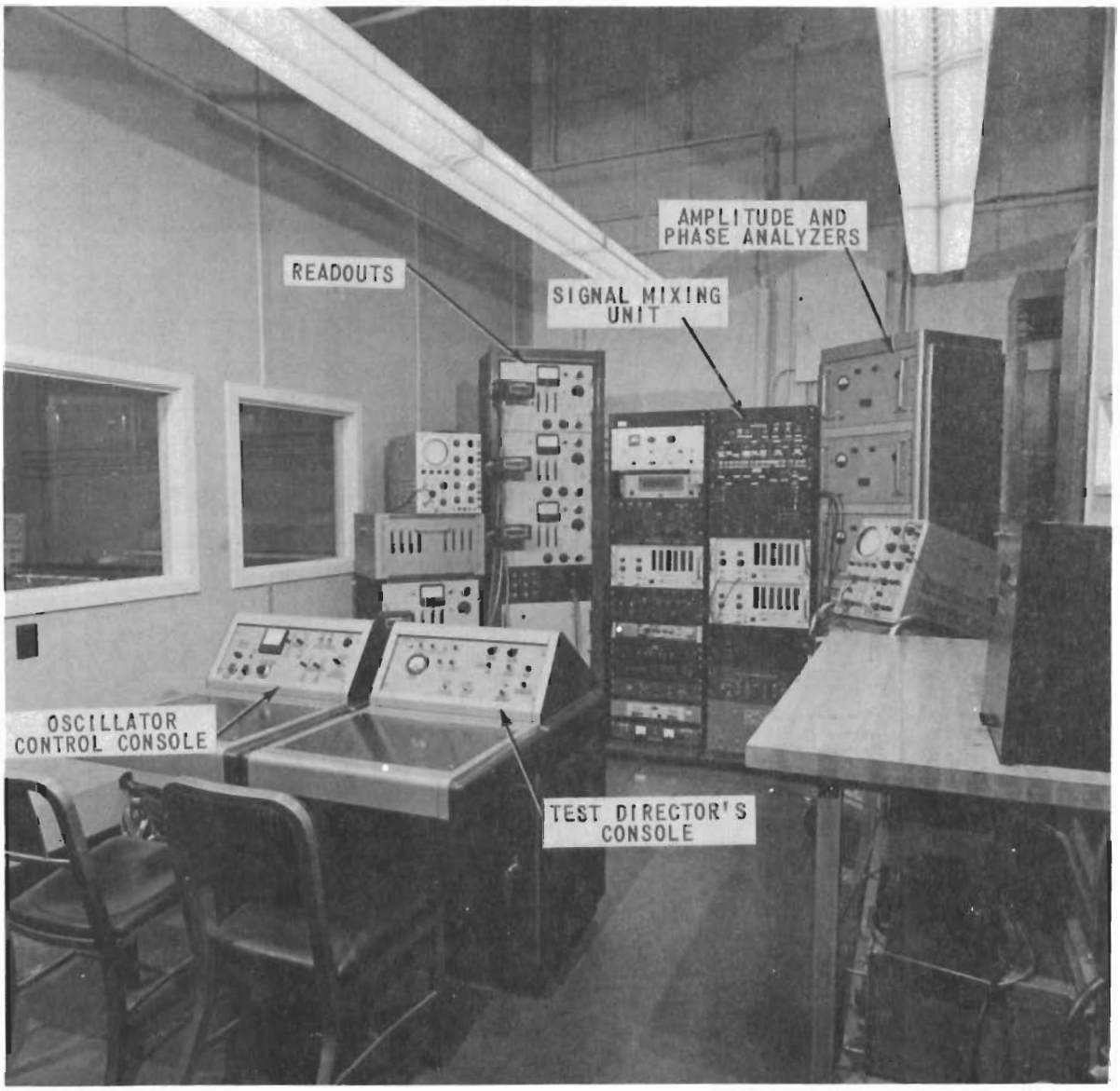

Figure 7 DYNAMIC TESTING CONTROL ROOM

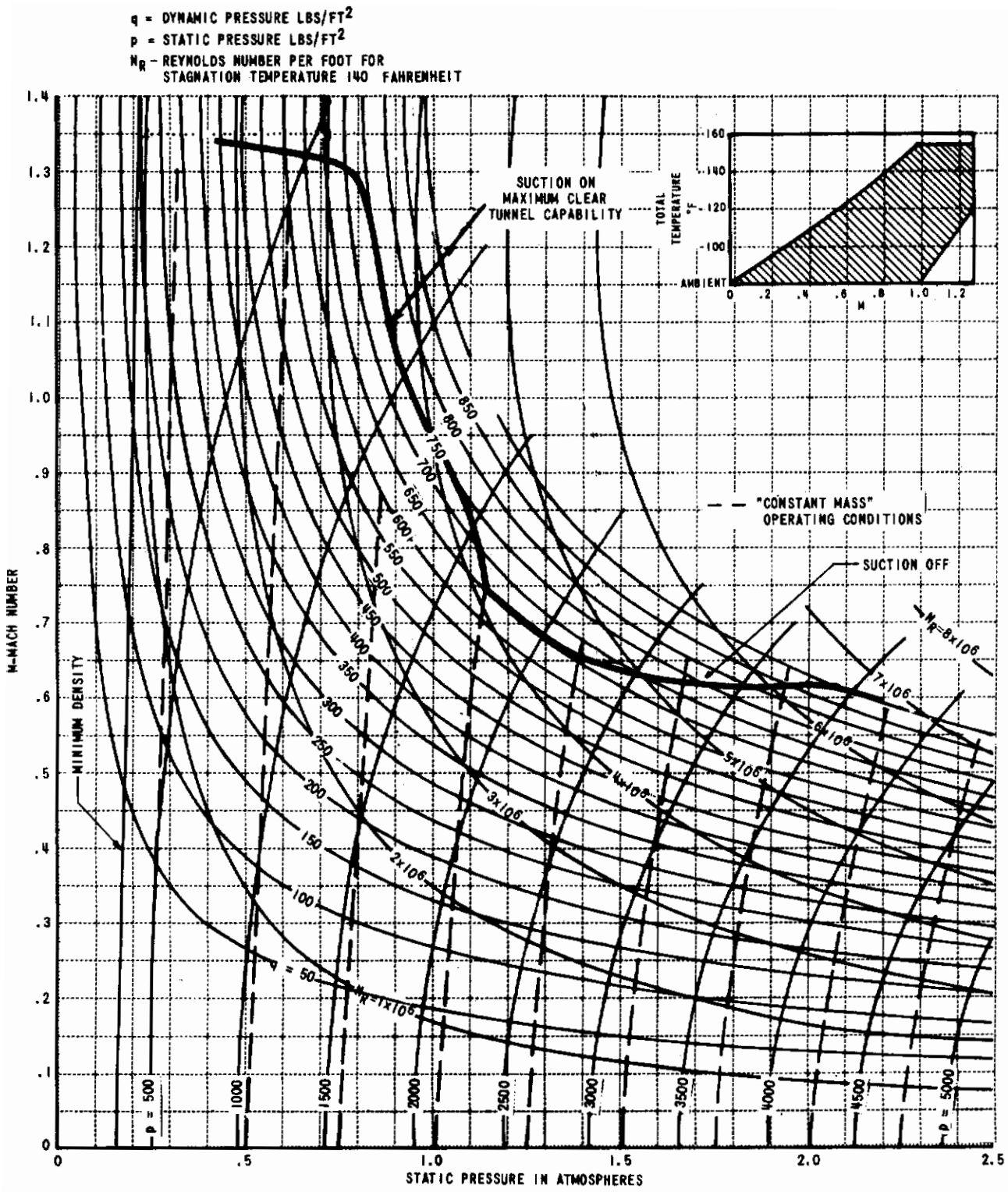

Figure 8 CAL 8-FOOT VARIABLE-DENSITY TRANSONIC WIND-TUNNEL OPERATING MAP

SECTION 4

THE MECHANICAL OSCILLATOR

Figure 9 shows the oscillator installed in the wind-tunnel test section, and Figure 10 is a sketch of the model support and oscillator system. The sting support for the model forms one arm of the forcing linkage system which is driven by connecting rods mounted eccentrically on two flywheels. Periodic motion even at low frequencies is assured by the large flywheel inertias. The total moment of inertia of the flywheels and other rotating parts is sufficient to maintain the angular velocity constant to within 1% even at a low oscillator speed of 3 cps. The long-term regulation depends upon the drive as well as the flywheels. A ten-horsepower DC motor drives the 1:1 geared flywheel shafts through 2:1 pulleys and "V" belts. (See Appendix I for a detailed description of the oscillator.) The motor speed is servo-regulated to within one-quarter revolution per second of constant speed. The flywheel, motor-servo system has an excellent long-time stability.

The desired model motion is obtained by adjusting the eccentric amplitudes and the angular relation between the flywheels while monitoring the actual model motion as measured by accelerometers within the model. Initially, the operator uses indications of the eccentric amplitudes and phasing to approximate the desired motion. (These indicators are described in Appendix I.) Each eccentric amplitude is controlled by means of small hydraulic motors which are mounted on the flywheels. Control over the phase relationship between the two flywheels is obtained by means of a hydraulic motor which permits arbitrary angular positioning between the drive gear and shaft on the aft flywheel. (Further details of the hydraulically actuated control system are presented in Appendix I.)

While the mechanical details of their operation are rather complicated, the actual controls provided to the operator are very simple (see Figure 11). On/off switches and a variable-resistance potentiometer provide the control for the oscillator driving motor. The amplitudes of the forward and aft eccentrics can be increased or decreased independently at either a fast or slow speed. Another variable-resistance potentiometer controls the rate of phase adjustment and a switch activates the phase control in either direction at this preset rate.

The dynamic loads produced by the oscillator in its own support structure are attenuated by mounting the oscillator on a large mass (about 14 tons) which is isolated from the wind-tunnel structure by a pneumatic suspension. The very low resonance frequency of this mount system practically eliminates the transmission of any dynamic loads to the tunnel structure and, at the same time, isolates the model from random vibrations produced by the tunnel itself.

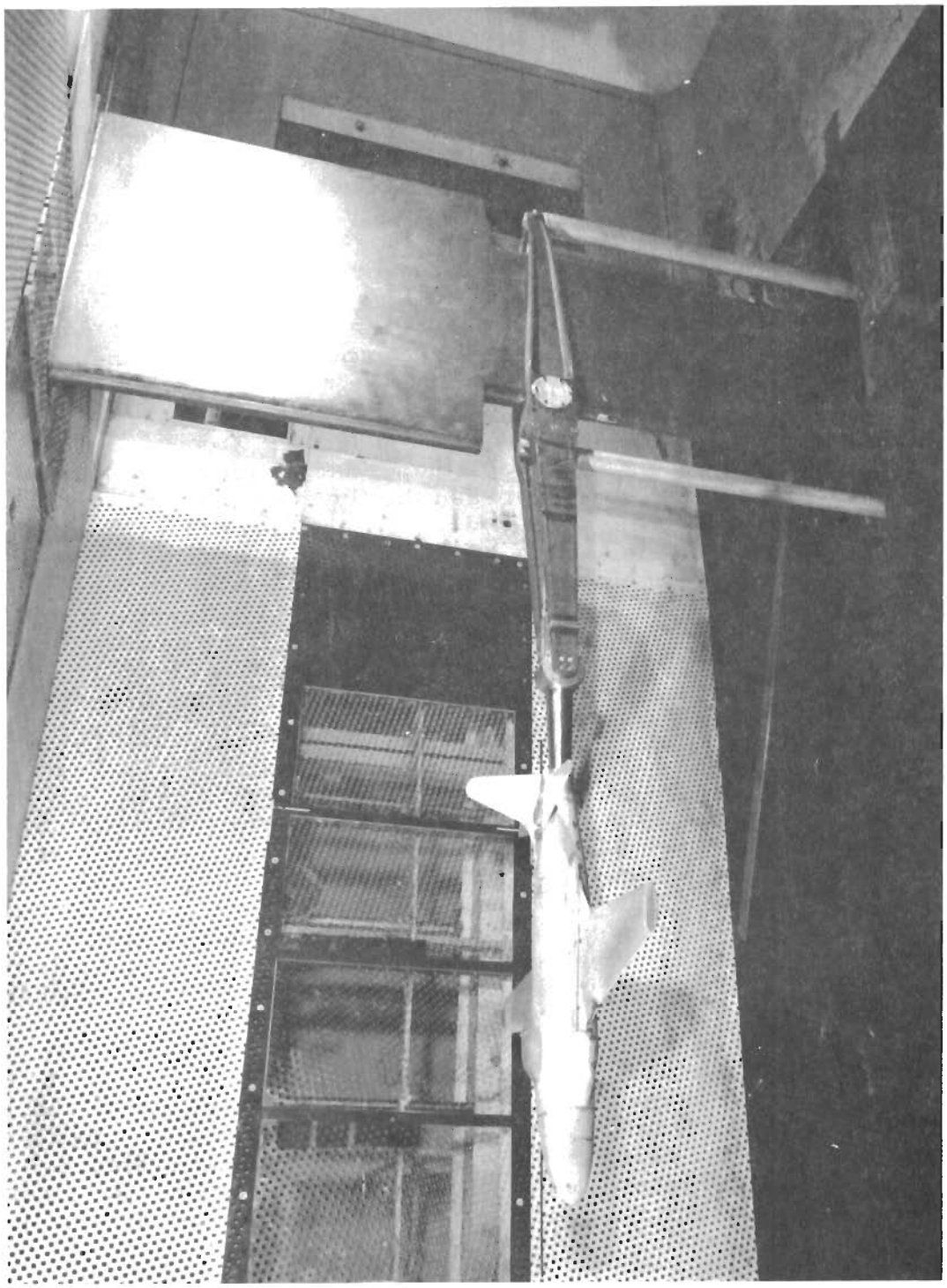

Figure 9 THE OSCILLATOR INSTALLED IN THE WIND TUNNEL

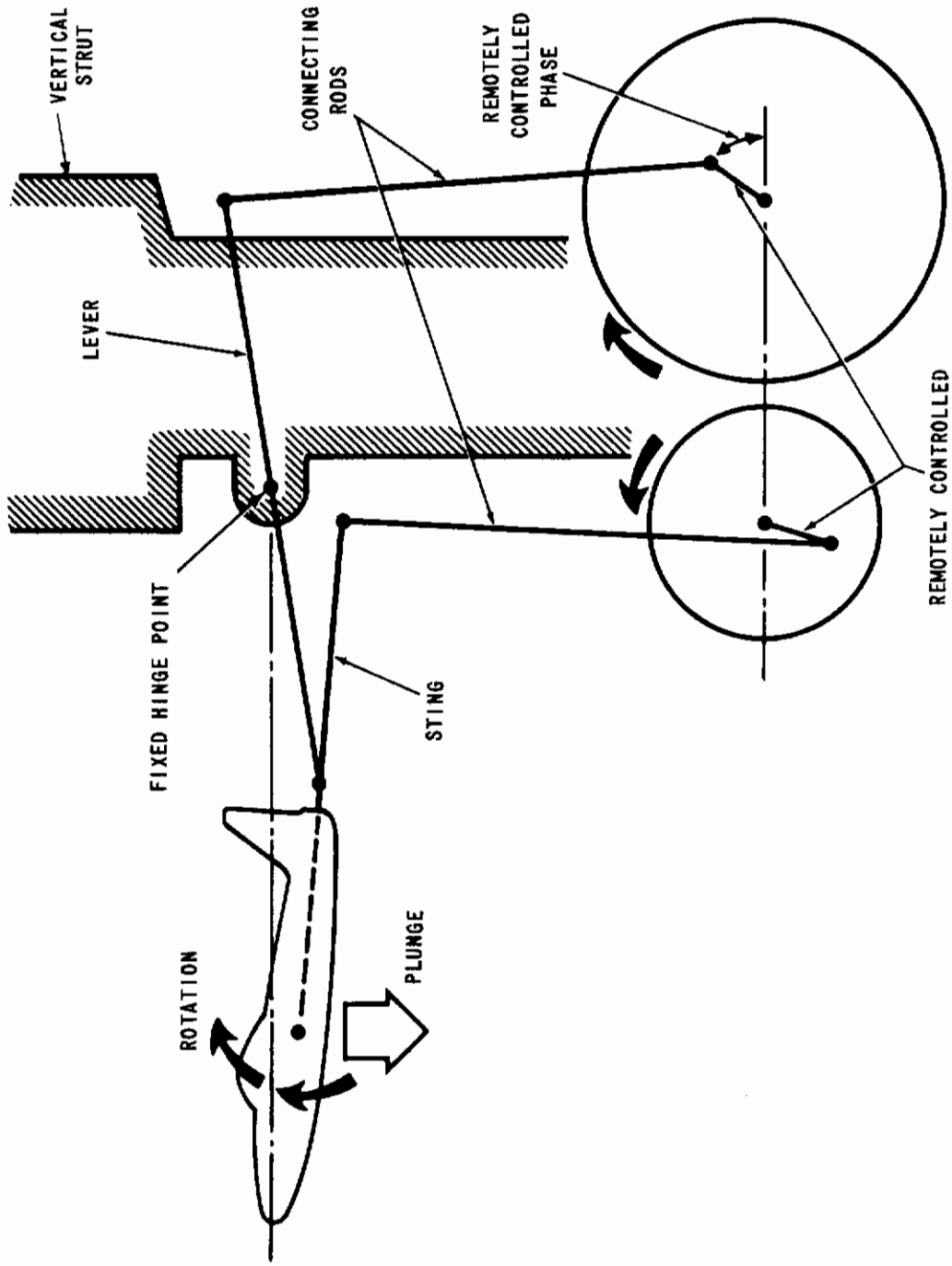

Figure 10 THE MODEL SUPPORT AND OSCILLATOR

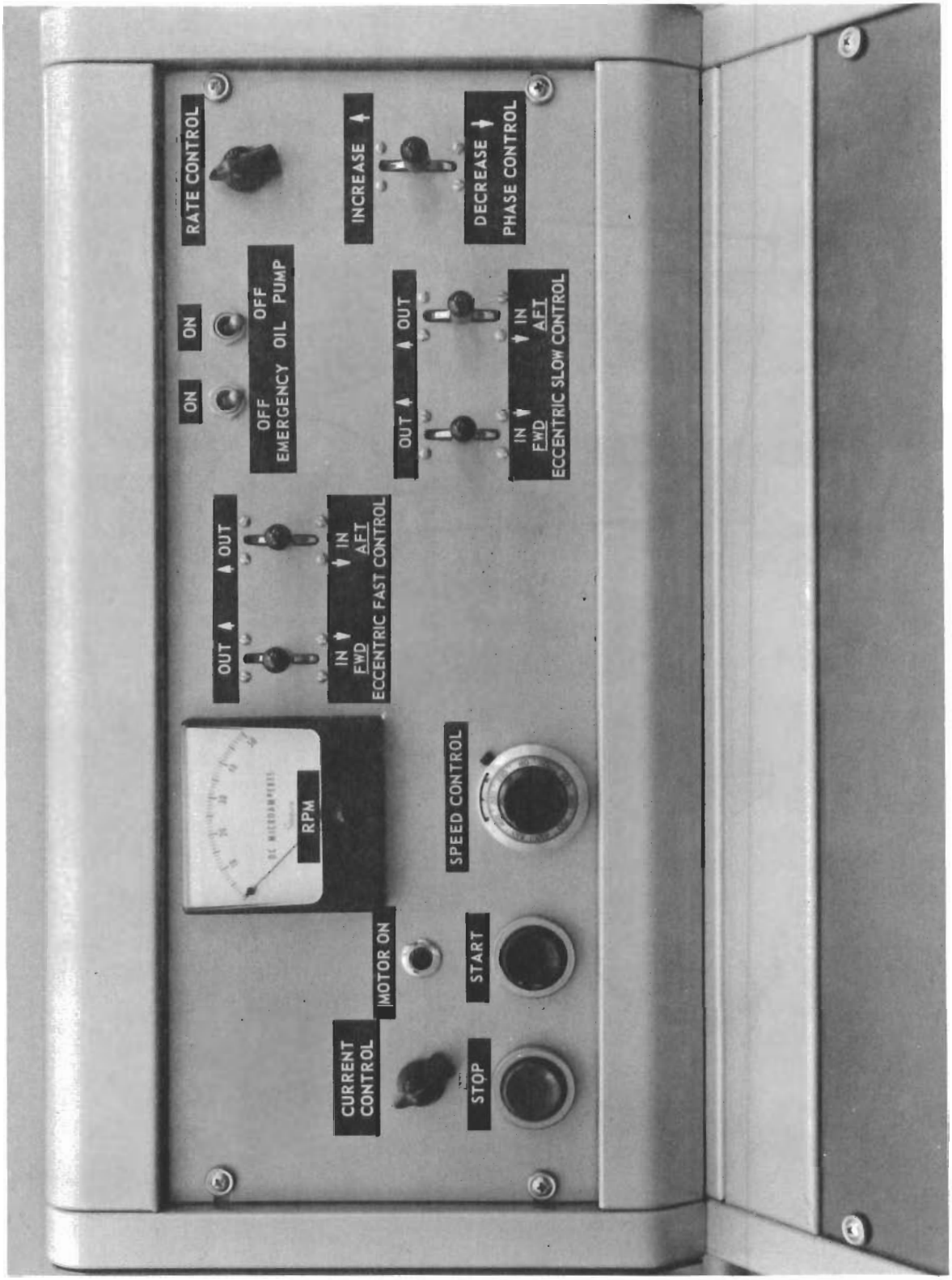

Figure 11 MECHANICAL OSCILLATOR CONTROL PANEL

The wave form of the model motion is excellent over most of the operating frequency range. The primary distortion of the wave form is attributable to the second-harmonic input due to the crank connecting rod kinematics. The distortions due to elasticity of the structure are significant at subharmonics of the system's resonant frequency. Tests performed with an 18-lb. dummy model indicated that, except at the discrete frequencies corresponding to the subharmonics, acceptable-to-good wave forms are achieved over the entire operating range, as shown in Figure 12. (The lowest natural frequency with an 18-lb. model on the support system is 17.3 cps.) The signals from accelerometers at the model were monitored on an oscilloscope and judged qualitatively to be good, acceptable, or unacceptable depending whether the harmonics and noise were, respectively, 0-10%, 10%-25%, or greater than 25% of the fundamental amplitude.

The mechanical oscillator has the following operating characteristics:

(1) it can provide a fundamental oscillating frequency of from 3-12 cps;

(2) at this fundamental frequency, it can provide a translational motion of up to 20 g's of translational acceleration or a vertical displacement of 1 ft. double amplitude, as shown in the double exposure of Figure 13;

(3) it can provide a rotational motion of the model at the fundamental frequency with angular accelerations in excess of 200 radians/sec.^{2} or a rotational displacement of 10° double amplitude, as shown in the double exposure of Figure 14; and

(4) the system can sustain a peak vertical load of 1200 lbs. at the model's center of gravity.

Further details on the design, construction, and operation of the mechanical oscillator are provided in Appendix I.

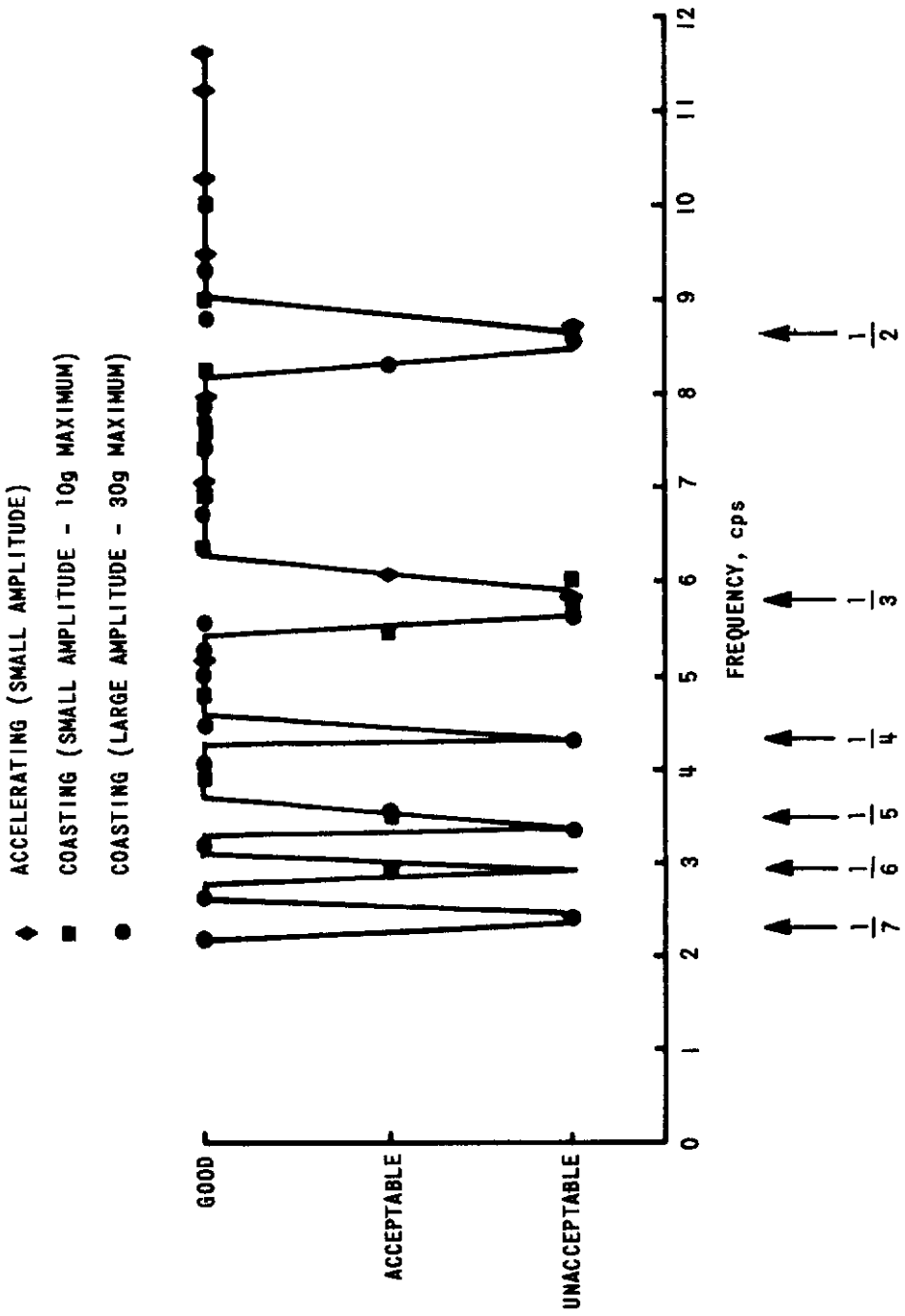

Figure 12 SINUSOIDAL WAVEFORM QUALITY OF THE MECHANICAL OSCILLATOR

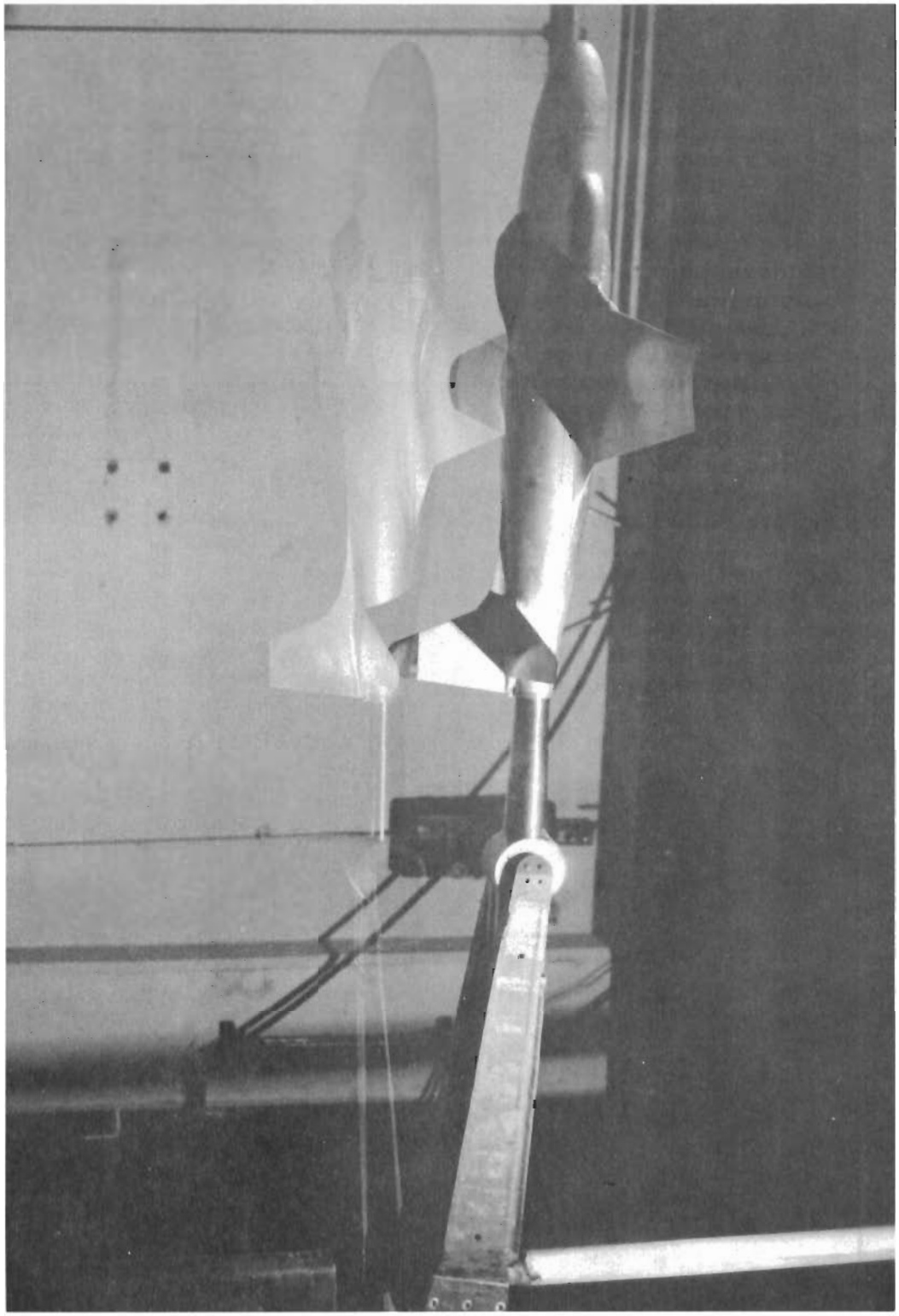

1 FOOT DOUBLE AMPLITUDE VERTICAL DISPLACEMENT OR 644 FT/SEC^2 LINEAR ACCELERATION

Figure 13 LIMITS OF PLUNGING MOTION

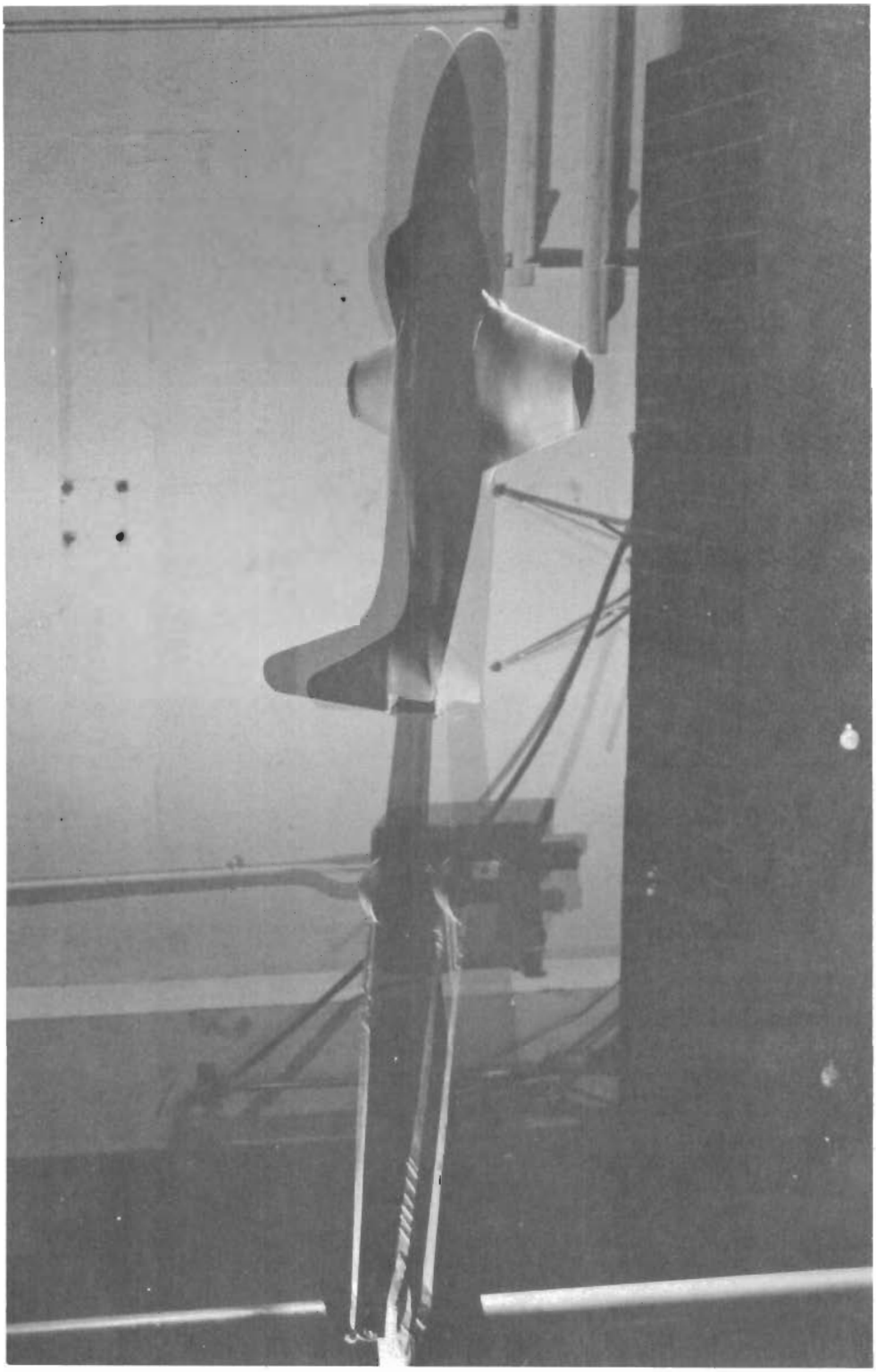

10° DOUBLE AMPLITUDE ROTATIONAL DISPLACEMENT OR 200 RAD/SEC^2 ANGULAR ACCELERATION

Figure 14 LIMITS OF ROTATIONAL MOTION

SECTION 5

THE MODEL

A one-tenth-scale model of an F-80 aircraft was utilized for purposes of checkout, shakedown, and evaluation of this dynamic testing system. (The model is shown in the photograph of Figure 15.) Although it is not a particularly modern design, the F-80 model was used primarily because of the relatively large amount of comparable data which exist from other wind-tunnel tests, calculations, and flight tests. This light, rigid, and strong model was built specifically to make dynamic wind-tunnel tests for comparison with flight test data. The model, including the metric portions of the transducers, has a greater weight (18 lbs.) and greater moment of inertia (0.375 slug ft.^{2}) than a true one-tenth-scale model. These factors have little significance for this investigation, however, because comparison of the dynamic wind-tunnel test data with full-scale flight test data is dependent upon reduced frequency, and the oscillator is capable of forcing the model motions at the appropriate reduced frequencies.

Nearly the entire model is aluminum alloy, including the semi-monocoque fuselage and the honeycomb-core wing and tail. The model is very rigid, being about ten times as stiff as a dynamically scaled model, to avoid introducing effects due to aeroelastic deformations of the model. Flexibility of the model not only would increase the possibility of losing the model because of flutter, but also would defeat the purpose of the tests — that is, the obtaining of accurate dynamic derivatives. Any attempt to scale the flexibility of the full-scale airplane for an evaluation of its effect would introduce requirements for even more complicated testing procedures. Model excitation should, in that case, be applied in the manner to be simulated, such as by means of a gust or elevator input.

The weight and moment of inertia of the model must be small so that reasonably large linear and angular accelerations can be applied without exceeding the capacity of the model and of the normal-force- and moment-measuring balance. Inertial loads at the longitudinal short-period frequency have the same magnitude as aerodynamic spring terms and are considerably greater than the damping loads. Deflection of the airframe is proportional to absolute stiffness for static air loads, but is proportional to stiffness-to-weight ratio for inertial loads. (For details on the model design and construction, the reader is referred to Reference 14.)

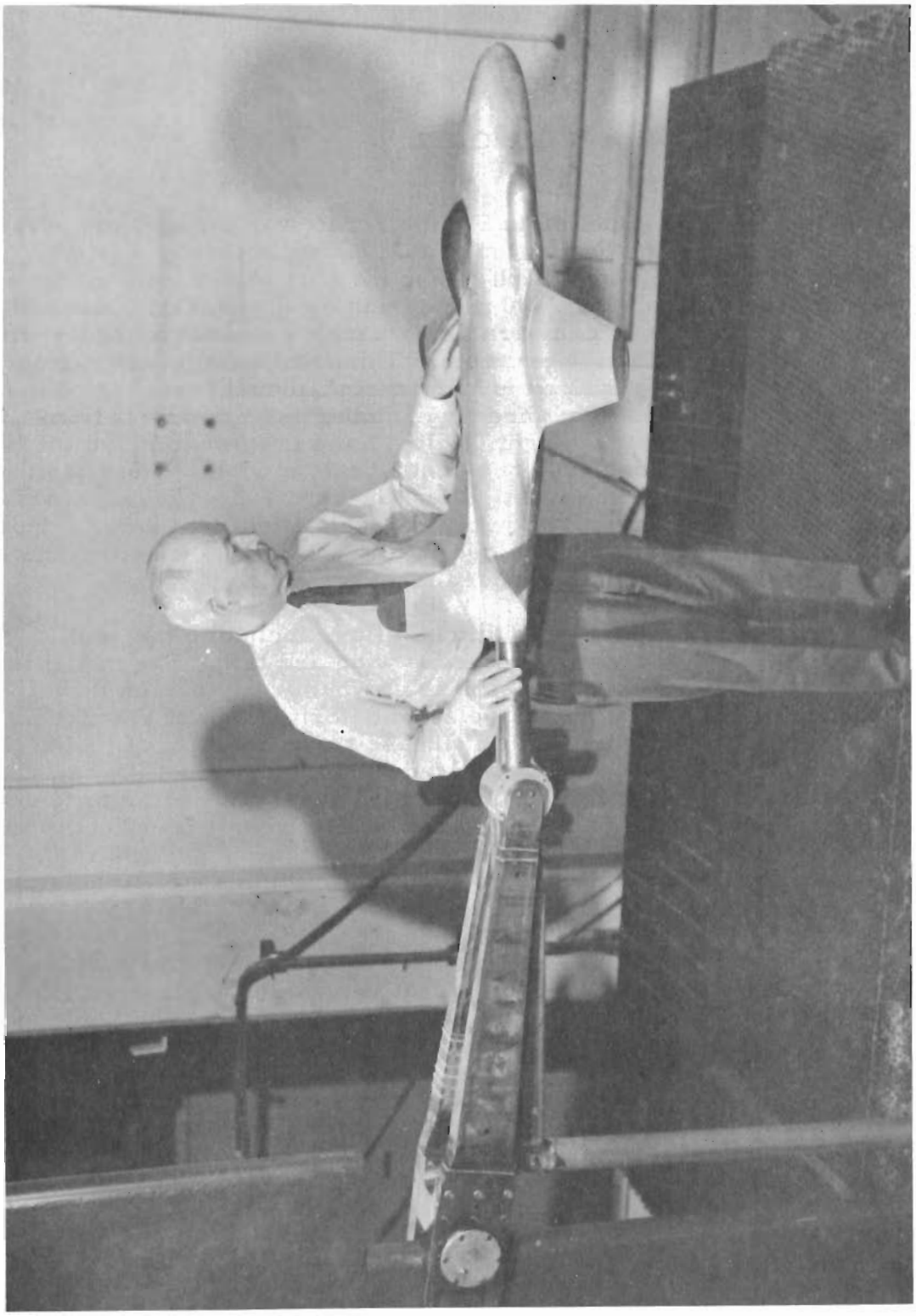

Figure 15 THE F-80 DYNAMIC TESTING MODEL

SECTION 6

THE FORCE AND MOTION SENSORS

The measurement system in the model is shown in the sketch of Figure 16(a) and in the photograph of Figure 16(b). The model is supported from the sting by a system of four flexures, three of which incorporate strain gages for measuring the loads on the model. The strain gages on two of these flexures (the forward strain beams) are connected to sum their output signals. (This signal is, henceforth, referred to as the "normal-force" measure although, actually, it includes a component proportional to the couple which reacts the pitching moment.) These two flexures are separated equilaterally about the plane of symmetry of the model to provide sufficient stiffness about the model's roll axis. The signal summing circuit automatically provides cancellation of signals caused by unintentional rolling-moment inputs to the model from the mechanical oscillating system. The model is precisely balanced so that its center of gravity is located longitudinally at the sensitive axes of the forward strain beams, which are located as closely as possible to the aerodynamic center of the model (in this case, the quarter chord of the wing). The sensitivity of the normal-force flexures is approximately 1.6 microvolts output per pound of force per volt of excitation.

A single flexure support is situated 6.5 in. aft of the forward flexures and on the model's longitudinal centerline. The strain-gage bridge attached to this flexure provides an output proportional to pitching moment only, and its sensitivity is approximately 23.8 microvolts per pound of force per volt of excitation. The normal-force and moment flexures support the model stiffly in all directions excepting along the longitudinal axis. A fourth flexure called the "axial strain beam" is attached between the model and sting to provide restraint along this axis without interfering with the operation of the sensing flexures. (See Appendix II for further details of the balance system.)

The vertical motion at the model's center of gravity is measured by a special linear accelerometer (see Figure 16). The standard version of this accelerometer consists of a seismic element and associated electronics housed in a single case which is too large to fit the space available at the center of gravity of the model. The modified unit obtained for this purpose consists of two parts — a sensing element housed in a small case, and an electronic components package in a separate case. As installed, the units are separated by a 7-ft. long cable. The sensing element can then be located at the model's center of gravity while the electronic package is located in the vertical strut just below the fixed hinge point of the linkage system. This linear accelerometer is of the servo-balance type employing a pendulous seismic element supported by a pivot and jewel bearings. The general characteristics of this accelerometer are as follows:

Range:	$\pm$30 g full scale
Output:	approximately 0.3 volt DC per g

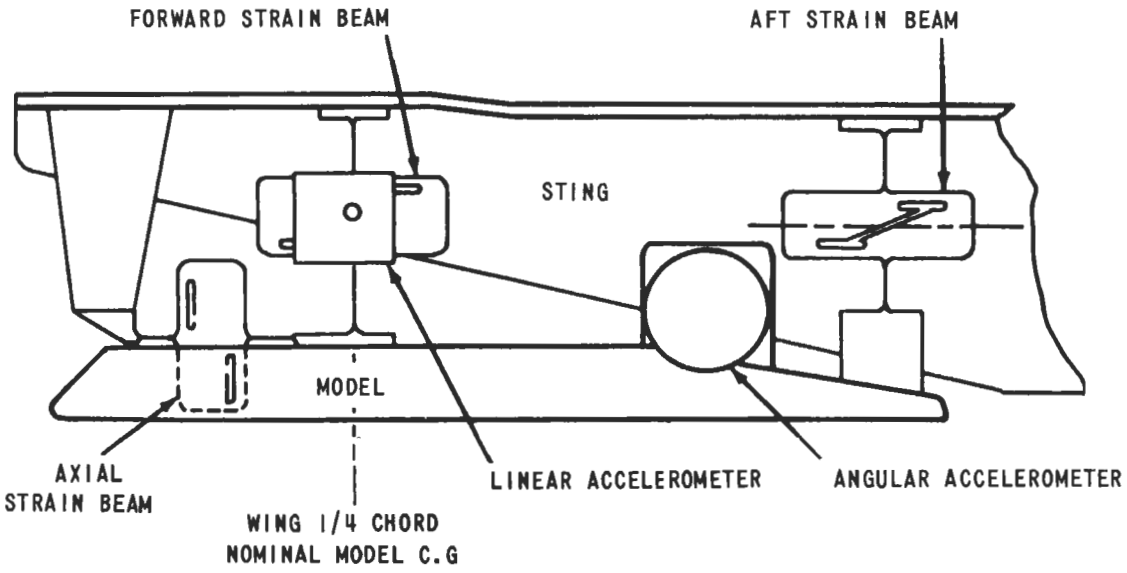

(a) SCHEMATIC

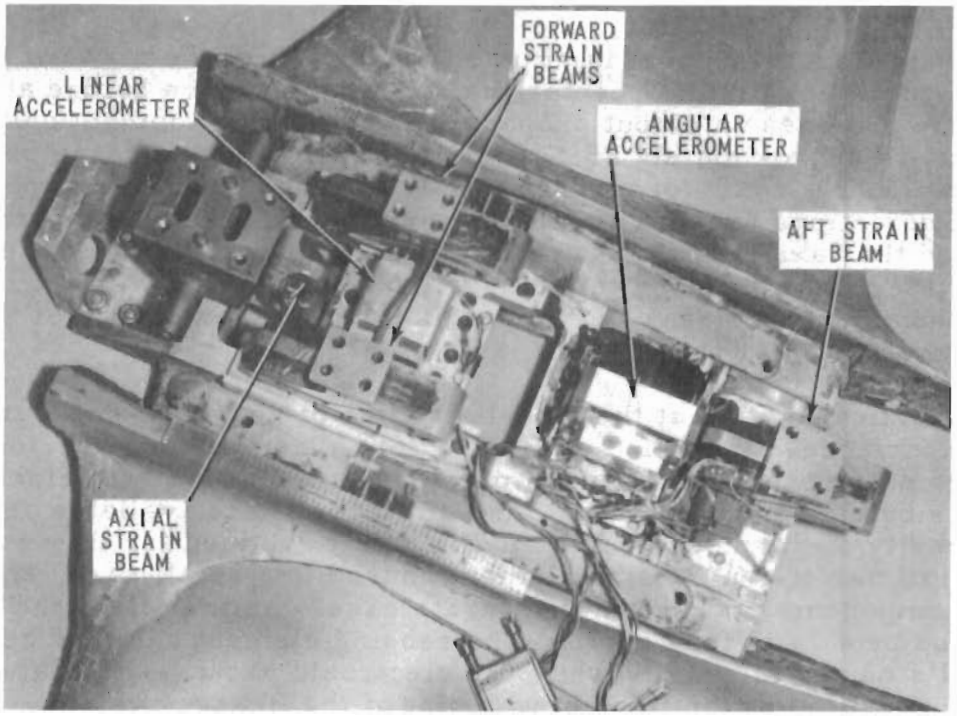

(b) INSTALLATION

Figure 16 THE FORCE AND MOTION SENSORS

Output impedance:	approximately 3,000 ohms
Natural frequency:	~ 200 cps
Damping:	~ 0.6 of critical
Phase shift (3-12 cps):	0.6°/cps
Input power:	±15 volts DC

Under all operational environments existing during wind-tunnel testing, this linear accelerometer exhibits an overall accuracy of 1% or better. (See Appendix II for further description of this unit.)

The model's rotary motion about a pitching axis through the model's center of gravity is measured by means of a very special angular accelerometer. An outline drawing of the angular accelerometer is shown in Figure 17(a). Figure 17(b) shows the instrument installed in the model. This instrument is of the servo type and employs feedback circuitry which results in high accuracy and stable performance. The instrument was developed especially for the dynamic testing system and is unique in its small size, ruggedness, insensitivity to inputs other than angular acceleration, and its attenuation of high-frequency noise inputs. The inertial sensing element in this transducer is designed for minimum pendulosity or mass unbalance. If this were not the case, prohibitively large errors would result from the instrument's response to linear accelerations when attempting to measure angular accelerations during model motions which included large linear accelerations (as in plunge and pitch). The general characteristics of this angular accelerometer are as follows:

Range:	±200 radians/sec.^{2} full scale
Output:	0.05 volts DC/rad/sec.^{2}
Output impedance:	approximately 10 ohms
Natural frequency:	approximately 50 cps
Damping:	0.7 of critical
Phase shift (3-12 cps):	approximately 5°/cps (with high-frequency noise rejection circuits in the feedback loop of the accelerometer)
Input power:	+28 volts DC, -28 volts DC, and 3 volts DC
Sensitivity to linear acceleration:	less than ±0.05 radian/sec.^{2}/g (under 15 g conditions)
Resolution:	better than 0.002% of full scale

(See Appendix II for further description of this unit.)

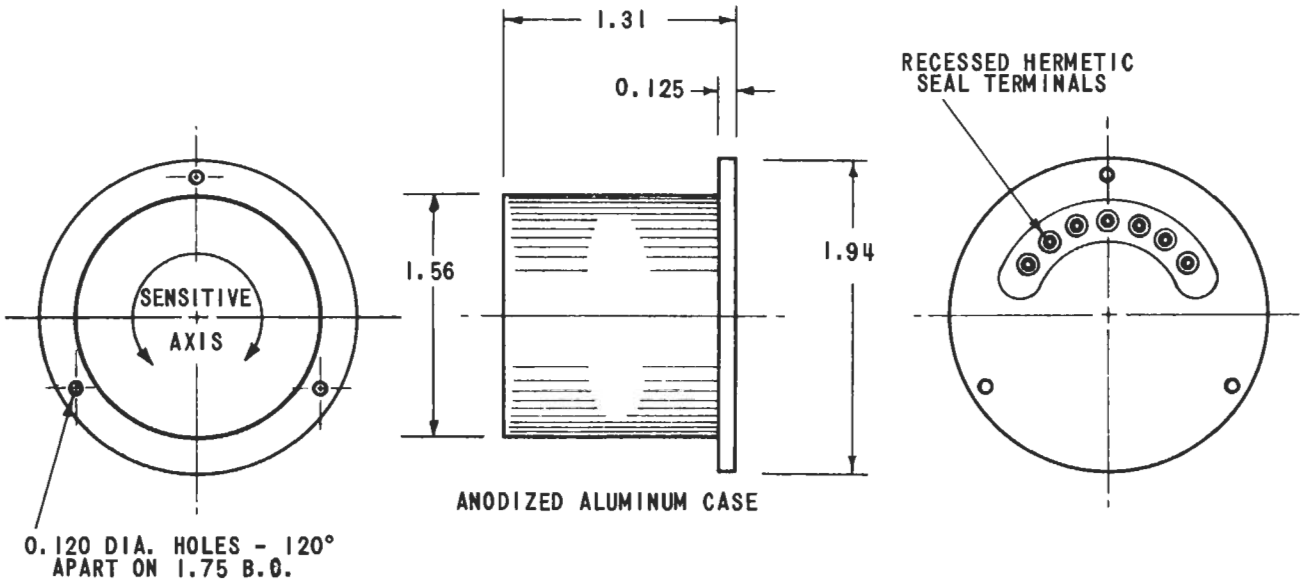

(a) SCHEMATIC

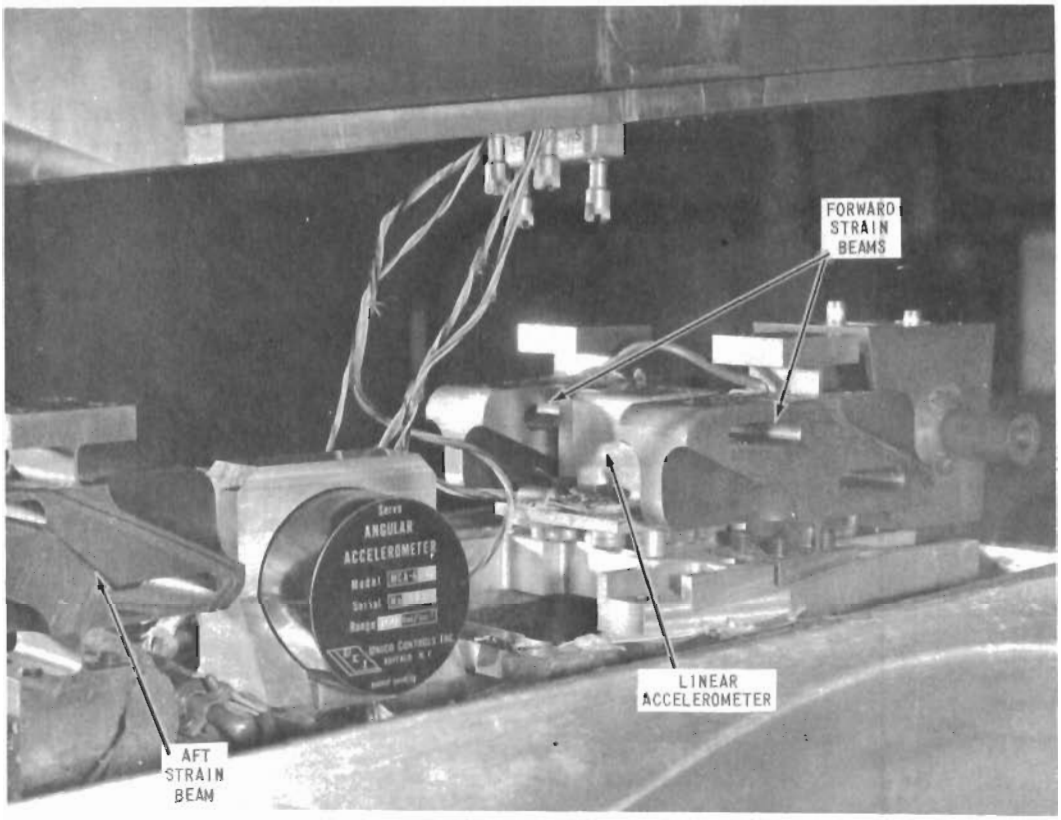

(b) INSTALLATION

Figure 17 THE ANGULAR ACCELEROMETER

Special techniques had to be developed to calibrate these transducers to the required degree of accuracy. This was particularly true in the case of the measurement of the crosstalk sensitivity of the angular accelerometer. To illustrate the difficulty: If this crosstalk is to be evaluated under environmental conditions of, say, 15 g's of linear acceleration at 7 cps, a rotational displacement of only $\pm$1-1/3 minutes of arc would produce a signal equal to the entire allowable output due to g sensitivity. The only transducer capable of measuring such small angular quantities in the presence of large linear accelerations was the angular accelerometer itself. The procedure used for calibration of the crosstalk sensitivity is described in Appendix II.

The center of gravity of the model had to be located precisely at the plane of the sensitive axes of the two forward strain beams. To accomplish this, the output of the moment-measuring beam was recorded with the model and the sting in, first, the upright (normal) and, then, the inverted position. The model was then ballasted until the pitching-moment-measuring balance readouts were the same for both configurations. The vertical location of the c.g. relative to the balance elastic axis was similarly checked by supporting the model vertically, first, nose up and, then, nose down and noting the change in the pitching moment.

The pitching-moment-measuring flexure was calibrated dynamically by measuring the output of its strain bridge with and without a known increment of moment of inertia while the model was oscillated in a pure rotational mode at various values of angular acceleration. The center of gravity of the incremental weight was located very precisely to coincide with the model's center of gravity. This technique not only enabled the calibration of the moment-measuring strain-gage beam, but the measurement of the moment of inertia of the model as well. (Further details of the force and motion sensors and their calibrations are discussed in Appendix II.)

The transducer signals from the model are passed through an "on-line" processing system to provide digitized readouts of the amplitudes and phases of the forces, moments, and accelerations at the oscillation frequency.

SECTION 7

SIGNAL PROCESSING

A block diagram of the signal processing system is shown in Figure 18. The signal processing system accepts, simultaneously, the four transducer outputs originating in the model at a particular frequency within the range of 3-12 cps, extracts the fundamental signals in the presence of random noise and harmonics, and automatically derives from these signals their phase angles and individual magnitudes. This information is displayed visually and is printed out and punched on IBM cards for later use in performing the final analysis.

The four signals from the force and motion transducers in the model which are related to the normal force, pitching moment, normal acceleration, and angular acceleration of the model are fed to a signal mixing unit. This unit contains DC amplifiers with gain controls in all four channels. The operations performed in the signal amplification and mixing unit are indicated in Figure 19. Phase-compensation controls (padders) are provided in the force, moment, and linear-acceleration channels to accommodate differences in dynamic characteristics of the transducers and to match these channels dynamically at each frequency to the angular-accelerometer channel. These signals can then be combined as desired. In particular, the forces and moments due to inertial reactions are compensated by corresponding signals of opposite polarity from the linear and angular accelerometers.

The heart of the signal processing system is a bank of four phase and amplitude analyzers which operate on the four signals from the mixing unit. Each analyzer channel provides a unique filter system which is self synchronous with respect to the oscillator frequency, so that harmonics or random noise in the input signal are strongly attenuated regardless of the frequency of its fundamental component. Two outputs from each channel are very accurate measures of the amplitude and phase of the component at the oscillator frequency. One output is a DC voltage proportional to the amplitude of the part of the signal which is at the fundamental oscillator frequency. The other output is a digitized presentation of the phase of this fundamental component with respect to the oscillator drive. Although these units were developed especially to satisfy the requirements of the dynamic testing system, they were obtained as CAL equipment because of their potential for more general applications. The phase and amplitude analyzers are described further in Appendix III.

Signal-matching units make the output circuits of these phase and amplitude analyzers compatible with the requirements of the input circuits of the available CAL wind-tunnel data readout system. Four of the normal digital voltmeters are equipped with special plug-in adapters to make them compatible with the four amplitude-measuring circuits in the signal processing system. Each voltmeter is also connected to a printer and a cardpunch unit.

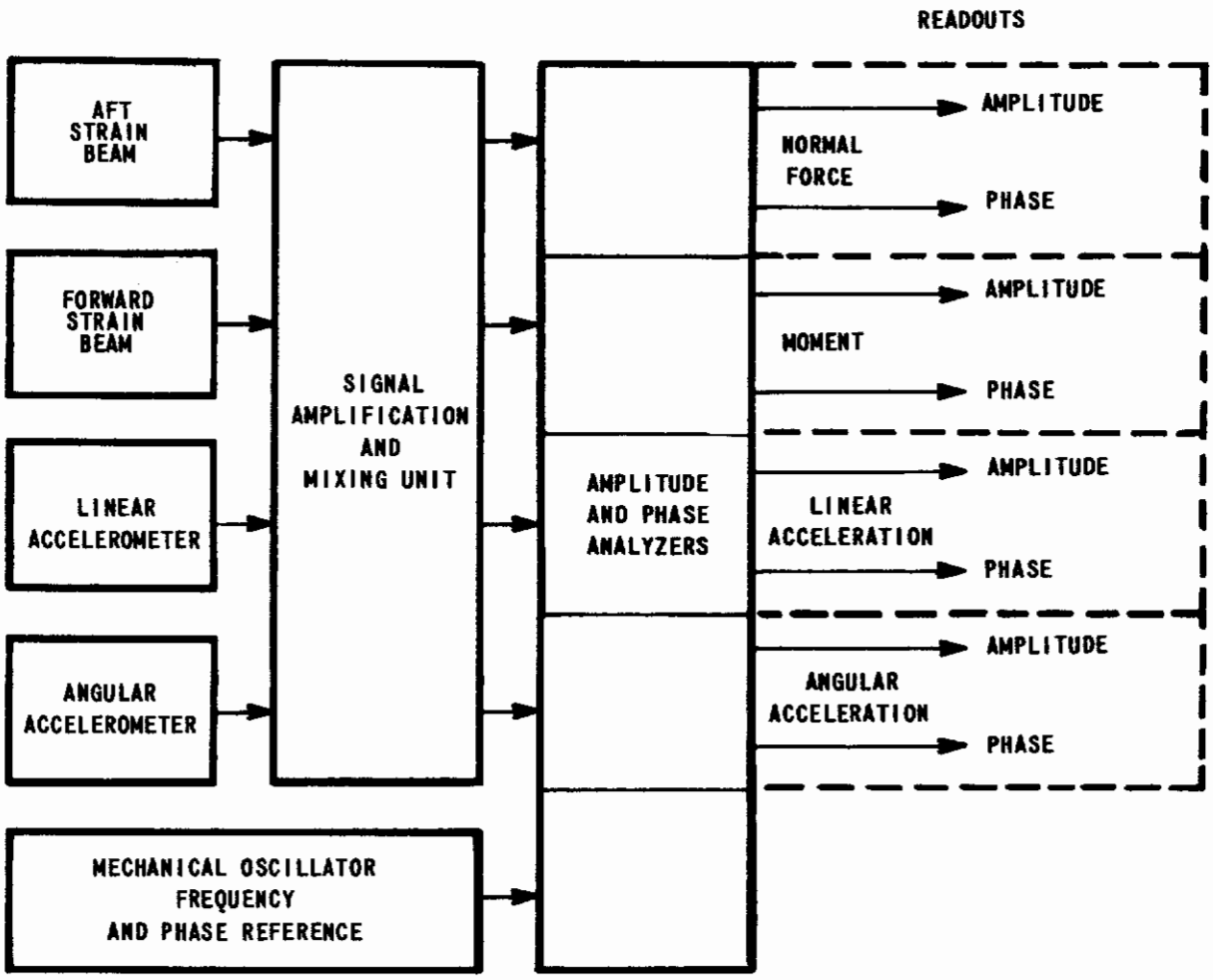

Figure 18 THE SIGNAL PROCESSING SYSTEM

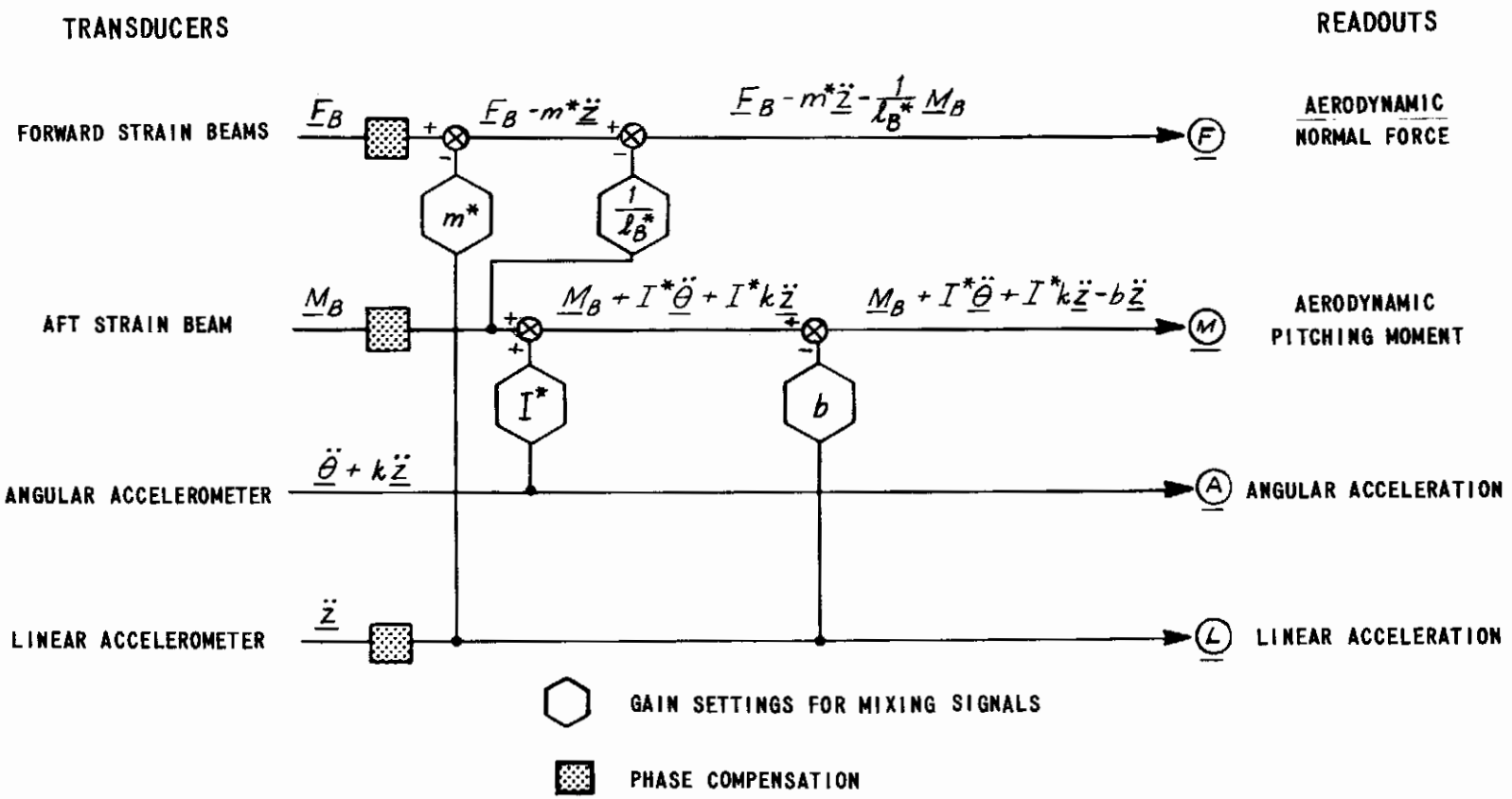

Figure 19 OPERATIONS PERFORMED IN THE SIGNAL MIXING UNIT

The phase signals are digitized within the analyzer units themselves. These are displayed on remote indicators and are also reproduced in printed and punched-card forms.

A special test signal generator, while not an active part of the data-signal-processing system itself, is, nevertheless, an important piece of support equipment which is used for "on-line" calibration of the signal processing system. The test signal generator is composed of two major parts — (1) a pure sinewave signal source for the frequency range of 3-12 cps, and (2) a precision measuring circuit called a "peak reader" which very accurately determines the amplitude of the test signal sinewave.

Further details of the signal processing system and the test signal generator are presented in Appendix III.

SECTION 8

SYSTEM ACCURACY REQUIREMENTS

The acceptable tolerances in the measured derivatives were arbitrarily selected to be the following, in order to establish the accuracy objectives for the system:

(1) The error in F_{α} shall be less than 10% of F_{α} .

(2) The error in M_{α} shall be less than 10% of M_{α} .

(3) The error in $M_{\dot{\alpha}} + M_{\dot{\theta}}$ shall be less than 10% of $M_{\dot{\alpha}} + M_{\dot{\theta}}$.

(4) The error in $M_{\dot{\alpha}}$ shall be less than 10% of $M_{\dot{\alpha}} + M_{\dot{\theta}}$.

(5) The error in $M_{\dot{\theta}}$ shall be less than 10% of $M_{\dot{\alpha}} + M_{\dot{\theta}}$.

Requirements on the system accuracy fall into two categories — one is the requirement on the accuracy with which the desired motion must be set up, and the other is the requirement on the accuracy with which that motion and the resulting force and moment must then be measured.

In the first category, the very precise control on the oscillator, together with the accurate on-line readouts of the model accelerations, enables the operator to adjust the model motion within extremely tight tolerances. For example, the control is sufficiently precise to adjust the model motion at 7 cps to within ± 0.4 radian/sec.^{2} of rotational acceleration, to well within ± 8 ft/sec.^{2} of the plunging acceleration, and to about $\pm 1/2^{\circ}$ of phase angle between rotation and plunging. These represent motion requirements in the pure pitching case where it is desirable to maintain the rate of change of angle of attack less than 0.03 radian/sec.

In the second category, every consideration has been given to maximizing the measurement accuracy of each element of the system. The transducers are designed to clearly separate their functions in order to tailor the sensitivity of each to the specific quantity to be measured. To assure that moment measurement is sufficiently independent of normal force, the model's center of gravity is positioned to within one one-hundredth of an inch of the elastic axis of the normal-force beam. Similarly, the angular accelerometer must, during plunging motion, be able to measure accurately small levels of angular acceleration in an environment of very high linear acceleration. The crosstalk sensitivity of this instrument is particularly low — the indicated rotational acceleration is less than 0.75 radian/sec.^{2} when it is exposed to pure linear accelerations as high as 480 ft/sec.^{2}. The model motions are also tailored to the particular measurement to be made. Ideally, with an errorless measuring system, the motion

of the model could be arbitrary. Since this perfection cannot be achieved, specific motions (such as pitching, plunging, and rotation in the case of longitudinal dynamics) are used to maximize particular components of the loads to be measured. This use of a particular motion for each measurement maximizes the accuracy possible within the resolution limitations of the data-processing system. In much the same way, readout accuracy is improved by canceling - in the mixing unit - the components of force and moment due to inertial loads.

The accuracy requirements on the system are discussed further in Appendix IV.

SECTION 9

SYSTEM EVALUATION TESTS

The F-80 model was used in a series of wind-tunnel tests for checkout, shakedown, and evaluation of the dynamic testing system.

Prior to the wind-on tests, a program of wind-off tests was performed to set up the desired gains, adjust the phase paddings on the signal channels, and combine the signals in the proper proportions in accordance with Figure 19. These wind-off tests proceeded as follows:

(1) The precise operating frequency was selected by observing the wave form of the model motion in pure plunging at various frequencies slightly above and slightly below the desired one. The linear accelerometer output was monitored on an oscilloscope for this purpose.

(2) With the mechanical oscillator running with small eccentricities and at the testing frequency, the test signal was introduced to all channels, the phase and amplitude analyzers were standardized to their zeros, the gain was set on the angular accelerometer channel to provide the desired number of counts of readout per volt of test signal in accordance with the calibration of that instrument, and the approximate gains were set on the other three channels.

(3) All phase readouts were set to the same value with the test signal into all four signal channels.

(4) Phase padding was increased in the linear accelerometer channel to provide the proper phase relationship with respect to the angular accelerometer at the testing frequency on the basis of the previously obtained calibrations of these two transducers. The final gain was then set on the linear accelerometer channel to provide the desired number of counts per g on the digital voltmeter readout. The test signal (which provides the counts per volt) and the calibration of the linear accelerometer (which provides the volts per g) are used for this purpose.

(5) The mechanical oscillator was operated at the testing frequency and the eccentrics were adjusted to provide a model motion of about 50 radians/sec.^{2} of angular acceleration and less than 0.1 g of linear acceleration.

(6) The padding in the moment channel was adjusted to provide a lag of 180° relative to the angular accelerometer. The final gain was then set on the moment channel to produce the desired number of counts per ft. lb. using the test signal and the calibration of the moment-beam sensitivity. (Since the moment in this configuration is due almost entirely to inertial reaction, a check of the previously measured inertia could be made by ratioing the indicated moment to the angular acceleration.)

(7) A signal from the angular accelerometer was combined in the mixing unit with the signal from the moment balance and a gain (I^* in Figure 19) was adjusted until the moment readout was zero. The moment due to inertial reaction was thus canceled.

(8) Phase padding on the normal-force channel was adjusted to provide 180° phase lag with respect to the angular accelerometer. The final gain on the normal-force channel could then be set to provide the desired number of counts per pound using the test signal and the calibration of the normal-force beams.

(9) The eccentrics of the mechanical oscillator were then adjusted to provide a model motion of 15 g's of linear acceleration and less than 0.4 radians/sec.^{2} of angular acceleration.

(10) A signal from the linear accelerometer was combined in the mixing unit with the signal from the moment balance, and the gain (b in Figure 19) was adjusted to reduce the component of the moment in phase with linear acceleration to zero. (The F-80 in pure plunging in still air had a significant residual moment due to aerodynamic load on the horizontal tail which was in phase with the linear velocity. See page 42 for further discussion of this point.)

(11) A signal from the linear accelerometer was combined with the signal from the normal-force beams in the mixing unit, and the gain (m^* in Figure 19) was adjusted to minimize the normal-force readout. This compensated for the force due to inertial reaction.

(12) A signal from the moment balance was combined with the signal from the forward (normal-force) beams in the mixing unit, and the gain ($\frac{1}{ft}$ in Figure 19) was adjusted to zero the normal-force readout. This compensated for the component of moment sensed by the forward beams.

(13) With the wind still off, the density in the sphere of the test section was reduced. The moment readout during pure plunging motion was recorded at several values of density. This provided a check that the residual moment was entirely due to horizontal tail drag, since the extrapolated straight line through these points passed through zero at zero density.

The system was then ready for wind-on tests. A series of wind-tunnel tests using the F-80 model at three frequencies and four Mach numbers demonstrated the versatility and overall accuracy of the dynamic testing system. The tests were run in the following order, all at conditions corresponding to 1/2 atmosphere at wind off:

(1) Pure rotation tests were run at 50 radians/sec.^{2} with less than 1/4 g of linear acceleration. The frequency was 7 cps (period equal to 0.1429 sec.). Data were taken at Mach numbers 0, 0.5, 0.7, 0.75, 0.8, and repeated at M = 0. (The chart of Figure 20 is convenient for relating rotational amplitudes, rates, accelerations and frequencies.)

(2) Pure plunging tests were run at 15 g's of linear acceleration and less than 0.4 radian/sec.^{2} of angular acceleration. Again, the frequency was 7 cps and the Mach numbers were 0, 0.5, 0.7, 0.75, 0.8, and repeated at M = 0. (The chart of Figure 21 is convenient for relating translational amplitudes, rates, accelerations and frequencies.)

(3) Pure pitching tests were performed at about 15 g's of linear acceleration, and a frequency of 7 cps. In all cases, the linear acceleration was adjusted to 15 g's $\pm$1/4 g, and the angular acceleration required at each Mach number was adjusted to within $\pm$0.4 radian/sec.^{2}. The amplitude of the angular acceleration in radians/sec.^{2} for pure pitching is given by $|\underline{A}| = \frac{2\pi}{U\tau}|\underline{L}|$ where U is the free stream velocity in fps, τ is the period in seconds, and $|\underline{L}|$ is the linear acceleration in ft/sec.^{2}. The motion was adjusted so that the phase of the angular acceleration lagged the linear acceleration by 90° $\pm$1/2°. At M = 0.5 (U = 550 fps), the required angular acceleration to cancel the angle of attack due to translational motion of 15 g's at 7 cps is 38.6 radians/sec.^{2}; at M = 0.7 (U = 767 fps), the angular acceleration is 27.7 radians/sec.^{2}; at M = 0.75 (U = 824 fps), the angular acceleration is 25.8 radians/sec.^{2}; and at M = 0.8 (U = 882 fps), the angular acceleration is 24.1 radians/sec.^{2}.

The entire test program was then repeated at a frequency of 5 cps, and pure rotation tests were also conducted at 10 cps.

A major consideration during the development of the dynamic testing system was the necessity for a sufficiently strong fundamental signal that would not be lost in the noise environment caused by vibrations and aerodynamic turbulence. Difficulties in this regard that were encountered in the early phases of the system's development are discussed in Appendix V. The F-80 tests demonstrated, however, that a very high signal-to-noise ratio was indeed maintained. This is due, in large part, to the high g levels that can be obtained, the good wave form, the firmness of the model-motion system, the isolation mounting of the mechanical oscillator, and the overall design of the instrumentation and signal processing system.

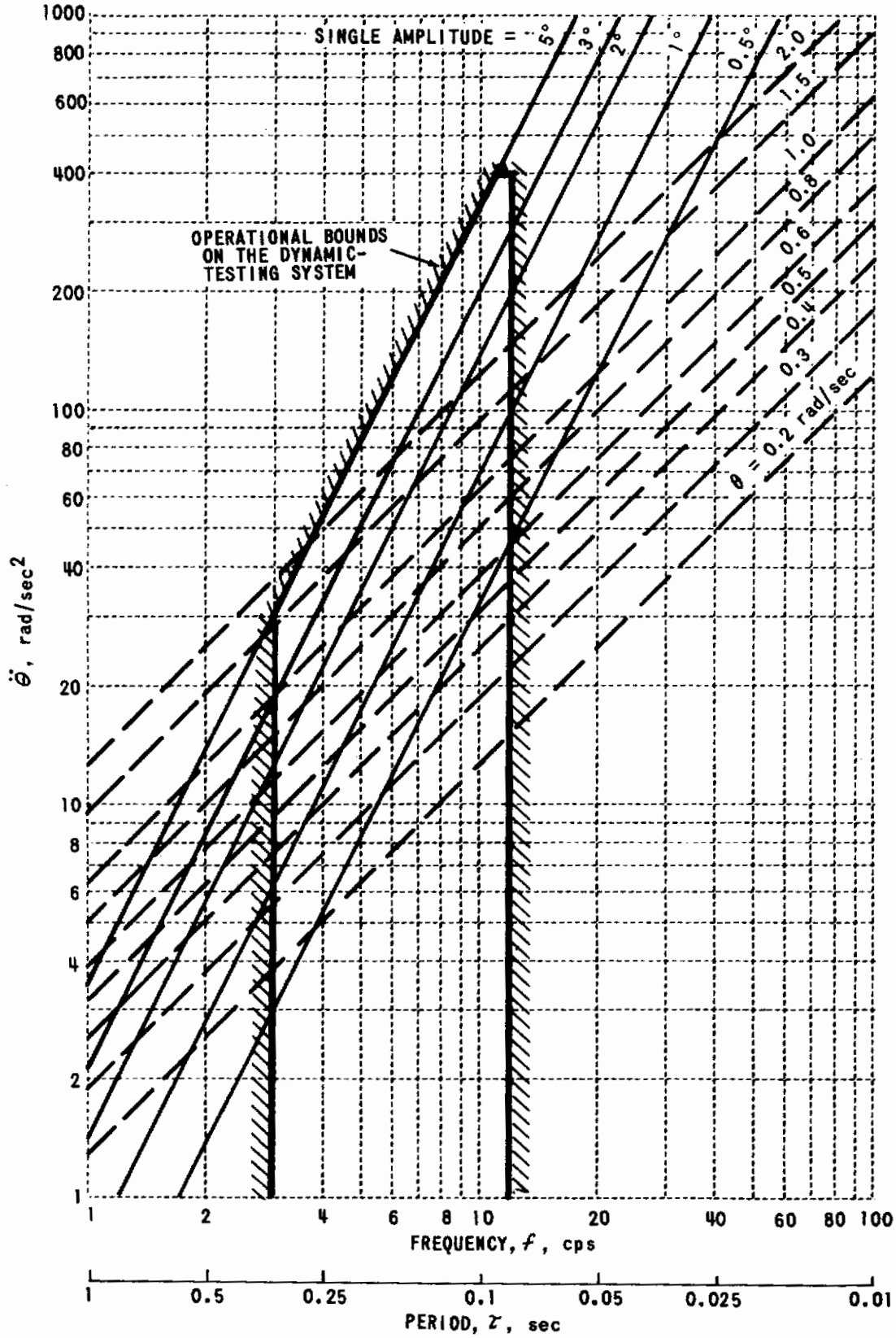

Figure 20 ANGULAR ACCELERATION, RATE, AND AMPLITUDE vs. FREQUENCY

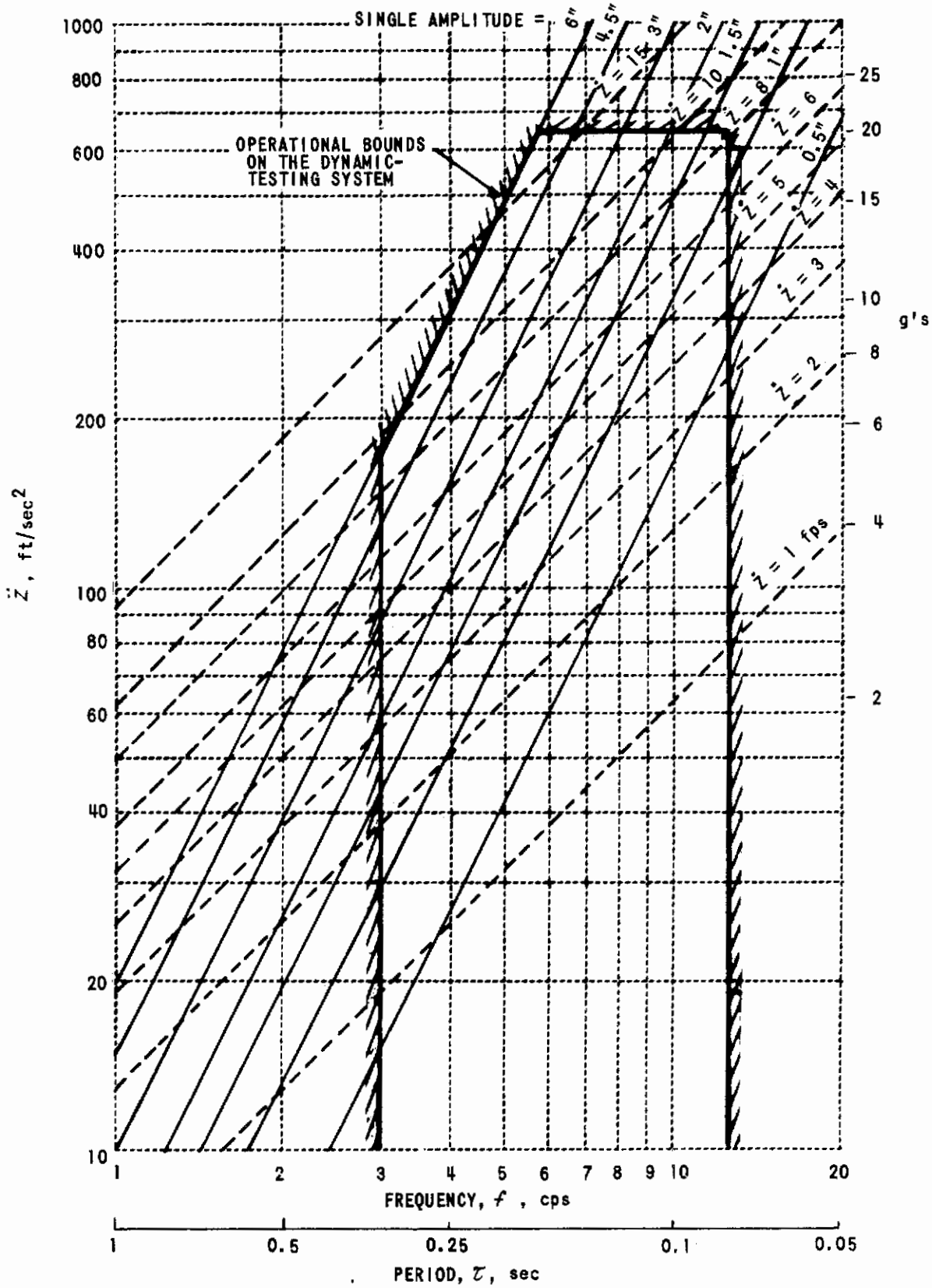

Figure 21 TRANSLATIONAL ACCELERATION, RATE, AND AMPLITUDE vs. FREQUENCY

SECTION 10

DATA REDUCTION AND ANALYSES

The data which were automatically printed out during these tests were analyzed in accordance with the equations developed in the following discussion:

$\underline{F_B}$ is the reactive force of the model on the normal-force strain beams defined as positive up,

$\underline{M_B}$ is the reactive moment of the model on the aft strain beam defined as positive for model nose up,

$\underline{\ddot{z}}$ is the linear (vertical) acceleration of the c. g. of the model defined as positive down, and

$\underline{\ddot{\theta}}$ is the angular acceleration of the model about its c. g. defined as positive for model nose up.

In the most general case, the loads carried by the forward and aft strain beams are, respectively,

$$\left.\begin{aligned} \underline{F_B} &= m\underline{\ddot{z}} + \frac{1}{\ell_B}\underline{M_B} + F_\alpha \underline{\theta} + F_{\dot\theta}\underline{\dot\theta} + F_{\dot\alpha}\underline{\dot\theta} + F_\alpha \frac{\dot z}{U} + F_{\dot\alpha}\frac{\ddot z}{U} \\ \text{and} \\ \underline{M_B} &= -I\underline{\ddot\theta} + m x_{c.g.}\underline{\ddot z} + M_\alpha \underline{\theta} + M_{\dot\theta}\underline{\dot\theta} + M_{\dot\alpha}\underline{\dot\theta} + M_\alpha \frac{\dot z}{U} + M_{\dot\alpha}\frac{\ddot z}{U} \end{aligned}\right\} \quad (1)$$

where m is the mass of the model plus metric part of the balance (including the linear and angular accelerometers),

ℓ_B is the distance between the sensitive axes of the forward and aft strain beams,

I is the pitching moment of inertia of the mass m about its c. g., and

$x_{c.g.}$ is the longitudinal displacement of the sensitive axis of the forward strain beams from the center of gravity of the mass m (positive aft).

and where the relation $\underline{\alpha} = \underline{\theta} + \frac{\dot z}{U}$ has been used in representing the aerodynamic loads in the remaining terms on the r. h. s. of equations (1). In accordance with the operations performed in the mixing unit, as shown in Figure 19, the aerodynamic normal-force and pitching moment are related to the balance measurements as follows:

$$\left.\begin{aligned} \underline{\textcircled{F}} &= \underline{F_B} - m^*\underline{\ddot z} - \frac{1}{\ell_B^*}\underline{M_B} \\ \text{and} \\ \underline{\textcircled{M}} &= \underline{M_B} + I^*\underline{\ddot\theta} + I^* k\underline{\ddot z} - b\underline{\ddot z} \end{aligned}\right\} \quad (2)$$

where m^* is used to cancel the normal force due to inertial reaction,

I^* is used to cancel the moment due to inertial reaction,

$\frac{1}{\ell_\theta^*}$ is used to cancel the component of moment sensed by the forward strain beams,

k is the crosstalk sensitivity of the angular accelerometer, and

b is used to correct for the effects of the crosstalk, k, and the c. g. location error, $x_{c.g.}$

For practical values of $x_{c.g.}$, the error introduced into the indicated linear acceleration is, in all cases of interest, negligible so that, in terms of the actual readout indications, the model motion is expressed as (see Figure 19)

$$\left.\begin{aligned} \underline{\ddot{z}} &= \underline{(L)} \\ \underline{\ddot{\theta}} &= \underline{(A)} - k\,\underline{(L)} \end{aligned}\right\} \quad (3)$$

and for sinusoidal motion

$$\left.\begin{aligned} \underline{\theta} &= -\left(\frac{\tau}{2\pi}\right)^2 \underline{\ddot{\theta}} \\ \underline{\dot{\theta}} &= \left(\frac{\tau}{2\pi_j}\right) \underline{\ddot{\theta}} \\ \underline{\dot{z}} &= \left(\frac{\tau}{2\pi_j}\right) \underline{\ddot{z}} \end{aligned}\right\} \quad (4)$$

Equations (1), (2), (3) and (4) are combined to give

$$\left.\begin{aligned} \underline{(F)} &= \left\{-F_\alpha \left(\frac{\tau}{2\pi}\right)^2 + F_{\dot\theta}\left(\frac{\tau}{2\pi_j}\right) + F_{\dot\alpha}\left(\frac{\tau}{2\pi_j}\right)\right\} \underline{(A)} \\ &\quad + \left\{U(m-m^*) + F_\alpha \left(\frac{\tau}{2\pi}\right)^2 kU - F_{\dot\theta}\left(\frac{\tau}{2\pi_j}\right) kU - F_{\dot\alpha}\left(\frac{\tau}{2\pi_j}\right) kU + F_\alpha \left(\frac{\tau}{2\pi_j}\right) + F_{\dot\alpha}\right\} \frac{\underline{(L)}}{U} \\ &\quad + \left(\frac{1}{\ell_\theta} - \frac{1}{\ell_\theta^*}\right) \underline{M_\theta} \\ \underline{(M)} &= \left\{I^* - I - M_\alpha \left(\frac{\tau}{2\pi}\right)^2 + M_{\dot\theta}\left(\frac{\tau}{2\pi_j}\right) + M_{\dot\alpha}\left(\frac{\tau}{2\pi_j}\right)\right\} \underline{(A)} \\ &\quad + \left\{\left(Ik + mx_{c.g.} - b\right)U + M_\alpha \left(\frac{\tau}{2\pi}\right)^2 kU - M_{\dot\theta}\left(\frac{\tau}{2\pi_j}\right) kU - M_{\dot\alpha}\left(\frac{\tau}{2\pi_j}\right) kU + M_\alpha \left(\frac{\tau}{2\pi_j}\right) + M_{\dot\alpha}\right\} \frac{\underline{(L)}}{U} \end{aligned}\right\} \quad (5)$$

For wind-off tests, equations (5) reduce to

$$\left.\begin{aligned} \underline{(F)} &= (m-m^*)\underline{(L)} + \left(\frac{1}{\ell_\theta} - \frac{1}{\ell_\theta^*}\right)\left[-I\,\underline{(A)} + (mx_{c.g.} + Ik)\underline{(L)}\right] \\ \underline{(M)} &= (I^* - I)\underline{(A)} + (mx_{c.g.} + Ik - b)\underline{(L)} + \underline{M_{TD}} \end{aligned}\right\} \quad (6)$$

where M_{TD} is the pitching moment due to the aerodynamic load on the horizontal tail during motion with no wind. This load is the "flat-plate drag" of the tail which exists when the tail is given a velocity normal to its surface

through still air. When plunging at 15 g's and 7 cps, for example, the translational velocity is about 11 ft/sec. For the F-80 in a 1/2-atmosphere environment, this velocity produced about 0.5 ft. lb. of moment 180° out of phase with $\ddot{z}$. The corresponding normal forces due to drag loads during wind-off plunging motion were negligible.

During the wind-off plunge tests, the gain m^* in Figure 19 was adjusted to minimize the normal-force readout and then the gain $1/\ell_B^*$ was adjusted to reduce this readout to zero. These compensate for the inertial reaction force and for the component of moment sensed by the forward strain beams. Hence, for wind-off conditions, the first of equations (6) is $\underline{(F)} = 0$. Further, in wind-off pure rotation tests, the gain I^* was adjusted until the moment readout was nearly zero (in general, less than 0.1 ft. lb.). Hence, it appears reasonable to assume that $I^* = I = 0.375$ ft. lbs. sec.^{2}.

Presumably, b had been adjusted to make the quantity $(mx_{c.g.} + I\dot{k} - b)$ equal to zero. During the wind-off tests, the gain b was adjusted by operating the model in pure plunge and varying b until the remaining moment vector led the linear acceleration by 90°, which would be the case if this residual moment were due entirely to tail drag. This was then checked by operating the model in pure plunging motion at 15 g's. The moment was measured at 1/8, 1/4, 1/2, and 1 atmosphere. The fact that this moment led the output of the linear accelerometer by 90° and that the values fell very nearly along a straight line through zero (to within about 1/10 of a ft. lb.) at zero density was an indication that the wind-off residual moment was, in fact, mostly due to the horizontal tail drag. Its value was determined to be about 0.5 ft. lb. at 15 g's and 7 cps in a 1/2-atmosphere environment. In computing the wind-off tares, this was the magnitude of the residual moment leading the linear acceleration by 90°, which was retained for a plunging acceleration of 483 ft/sec.^{2} at 7 cps and 1/2 atmosphere. The moment due to tail drag was adjusted for other conditions of frequency and linear acceleration amplitude (since it is proportional to the square of the velocity at the tail) by the following: $0.5(\underline{(L)}/483)^2(7/f)^2$, where f is the frequency in cycles per second. It was considered in rotation and in pitch in the following manner. The effective acceleration at the horizontal tail in ft/sec.^{2} was approximated by $(\underline{(L)} + \ell_t \times \underline{(A)}) = \underline{(L)} + 1.5\underline{(A)}$ where ℓ_t is the tail length equal to 1.5 ft. The wind-off moment due the tail drag was oriented at 90° ahead of this vector with the magnitude of $((|\underline{(L)} + 1.5\underline{(A)}|)/f)^2 \times 10^{-4}$. The vector required to correct the wind-off measured moment to the above vector was the correction made to each wind-on moment vector with the corresponding $|(L)|$ and $|(A)|$.

After adjusting the gains of combined signals, as indicated during the wind-off test program, the appropriate forms of equations (5) for reducing the wind-on test data are then (as shown on the next page):

Pure Rotation

$$\left.\begin{aligned} \underline{\textcircled{F}} &= \left\{ F_\alpha \left(\frac{\tau}{2\pi j}\right) + \left(F_{\dot\alpha} + F_{\dot\theta}\right)\right\} \frac{\tau \underline{\textcircled{A}}}{2\pi j} \\ \underline{\textcircled{M}} &= \left\{ M_\alpha \left(\frac{\tau}{2\pi j}\right) + \left(M_{\dot\alpha} + M_{\dot\theta}\right)\right\} \frac{\tau \underline{\textcircled{A}}}{2\pi j} \end{aligned}\right\} \quad (7)$$

Pure Plunge

$$\underline{\textcircled{F}} = \left\{ F_{\dot\alpha} + F_\alpha \left(\frac{\tau}{2\pi}\right)^2 kU + \left[F_\alpha - \left(F_{\dot\alpha} + F_{\dot\theta}\right) kU\right]\left(\frac{\tau}{2\pi j}\right)\right\} \frac{\underline{\textcircled{L}}}{U}$$

$$\underline{\textcircled{M}} = \left\{ M_{\dot\alpha} + M_\alpha \left(\frac{\tau}{2\pi}\right)^2 kU + \left[M_\alpha - \left(M_{\dot\alpha} + M_{\dot\theta}\right) kU\right]\left(\frac{\tau}{2\pi j}\right)\right\} \frac{\underline{\textcircled{L}}}{U}$$

The crosstalk sensitivity of the angular accelerometer, k, was sufficiently small so that negligible error was introduced when $F_\alpha \left(\frac{\tau}{2\pi}\right)^2 kU$ was neglected with respect to $F_{\dot\alpha}$, $\left(F_{\dot\alpha} + F_{\dot\theta}\right) kU$ was neglected with respect to F_α, $M_\alpha \left(\frac{\tau}{2\pi}\right)^2 kU$ was neglected with respect to $M_{\dot\alpha}$, and $\left(M_{\dot\alpha} + M_{\dot\theta}\right) kU$ was neglected with respect to M_α. Then

$$\left.\begin{aligned} \underline{\textcircled{F}} &\cong \left\{ F_{\dot\alpha} + F_\alpha \left(\frac{\tau}{2\pi j}\right)\right\} \frac{\underline{\textcircled{L}}}{U} \\ \underline{\textcircled{M}} &\cong \left\{ M_{\dot\alpha} + M_\alpha \left(\frac{\tau}{2\pi j}\right)\right\} \frac{\underline{\textcircled{L}}}{U} \end{aligned}\right\} \quad (8)$$

Finally, for

Pure Pitch

$$\underline{\textcircled{F}} = F_{\dot\theta} \left(\frac{\tau}{2\pi j}\right) \underline{\textcircled{A}} + \left\{ F_\alpha \left(\frac{\tau}{2\pi j}\right) + F_{\dot\alpha}\right\} \left(\frac{\tau \underline{\textcircled{A}}}{2\pi j} + \frac{\underline{\textcircled{L}}}{U}\right) + \left\{ F_\alpha \left(\frac{\tau}{2\pi}\right)^2 - \left(F_{\dot\alpha} + F_{\dot\theta}\right)\left(\frac{\tau}{2\pi j}\right)\right\} (kU) \frac{\underline{\textcircled{L}}}{U}$$

$$\underline{\textcircled{M}} = M_{\dot\theta} \left(\frac{\tau}{2\pi j}\right) \underline{\textcircled{A}} + \left\{ M_\alpha \left(\frac{\tau}{2\pi j}\right) + M_{\dot\alpha}\right\} \left(\frac{\tau \underline{\textcircled{A}}}{2\pi j} + \frac{\underline{\textcircled{L}}}{U}\right) + \left\{ M_\alpha \left(\frac{\tau}{2\pi}\right)^2 - \left(M_{\dot\alpha} + M_{\dot\theta}\right)\left(\frac{\tau}{2\pi j}\right)\right\} (kU) \frac{\underline{\textcircled{L}}}{U}$$

In terms of the readouts, "pure" pitch is set up by making $\frac{\tau}{2\pi j}\underline{\textcircled{A}} + (\underline{\textcircled{L}}/U)$ equal to zero. If this is done accurately, then the second term in each equation is zero and $\dot{\theta} \cong -\ddot{z}/U$, the difference being only the cross-talk. The consequent errors in $\underline{\textcircled{F}}$ and $\underline{\textcircled{M}}$ are given by the third terms. The value of k was sufficiently small (about 6×10^{-4} rad/sec.^{2}/ft/sec.^{2}, as shown in Appendix II) to make these negligible, so that

$$\left.\begin{aligned} \underline{\textcircled{F}} &\cong F_{\dot{\theta}} \left(\frac{\tau \underline{\textcircled{A}}}{2\pi j}\right) \\ \underline{\textcircled{M}} &\cong M_{\dot{\theta}} \left(\frac{\tau \underline{\textcircled{A}}}{2\pi j}\right) \end{aligned}\right\} \qquad (9)$$

The resolution of the force and moment vectors, given above in equations (7), (8) and (9), into their components in phase and in quadrature with the relevant motion in each of the three cases permits the evaluation of the lift and moment derivatives. (See Appendix VI for a detailed discussion of the data reduction procedures.)

Figure 22 presents an example of a polar plot for pure rotational motion; in this case, at 7 cps and a Mach number of 0.75. The purity of the rotational motion is indicated by the fact that the rate of change of angle of attack due to translational acceleration was only about one one-thousandth of that due to rotational velocity. The vector representing the resultant aerodynamic pitching moment is shown in its measured phase relation to the rate of change of angle of attack. The component of this moment vector in phase with the rate of change of angle of attack is a dynamic measure of the total rotary derivative, $M_{\dot{\alpha}} + M_{\dot{\theta}}$. The component of the moment vector in quadrature with the rate of change of angle of attack is a dynamic measure of the moment-curve slope M_{α}.

The results of a typical case of pure plunge, once again at 7 cps and Mach 0.75 are shown in Figure 23. The purity of the translatory motion is again demonstrated by the fact that the rate of change of angle of attack due to rotational motion was, in this case, less than two one-thousandths of that due to the translatory motion. This is the particular motion that dictates the requirement for extremely low crosstalk sensitivity of the angular accelerometer. The total aerodynamic moment is again plotted in its proper relation to the rate of change of angle of attack. The component of the indicated aerodynamic moment in quadrature with the rate of change of angle of attack is another independent dynamic measure of the moment-curve slope M_{α}. The other component in this case is proportional to the pitching moment due only to rate of change of angle of attack, that is, $M_{\dot{\alpha}}$.

Finally, the results of a typical case of pure pitch, also at 7 cps and Mach 0.75, are presented in Figure 24. One motion vector indicates the rate of change of angle of attack due to the rotational velocity; the other indicates the rate of change of angle of attack due to the translational acceleration. If this motion has been set up accurately, then these two vectors should be of equal amplitude and opposite phase. In this example,

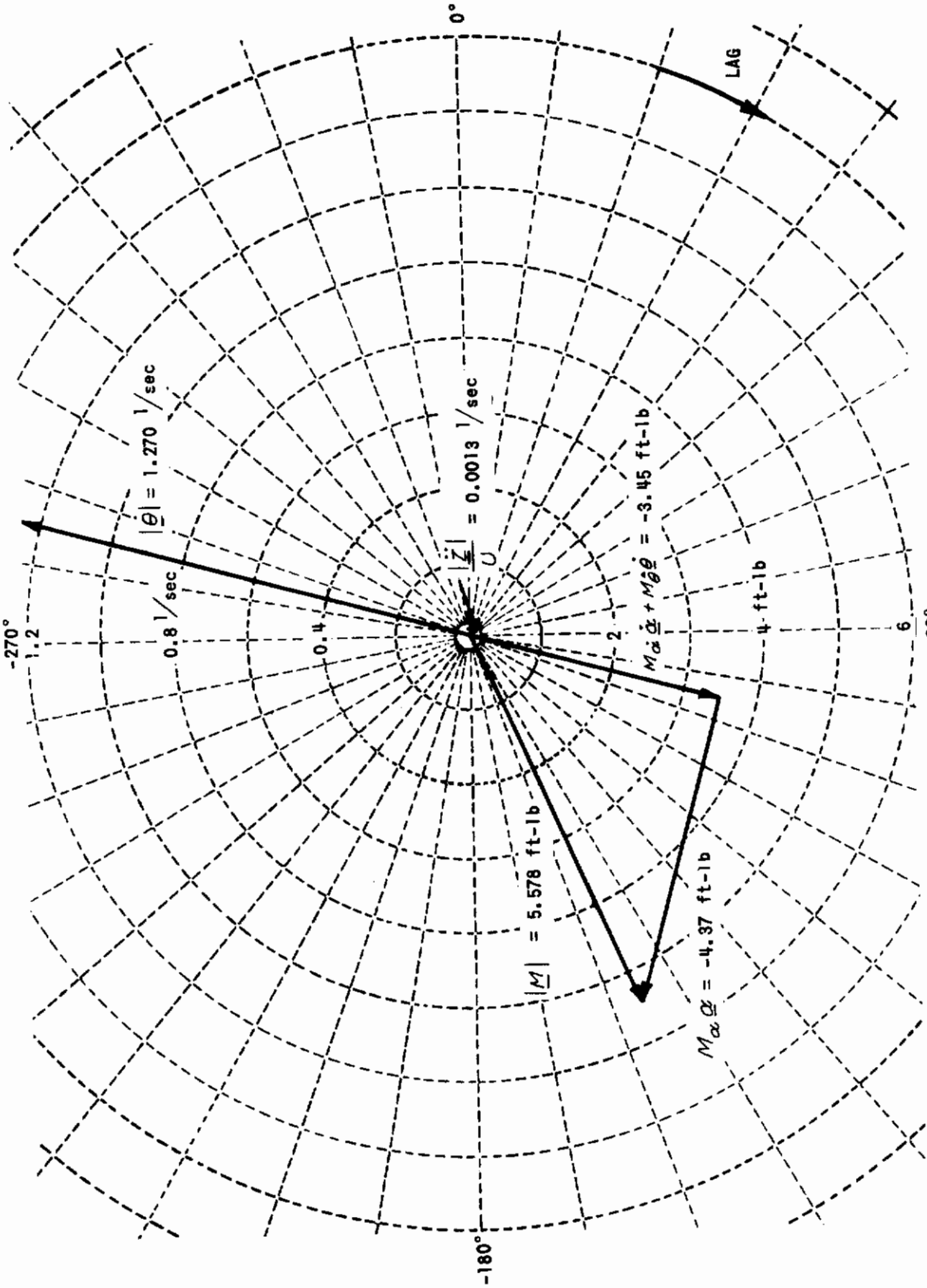

Figure 22 POLAR PLOT OF PITCHING MOMENT DUE TO ROTATION AT 7 cps, M = 0.75

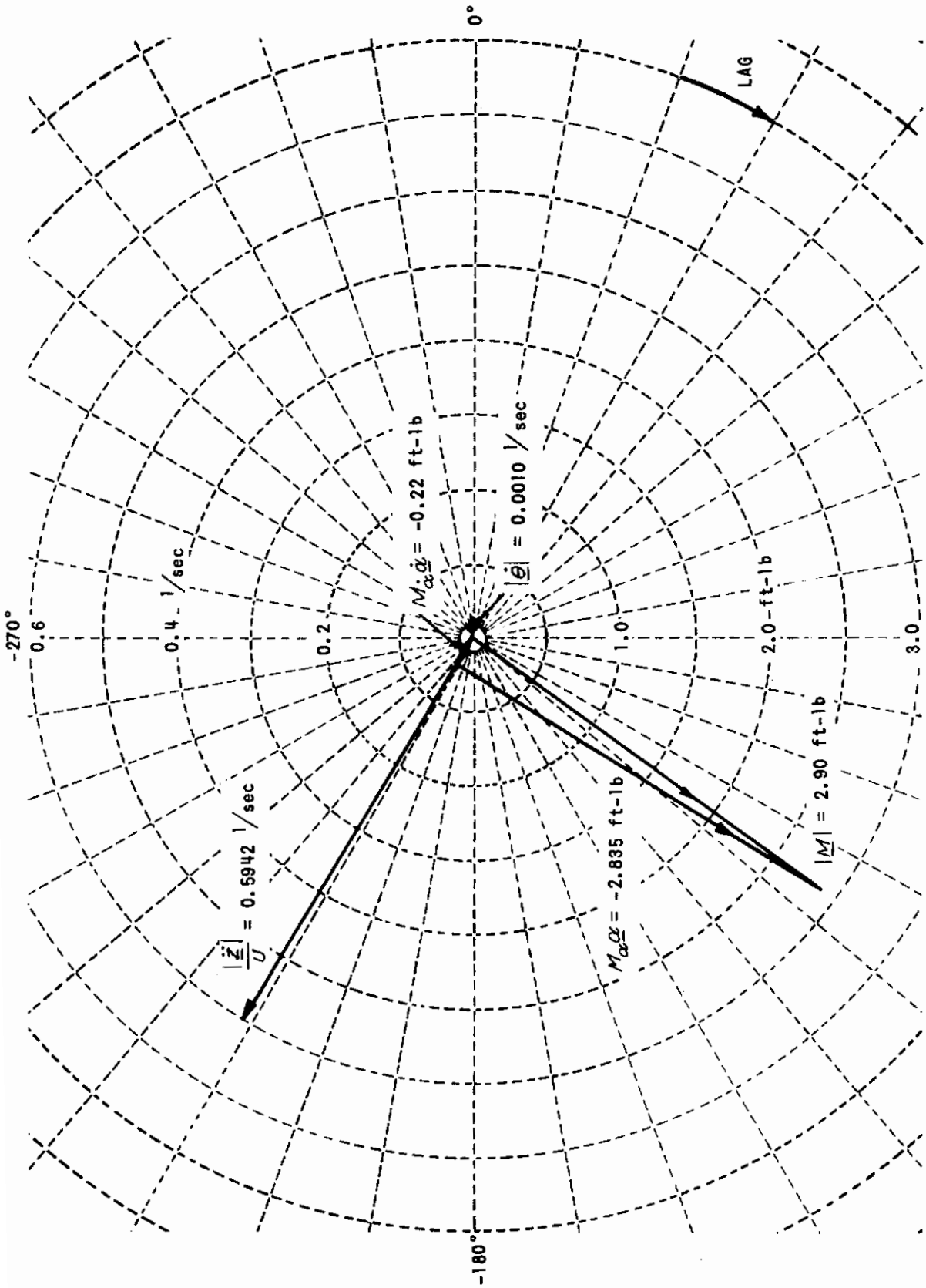

Figure 23 POLAR PLOT OF PITCHING MOMENT DUE TO PLUNGE AT 7 cps, M = 0.75

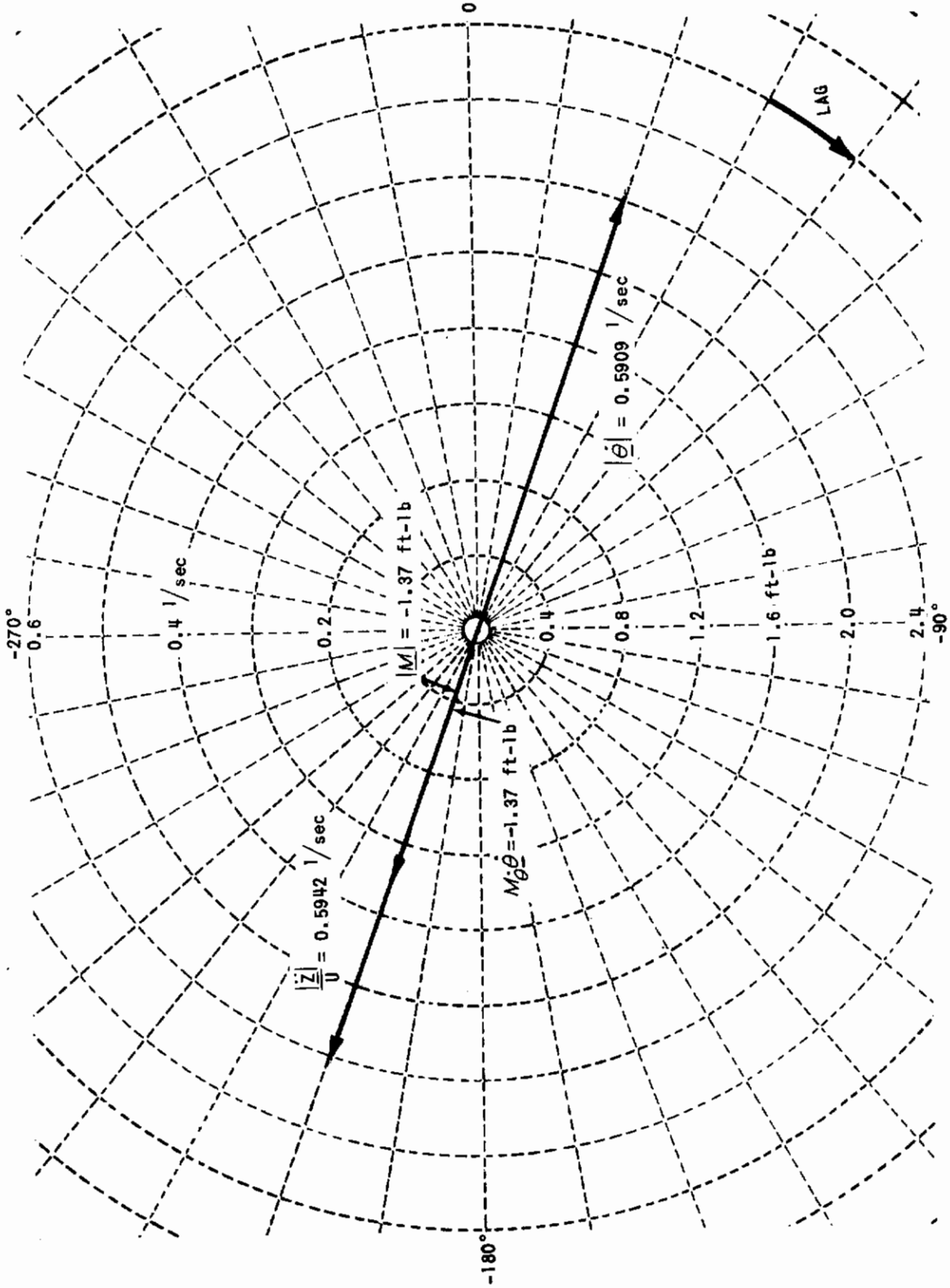

Figure 24 POLAR PLOT OF PITCHING MOMENT DUE TO PITCH AT 7 cps, M = 0.75

there is about a half of one percent difference in amplitudes of the vectors and about a half-degree error in phase. This is typical of the accuracy with which the motions can be set up. The measured total pitching moment is shown in its relation to the indicated rotational velocity vector. The component of this pitching moment in phase with the rotational velocity is a measure of the moment due to pitch rate alone, that is, $M_{\dot{\theta}}$. The other component should theoretically be zero. (In this particular example, it was, in fact, zero to two decimal places.)

A similar set of polar plots concerns the normal-force measurements, examples of which are shown in Figures 25 through 27.

These tests provided, for the first time, a complete systematic set of dynamic measurements of aerodynamic lift and pitching moment.

The results for the lift derivatives and moment derivatives for the F-80 model obtained during these dynamic wind-tunnel tests are presented in Tables I and II.

The measurements of C_{L_α} at 5 and 7 cps from rotation and from plunge are in excellent agreement. They are, furthermore, in good agreement with the general band of data covered by calculated, flight-test and static wind-tunnel results as shown in Figure 28. The difference between the static lift curve slope and the unsteady lift curve slope is negligible for the reduced frequencies tested and for the near zero lift configuration.

In the case of the moments, the dynamic measurements of C_{m_α} at 5 cps, 7 cps, and 10 cps from rotation are in excellent agreement. This agreement demonstrates the repeatibility of the test data, since these tests were completely independent; in fact, they were performed on different days. The C_{m_α} values from these dynamic measurements are in good agreement with the band covered by flight-test data and calculations as shown in Figure 29.

The dynamic measurements of C_{m_α} from plunge tests at 5 and 7 cps are also in good agreement with each other, but, in the region of Mach 0.7 to 0.8, there are significant differences between the results taken from rotation tests and those from plunge tests. The amplitudes of the oscillatory angle of attack during the rotation tests were about double those achieved in plunge at the highest speeds, and the differences can be attributed to the nonlinearity of the moment curve. This is indicated in Figure 30 where the dynamic measures of C_{m_α} from rotation and from plunge at 7 cps are spotted with the appropriate angle-of-attack amplitude denoted in each case for comparison with static measures of C_{m_α} made at various angles of attack. The variation of C_{m_α} with amplitude of the oscillatory angle of attack is consistent with that observed in the static test results which were taken from data presented in Reference 18. The spread in the dynamic values of C_{m_α} is within that observed in static measurements over a comparable angle-of-attack variation. The nonlinearity of C_{m_α} is particularly strong at Mach numbers between 0.7 and 0.8.

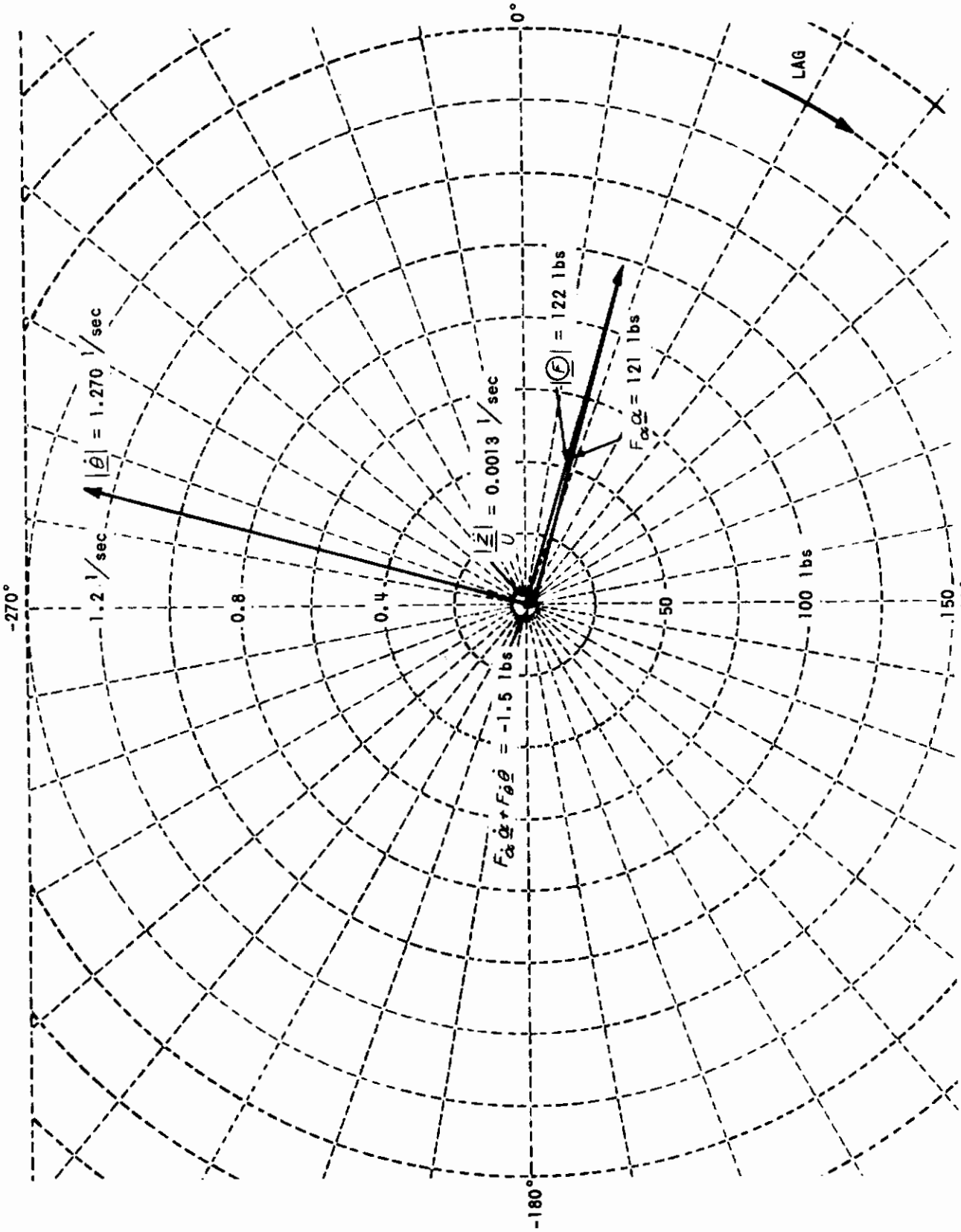

Figure 25 POLAR PLOT OF LIFT DUE TO ROTATION AT 7 cps, M = 0.75

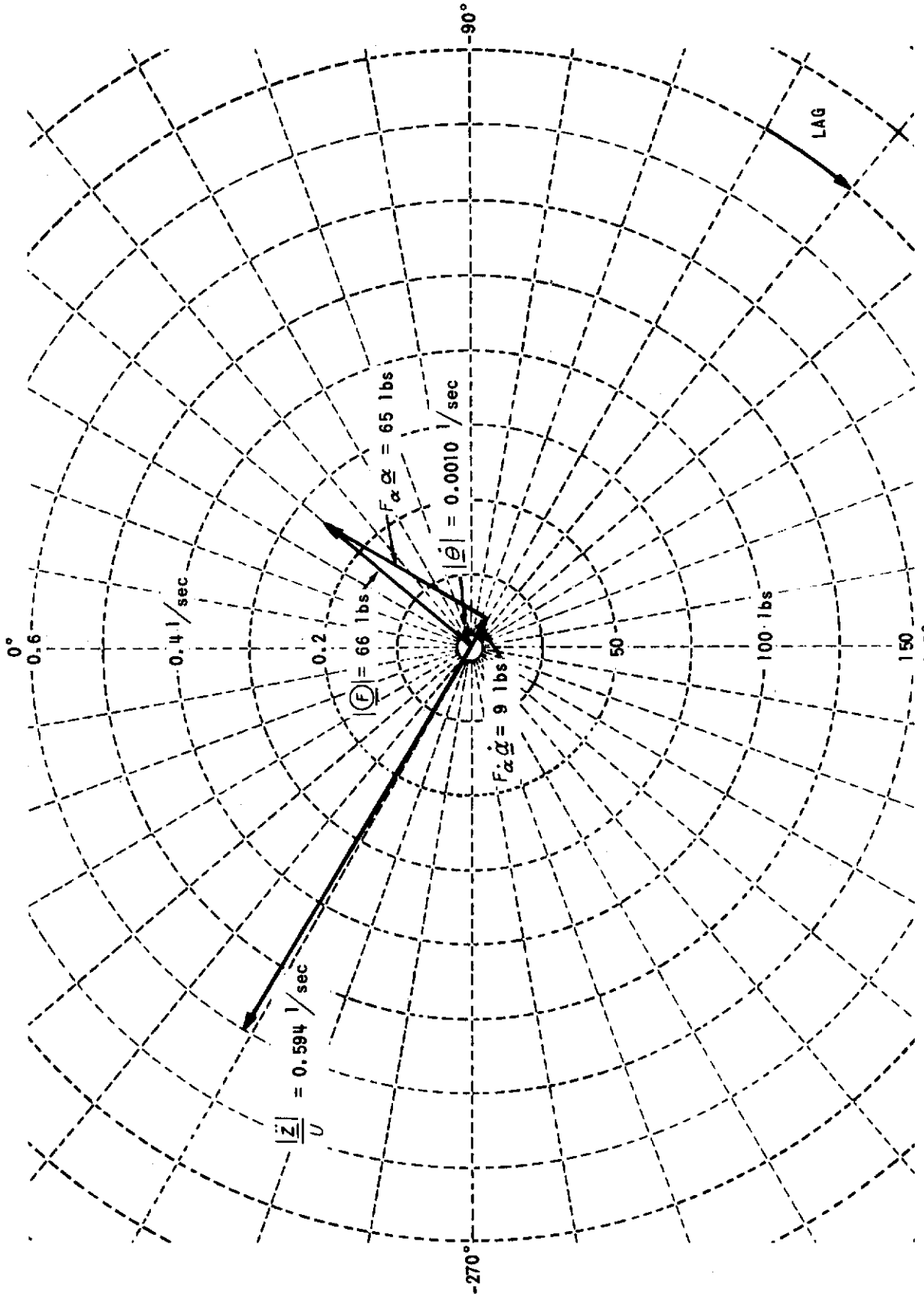

Figure 26 POLAR PLOT OF LIFT DUE TO PLUNGE AT 7 cps, M = 0.75

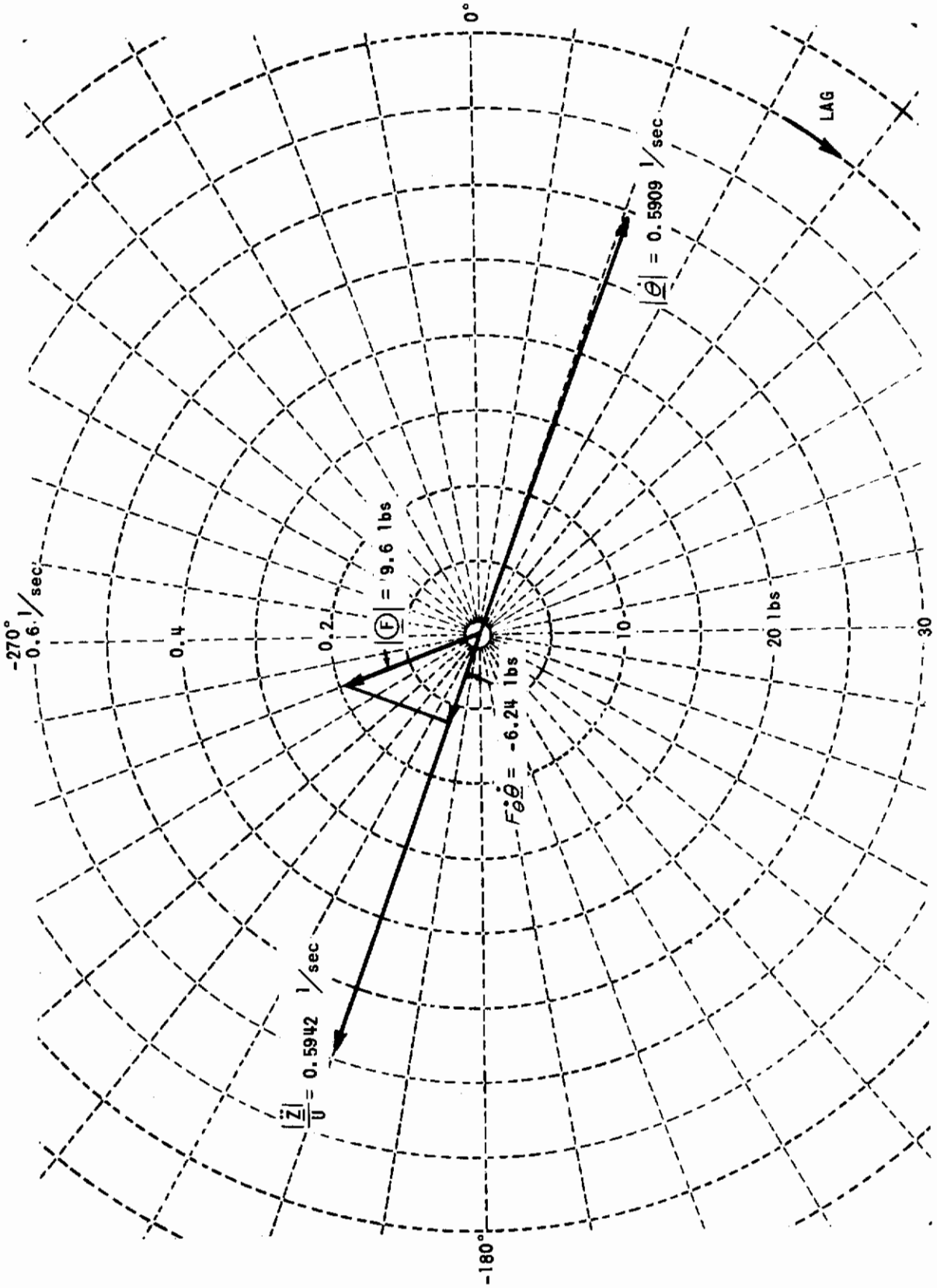

Figure 27 POLAR PLOT OF LIFT DUE TO PITCH AT 7 cps, M = 0.75

Table I
LIFT DERIVATIVES FOR F-80 MODEL FROM DYNAMIC TESTS

	ROTATION					
	5 cps		7 cps		10 cps	
M	$C_{L_{\dot\alpha}} + C_{L_{\dot\theta}}$	C_{L_α}	$C_{L_{\dot\alpha}} + C_{L_{\dot\theta}}$	C_{L_α}	$C_{L_{\dot\alpha}} + C_{L_{\dot\theta}}$	C_{L_α}
.5	34.2	5.31	6.1	5.17	17.8	4.77
.7	34.8	5.84	-3.9	5.67	4.1	5.2
.75	35.4	5.85	-4.0	5.84	7.3	5.1
.8	34.9	4.77	2.6	4.70	-	-

	PLUNGE					
	5 cps		7 cps		10 cps	
M	$C_{L_{\dot\alpha}}$	C_{L_α}	$C_{L_{\dot\alpha}}$	C_{L_α}	$C_{L_{\dot\alpha}}$	C_{L_α}
.5	—	5.30	39.1	5.08	—	—
.7	—	5.66	44.3	6.10	—	—
.75	—	5.59	52.1	6.49	—	—
.8	—	4.64	47.6	4.97	—	—

	PITCH					
	5 cps		7 cps		10 cps	
M	$C_{L_{\dot\theta}}$	—	$C_{L_{\dot\theta}}$	—	$C_{L_{\dot\theta}}$	—
.5	—	—	14.471	|0.2|	—	—
.7	—	—	-34.95	|0.5|	—	—
.75	—	—	-35.2	|0.5|	—	—
.8	—	—	-20.2	|0.4|	—	—

Table II
MOMENT DERIVATIVES FOR F-80 MODEL FROM DYNAMIC TESTS

	ROTATION					
	5 cps		7 cps		10 cps	
M	$C_{m_{\dot{\alpha}}} + C_{m_{\dot{\theta}}}$	C_{m_α}	$C_{m_{\dot{\alpha}}} + C_{m_{\dot{\theta}}}$	C_{m_α}	$C_{m_{\dot{\alpha}}} + C_{m_{\dot{\theta}}}$	C_{m_α}
.5	-13.2	-0.38	-13.0	-0.36	-12.8	-0.39
.7	-12.8	-0.28	-13.1	-0.30	-13.0	-0.35
.75	-13.7	-0.31	-13.6	-0.31	-13.7	-0.37
.8	-14.7	-0.23	-14.3	-0.24	—	—

	PLUNGE					
	5 cps		7 cps		10 cps	
M	$C_{m_{\dot{\alpha}}}$	C_{m_α}	$C_{m_{\dot{\alpha}}}$	C_{m_α}	$C_{m_{\dot{\alpha}}}$	C_{m_α}
.5	-5.0	-0.38	-3.4	-0.38	—	—
.7	+0.2	-0.45	-0.2	-0.42	—	—
.75	-1.2	-0.42	-1.9	-0.42	—	—
.8	-3.9	-0.34	-2.3	-0.31	—	—

	PITCH					
	5 cps		7 cps		10 cps	
M	$C_{m_{\dot{\theta}}}$	—	$C_{m_{\dot{\theta}}}$	—	$C_{m_{\dot{\theta}}}$	—
.5	-10.3	|0.01|	-10.9	|0.00|	—	—
.7	-13.4	|0.00|	-11.4	|0.00|	—	—
.75	-13.4	|0.01|	-11.5	|0.00|	—	—
.8	-14.2	|0.01|	-12.7	|0.01|	—	—

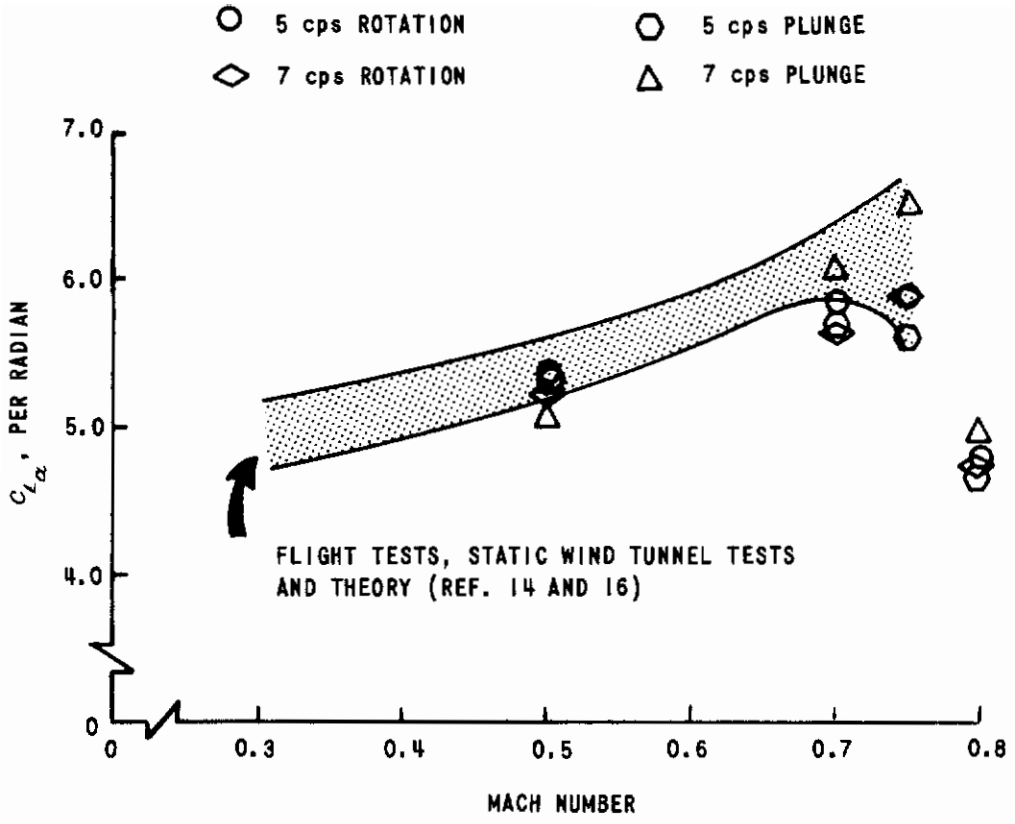

Figure 28 LIFT CURVE SLOPE vs. MACH NUMBER

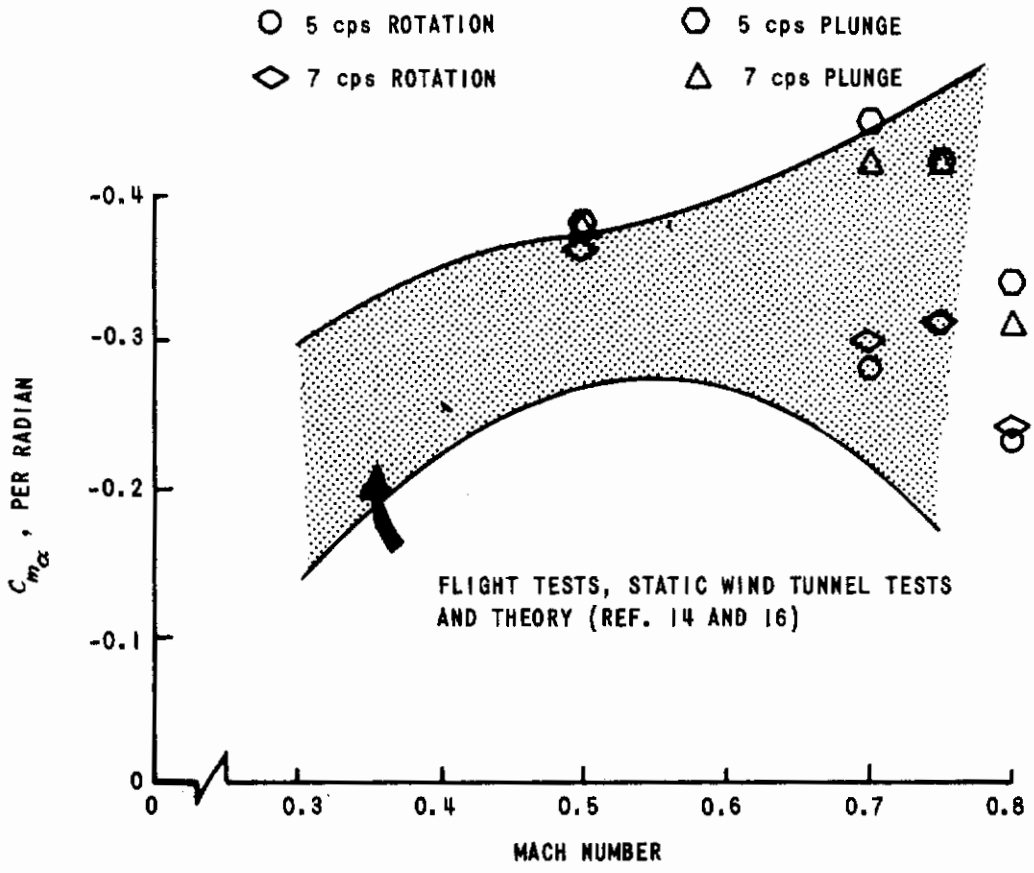

Figure 29 MOMENT CURVE SLOPE vs. MACH NUMBER

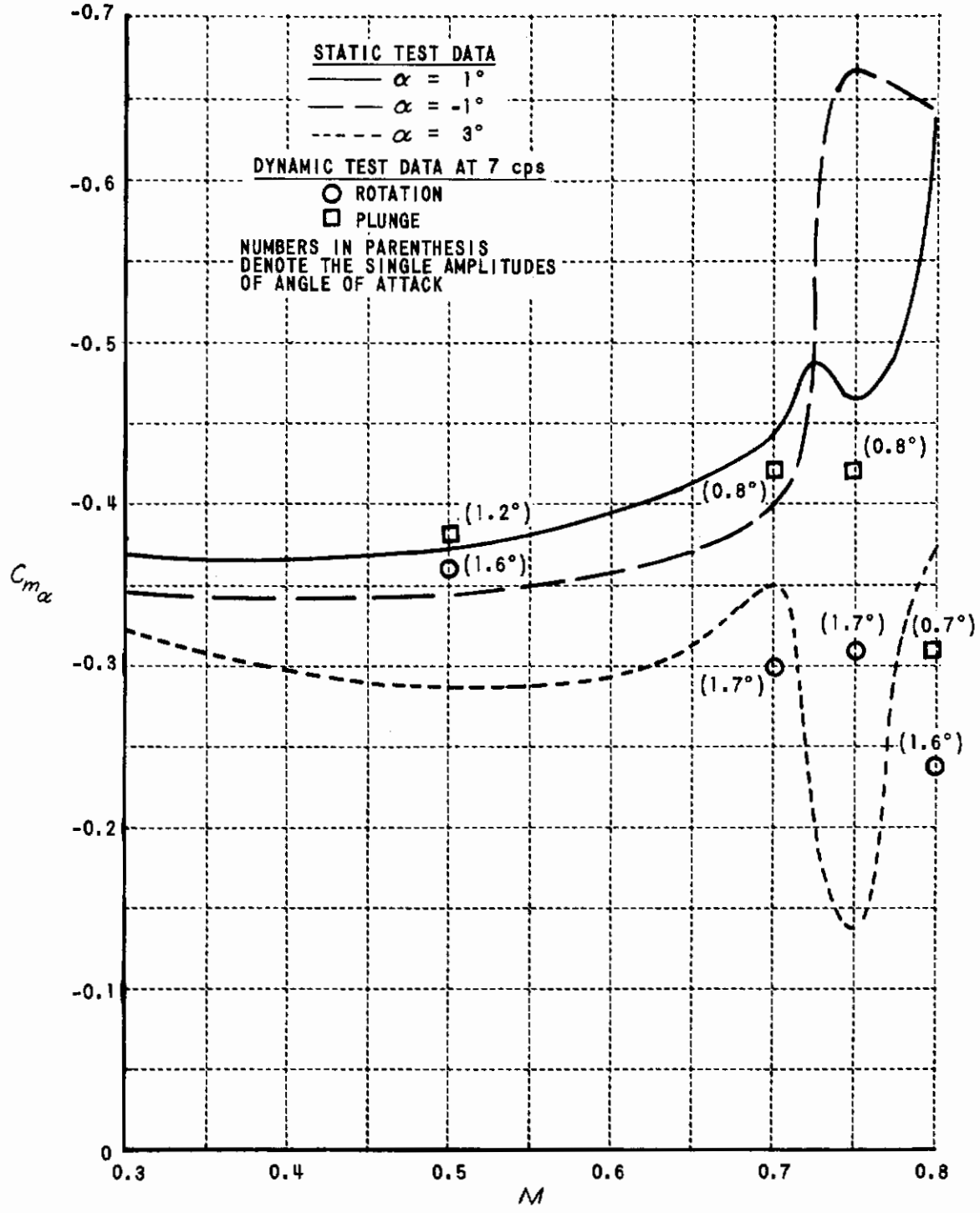

Figure 30 COMPARISON OF STATIC AND DYNAMIC MEASUREMENTS OF MOMENT CURVE SLOPE vs. MACH NUMBER FOR VARIOUS AMPLITUDES OF ANGLE OF ATTACK

Finally, the total rotary damping derivative versus Mach number showing the band of reference data and the measurements from rotation tests are presented in Figure 31. Again, note the agreement of measurements at 5 and 7 cps. These data points from rotation tests also compare favorably with the total derivative as determined from the sum of the components measured in the plunge and pitch tests. All the points lie well within the band of reference data. Some of the differences in the data are probably attributable to nonlinear effects similar to those which influenced the measurement of C_{m_α} . During plunging and pitching tests, the rate of change of angle of attack and the pitch rate, respectively, are governed by the magnitude of the plunging acceleration that can be obtained. During pure rotation tests, it is relatively easy to attain significantly higher pitch rates, and this was the case during the F-80 test program.

The measured values of the rotary lift derivatives, $C_{L_{\dot\alpha}} + C_{L_{\dot\theta}}$ presented in Table I, are inaccurate because the corresponding vector components of the lift forces generally constituted less than 10% of the total aerodynamic forces for the F-80. This is particularly evident in the typical polar plot of the lift due to rotation in Figure 25 and its comparison with the corresponding polar plot of pitching moment in Figure 22. The scatter in these derivatives can be accounted for by errors in the phase angles between the normal force vectors and the motion vectors of less than 2°. These results could have been significantly improved had the normal force measurements been made with the same care as were the moments. (This was substantiated in the tests performed on an F-104 model reported in Reference 19.)

Table II shows that the values for $C_{m_{\dot\alpha}}$ from plunge at 5 and 7 cps compare well at each Mach number, as do the values for $C_{m_{\dot\theta}}$ from pitch at 5 and 7 cps. The second column of data under the pitch tests at each frequency denotes the measured value of the component of moment (or load) due to angle of attack. This should be zero if the motion was set up accurately. These values, therefore, constitute a measure of the "purity" of the pitching motion.

Recall that the accuracy objective of this system was the ability to measure $C_{m_{\dot\alpha}}$ and $C_{m_{\dot\theta}}$ each to within $\pm 10\%$ of their sum as measured in pure rotation. This, then, means that the sum of $C_{m_{\dot\alpha}}$ from plunge and $C_{m_{\dot\theta}}$ from pitch should be within $\pm 20\%$ of $(C_{m_{\dot\alpha}} + C_{m_{\dot\theta}})$ as measured in rotation. In all cases but one, this objective has been very adequately achieved. In the one exceptional case (5 cps at M = 0.8), the difference is 23%.

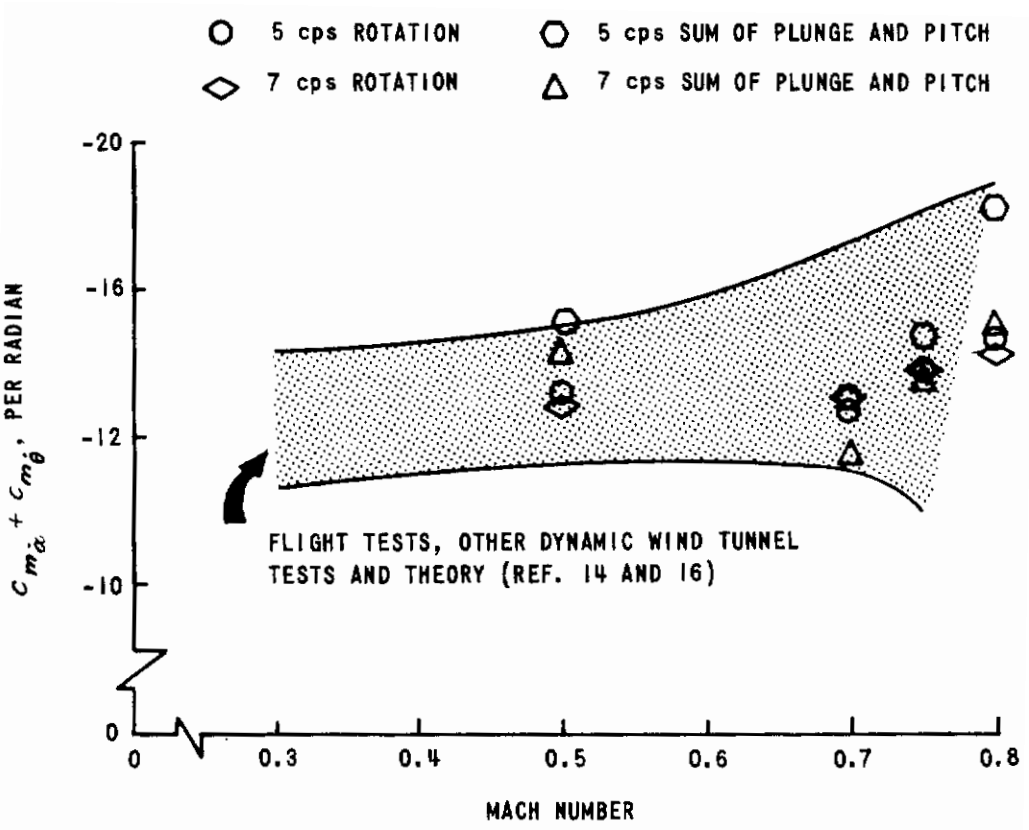

Figure 31 ROTARY DAMPING DERIVATIVE vs. MACH NUMBER

SECTION 11

FUTURE APPLICATIONS OF THE DYNAMIC TESTING SYSTEM

Since the F-80 model is limited to subsonic speeds because of buffeting, additional investigations were performed with a more advanced model through transonic speeds. The results of a similar series of tests on an F-104 model at speeds up to M = 1.2 are presented in Reference 19.

The additional capabilities built into the present equipment are noteworthy, although there are no definite plans for their use. All tests to date have been performed with the model at a mean angle of attack close to that for trim. The static angle of attack of the model can be adjusted, however, so that the model can be oscillated about various values of mean angle of attack. For tests conducted with large mean angles of attack, the concomitant large static balance moments should be compensated, however, by adjustments in the stabilizer angle. Also, lateral dynamic tests, similar to the longitudinal experiments, can be carried out by rotating the model 90° on the balance support.

The system can now be used in routine dynamic wind-tunnel tests comparable to current static wind-tunnel testing programs. These will provide a body of reference data to aid in estimating the dynamic stability characteristics and handling qualities of new designs. Apart from such design studies, dynamic wind-tunnel tests will be used for the purpose of checking the validity of theoretical calculations in those cases where appropriate theories are available. Most significantly, however, the dynamic testing system will be used for basic research studies to advance the understanding of unsteady transonic flow in general. In particular, the objective of this research will be to aid the development of a proven adequate analytical technique for predicting the unsteady aerodynamic loads at transonic speeds and at the low reduced frequencies typical of aircraft rigid-body dynamics.

The dynamic testing system is currently being prepared for use in a program, the objective of which is to determine the validity of available methods for predicting unsteady pressures in transonic flow by comparison with experimental results. Measurements will be made of the unsteady pressures at the surface of an inexorably oscillated rigid wing model, as well as of the integrated aerodynamic forces and moments on the model produced by this motion. These results, along with flow visualization, will then provide the bases for verification of available theoretical methods. The model to be tested is a 70°-delta single-wedge configuration. Twenty-six pressure transducers are to be installed in the model. Wind-tunnel tests will be performed at several combinations of Mach number and Reynolds number, while the model is oscillated at various discrete frequencies in rotation, plunge, and pitch. This program is a joint effort by CAL and North American Aviation, Inc. and is cosponsored by the Aerospace Dynamics Branch and the Control Criteria Branch of the Air Force Flight Dynamics Laboratory.

The available transonic unsteady theory, based on linearized equations of motion, is obtained from the assumption of high reduced frequency in addition to the assumption of small amplitude oscillation. Experimental verification of this theory is thus far inconclusive; but trends indicate that, for rigid-body dynamic stability, the current linear theory will have limited applicability. In attempting to formulate a theory for transonic unsteady aerodynamic predictions, experimental data will be used not only to evaluate available theories but to inspire new developments as well. A definitive program of research is required to provide experimental data accurate enough to be useful in further development of techniques for predicting transonic unsteady aerodynamic loads. The objectives of such a program are most effectively served by utilizing the CAL/Air Force Dynamic Wind-Tunnel Testing System. This facility, with its specialized signal processing and readout equipment, provides a unique capability for dynamic measurements in a wind tunnel which is ideally suited to the requirements of such a research program. It offers, for the first time, an opportunity for prescribed variations of motion content (that is, rotation and translation) and for a systematic investigation of effects of frequency, Mach number, Reynolds number, and configuration parameters on the fundamental constituents of longitudinal and lateral dynamic stability characteristics at transonic speeds.

SECTION 12

CONCLUDING REMARKS

The concept of the CAL/Air Force Dynamic Wind-Tunnel Testing System is neither new nor unique. Its versatility and the accuracy with which desired model motions can be provided are unusual, however. These result from the ability of the operator to monitor and adjust, continuously, the motion of the model itself. This capability is due, in large part, to the successful development in the course of this program of two particular components of the system — the angular accelerometer and the phase and amplitude analyzer. The requirements on these two units were not fully appreciated at the initiation of the design of the system. It developed, however, that there was not an angular accelerometer on the market of the required small size, ruggedness and insensitivity to linear accelerations. Further, prior to the development of the phase and amplitude analyzers, there was no practical, accurate means of continuously monitoring both the phase and the amplitude of a particular low-frequency component of a noisy analog signal.

There appears to be a sufficiently large sample of experimental evidence to verify that the objectives of overall accuracy for the dynamic testing system have been achieved. The measurements of the longitudinal aerodynamic derivatives of the F-80 model have served to demonstrate the capabilities of the system.

The ability to measure the separate components of the total rotary damping moment, while important in its own right, is equally significant for its indication of the accuracies which have been achieved. The very precise control on the oscillator, together with the accurate on-line readouts of the model accelerations, enables the operator to adjust the model motion within extremely tight tolerances. Very high measurement accuracies have been obtained by minimizing crosstalk sensitivities and tailoring the transducers to their particular measurements.

These tests indicated, however, that certain modifications in the equipment were needed to improve the operational efficiency. Mostly, these have entailed a rearrangement of the equipment in the dynamic testing control room to reduce the amount of eye scanning required of the operator and the test director when monitoring operating conditions. Controls have been consolidated and arranged in a fashion intended to facilitate the operation. Such controls as the fast and slow adjustments on the eccentric amplitudes have been physically separated to prevent inadvertent radical motion changes at critical speeds.

As indicated previously in this report, nonlinear aerodynamic effects apparently introduced some discrepancies in the comparisons between derivative measurements in pure rotation tests and comparable measurements in the pure plunging and pure pitching tests. This was evident in the static moment derivatives as measured in rotation and in plunge and, to a lesser extent, in the comparisons between the total rotary damping derivative measured in rotation and the sum of the components of this total derivative as measured in plunge and pitch. For future tests, it is recommended, therefore, that the amplitudes of the angular acceleration during pure rotation tests should be governed by those used during the pure pitching tests. The comparisons would be simpler if all three tests were performed at comparable amplitudes and, perhaps, at several different levels. The reduction in the amplitude of the rotation tests would not have a significant effect on the accuracy of those measurements.

It is recommended that the two-component linear accelerometer be replaced by a suitable single-component unit which is now available. The linear accelerometer caused some trouble due to a small signal apparently generated by the flexing of the seven-foot-long cable joining the seismic element in the model and its electronics package in the vertical strut.

A study should be made of the feasibility of increasing the highest operating frequency of the dynamic testing system. For the size of the F-80 model, the present operating range of 3-12 cps is consistent with the reduced frequency of the longitudinal, short-period mode of the full-scale F-80. Nevertheless, advantages accrue from the ability to test at higher frequencies. Most important is the fact that the rate-dependent aerodynamic terms become progressively easier to measure with increasing frequency. Further, for studies in the transonic speed range, it is desirable to be able to examine at least the lower bounds of Landahl's unsteady transonic theory which is linearized on the basis of high reduced frequencies.[20] To a limited extent, this can be accomplished with relatively little modification to the present system by making use of the nearly pure second-harmonic rotational motion which is generated during pure plunging.

The highest operating fundamental frequency is limited by the lowest resonance frequency of the dynamic testing system. With the 18-lb. F-80 model, this resonance frequency has been measured to be 17.3 cps. Very preliminary calculations indicate that this natural frequency could be increased by at least 5 cps by accomplishing some or all of the following:

(1) Reduce the flywheel inertias. The flywheel inertias were designed for good wave form at 3 cps which is, however, too low to be of practical interest.

(2) Add bearing supports to the flywheel shafts.

(3) Redesign the sting to maximize its stiffness. This would eliminate the present articulation between the forward and aft stings which enables incremental changes in the mean

angle of attack. (This capability might better be provided by changing the length of the forward connecting rod.)

(4) Replace the present 10 HP drive motor with a 25 HP motor and DC power supply.

There should be a study to derive testing and data analysis procedures for using bent stings on the dynamic testing system to investigate unsteady cross coupling aerodynamics.

Consideration should also be given to increasing the data handling capacity of the system. Expansion of the current four channels to six or even eight would probably be accommodated most economically by the addition of phase and amplitude analyzing channels. For a substantially larger data handling capacity, however, as, for example, in the case of unsteady pressure distribution measurements, a completely new approach to this problem would have to be devised.

Finally, and perhaps most importantly, it is recommended that a study be initiated to determine the feasibility of providing this system with a closed-loop feedback control by means of which any combination of translation and rotation of the model could be provided automatically. Under present circumstances, it takes a considerable amount of training and experience to learn safe and efficient operation of the controls. Conceptually, all that is lacking for a servo control system is the logic between the signals from the model motion sensors and the signals to the eccentric amplitude and phase adjusters.

APPENDIX I

THE MECHANICAL OSCILLATOR*

General Description

The design of the mechanical oscillator was influenced primarily by the following considerations:

(1) It should be capable of providing a fundamental oscillating frequency of from 3-12 cps. The motion is to have good harmonic waveform at even the low frequencies, and the speed regulation should have good long-time stability. The lowest natural frequency of the system should be sufficiently high with respect to the highest oscillator frequency to prevent significant excitation and concomitant distortion of the sinusoidal waveform of the motion.

(2) It should provide translational accelerations of the model of up to 20 g's at the fundamental frequency or displacements of 1-ft. double amplitude. It should provide a rotational motion of the model at the fundamental frequency with angular accelerations in excess of 200 radians/sec.^{2} or a rotational displacement of 10° double amplitude.

(3) The amplitudes of the translatory and rotational motions and the phase between them should be adjustable while the system is in operation in the wind tunnel.

(4) It should be capable of sustaining a peak vertical load of 1200 lbs. at the model's center of gravity.

(5) It should be designed for use in the CAL 8-Ft. Variable-Density Transonic Wind Tunnel, and the system should be isolated from the tunnel structure.

(6) The design should provide reasonable margins of safety of the maximum stress levels compared with the allowables based on fatigue life of the material.

---

* The authors wish to acknowledge the special contributions to this phase of the dynamic testing system development of Mr. George Duryea who is currently a Staff Design Engineer in CAL's Applied Hypersonic Research Department.

Some of the major effects of these considerations are discussed in the following sections with regard to the main subassemblies of the mechanical oscillator, namely,

(1) the cart and its suspension system,
(2) the oscillator drive and flywheels,
(3) the oscillator controls,
(4) the eccentric amplitude and phase indicators, and
(5) the sting support and linkage system.

The Cart and Its Suspension System

Self-propelled carts are used in the CAL Transonic Wind Tunnel which permit the complete test equipment to be set up and calibrated outside the wind tunnel prior to moving the entire system into the tunnel for wind-on tests. In the case of the dynamic testing system, the cart is a permanent base for the mechanical oscillator.

The cart consists of its subcart and the floor of the cart which becomes integral with the tunnel floor when the system is installed in the wind tunnel. For entry into and exit from the test section of the tunnel, the cart is in the low position indicated in the following sketch.

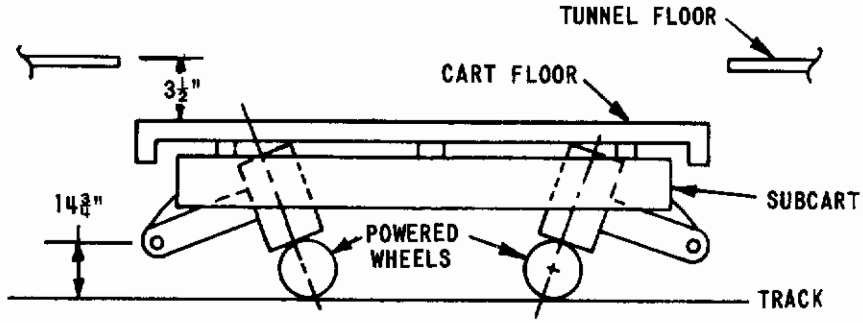

The subcart is supporting the cart floor in this configuration. Once the cart is in its operating position in the tunnel, the subcart can be used to raise the cart floor to the level of the tunnel floor, as indicated in the following sketch.

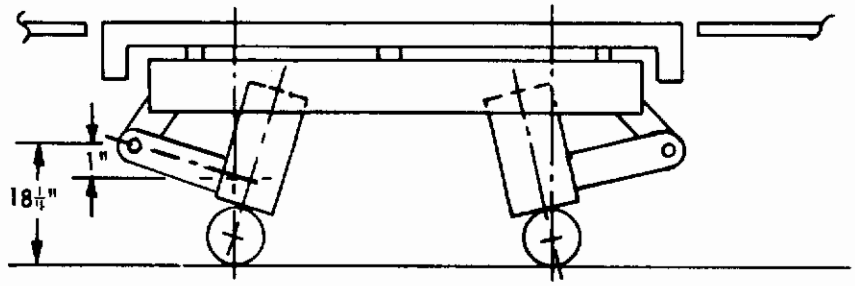

Notice that the cart legs have passed the vertical. The cart floor is then pinned to the tunnel floor in its operating position and the subcart is lowered to 1 in. below its supporting position with its legs vertical, as indicated in the following sketch.

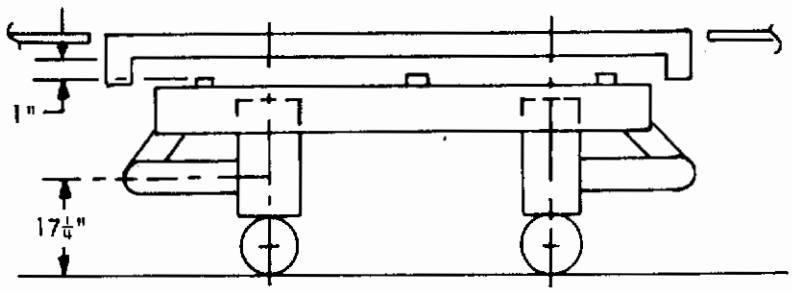

Very early in the design, it was decided that it would not be feasible to reduce the large reaction loads associated with large plunging amplitudes within the oscillator mechanism itself. Instead, the oscillatory loads transmitted to the tunnel structure are reduced by mounting the entire cart which supports the oscillator on very soft springs. Pneumatic, flexible-diaphragm type springs were selected for this purpose. A self-leveling feature is designed into the system so that the model attitude remains fixed even while tunnel operating conditions change. Because of the soft suspension, a change in the force on the model could cause a change in the model attitude. However, leveling valves introduce compensating changes in the internal pressures of each of the air springs, thereby returning the model to its original attitude. These leveling valves have built-in low-pass filtering characteristics so that they do not respond significantly to frequencies above 1/4 cycle and, therefore, they do not interfere with the model oscillation tests in the range of 3-12 cps.

Dynamic forces and moments transmitted from the oscillator to the wind-tunnel structure are reduced by almost an order of magnitude as a result of the very soft pneumatic springs and the very heavy (about 28,000 lbs.) subcart. Measurements of transmissibility indicated that the peak dynamic load applied to the wind-tunnel structure could be expected to be less than 300 lbs.

The self-leveling characteristic of the air-spring suspension system also automatically provides the desired decoupling of the rotational and translational degrees of freedom of the cart.

The pneumatic suspension system utilized "Airide" springs 1X5 (850 cu. in. reservoir). On the basis of data supplied by the manufacturer, the natural frequency was calculated to be 1.22 cps. This compares quite well with the 1.29 cps subsequently measured.

The cart suspension system is shown in the sketch of Figure 32.

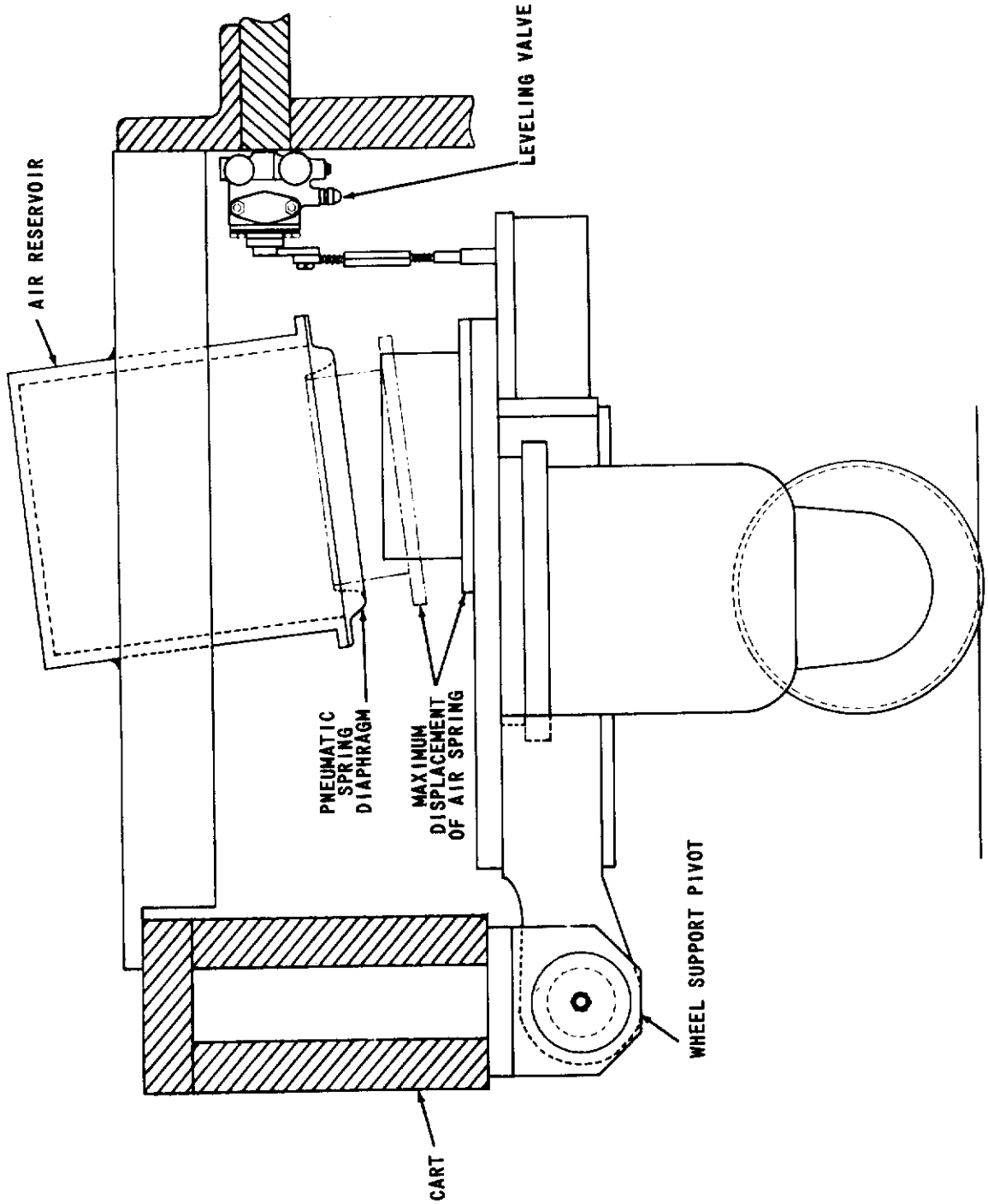

Figure 32 THE PNEUMATIC SUSPENSION SYSTEM - RIGHT FORWARD WHEEL ASSEMBLY

The Oscillator Drive and Flywheels

The motor housing, V-belts, gearing and flywheels are pictured as installed in the subcart in Figure 33. The motor is a direct-current type with a tachometer-generator feedback control and a full-wave-rectification type power supply. Speed regulation of the motor itself without the flywheels is $\pm 1/2\%$ of its rated speed, 1750 rpm. The motor is enclosed in a housing which permits it to be pressurized to 1/2 atmosphere above ambient. This is to prevent commutator arcing when tunnel density is reduced. The motor driveshaft passes through a Teflon seal to a pulley from which two V-belts take off the drive power to the gear pulley in a 2:1 speed ratio. The precision-ground spur gears are both 38 in. pitch diameter. The small and large flywheels mounted on the gearshafts therefore turn at precisely the same speed but in opposite directions. Lubrication is supplied to the gears and the gearshaft bearings by a forced spray system which is built into the subcart.

Eccentric cranks protrude from the otherwise clear face of each flywheel. Figure 34 shows the bottom of the forward connecting rod attached through its bearing to the eccentric of the small flywheel. Assembly of the aft connecting rod to the large flywheel is similar.

The flywheels were designed to be large enough to resist changes of speed within one cycle imposed by the variation of torque due to air load and inertia load. An objective of 1% speed variation was set, this figure being somewhat less than the effective speed variation introduced by the finite crank length. The percentage variation of speed will always be greatest at the lowest operating speed, which was assumed to be 3 cps for the purpose of the flywheel design. The maximum allowable model load (air load plus inertia) was set at 1200 lbs. by model structural limits. The required moment of inertia was determined to be 3640 in. lbs. sec.^{2}. For a disc of radius, R, and thickness, t, the inertia for the flywheels is given by 0.00114 tR^4 in. lbs. sec.^{2}. The approximate design drive inertia was then given by:

large flywheel	t = 10 in., R = 21 in.:	tR^4 =	1,940,000
two gears	t = 3 in., R = 19 in.:	tR^4 =	780,000
small flywheel	t = 8 in., R = 13 in.:	tR^4 =	229,000
phase housing	t = 4 in., R = 16 in.:	tR^4 =	260,000
Total			3,209,000

The approximate drive inertia is therefore given by 0.00114 x 3,209,000 = 3658 in. lbs. sec.^{2}. The actual weight of the rotating elements alone is 6,274 lbs.

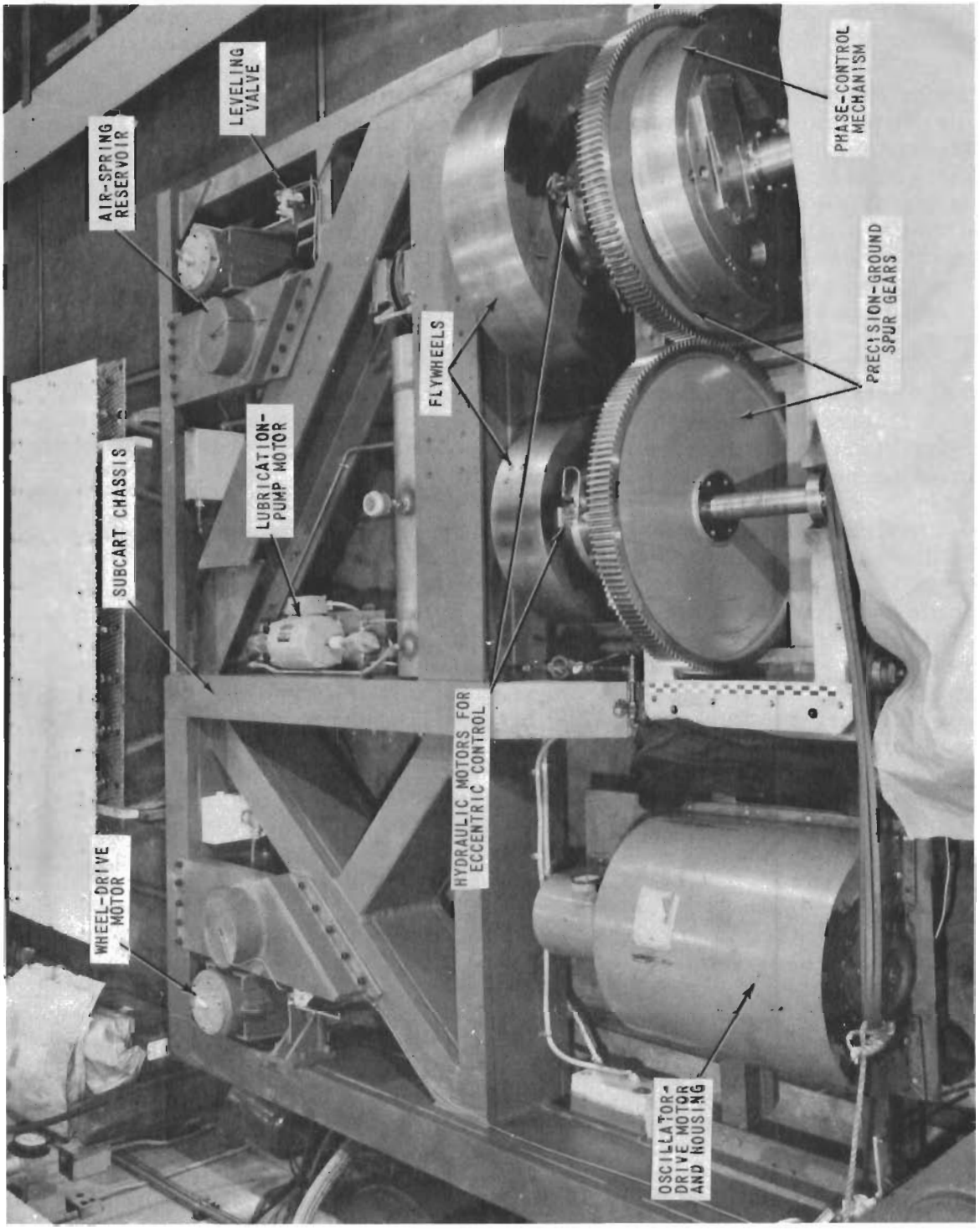

Figure 33 THE SUBCART

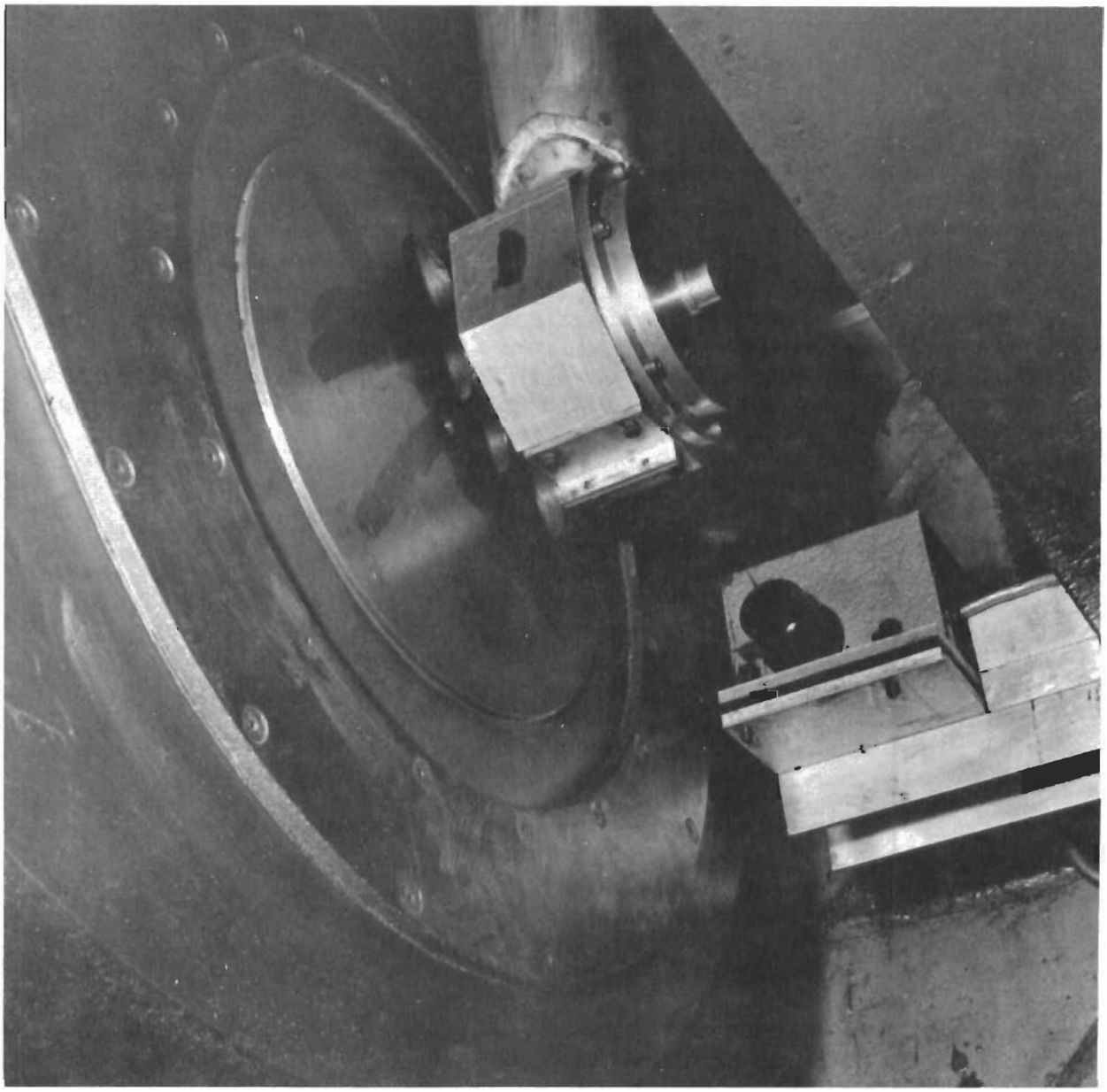

Figure 34 THE ECCENTRIC CRANK AND CONNECTING ROD ASSEMBLY

The Oscillator Controls

It is desired to provide the model with any combination of planar translational and rotational sinusoidal motion. To achieve this freedom of model motion, the amplitudes of the eccentrics and the phase between them are continuously and precisely adjustable. If, for example, the model is to have pure translational motion, then (under the assumption of rigid-body kinematics) the two connecting rods must be made to oscillate through the same amplitude and with a phase angle between them of 180°, i. e., when one is up, the other is down. If pure rotation about the model's c. g. is the desired motion, then the amplitude of oscillation of the aft connecting rod must be made about half that of the forward connecting rod and the phase must again be 180°. Motions which are combinations of translation and rotation, such as pure pitching, require other combinations of amplitudes of the two eccentrics and phase between them. These controls of the eccentrics are provided through mechanisms installed within the rotating parts of the oscillator drive and utilize hydraulic motors and hydraulic brakes.

In order to supply hydraulic fluid at high pressure (1500 psi) from an outside source to these rotating mechanisms, a special transfer system was designed. The housing and spindle of this transfer system are similar to those of a multiport servo valve. The housing of the transfer unit is supported in a fixed axial position relative to the rotating spindle by ball bearings and is restrained from turning with the spindle only by the radially attached hydraulic hoses. At the inner end of the spindle, tubing routes the hydraulic fluid through the hollow flywheel axle to the drive motors for the control mechanisms. A scavenging system returns all hydraulic fluid through the transfer unit to the outside supply. The complexity of the installation of this motion-change mechanism is apparent in Figure 35. This drawing is clarified somewhat when it is viewed in the light of the photographs in Figures 33 and 34.

The eccentric amplitudes are each controlled by means of one of the small hydraulic motors mounted on the flywheels. Each motor drives a drum whose periphery goes through the center of the flywheel, and whose axis is parallel to that of the flywheel. A stub shaft on the drum completes the crank of the crank-connecting rod design. The eccentric drum is mounted on tapered roller bearings in order to insure a minimum radial play during amplitude adjustment. An annular brake locks the drum, except while an eccentric adjustment is being made.

Control over the phase relationship between the flywheels is obtained by means of a hydraulic motor which permits arbitrary angular positioning between the drive gear and shaft on the aft flywheel. Again, a hydraulically actuated brake locks these in position, except while adjustment is being made.

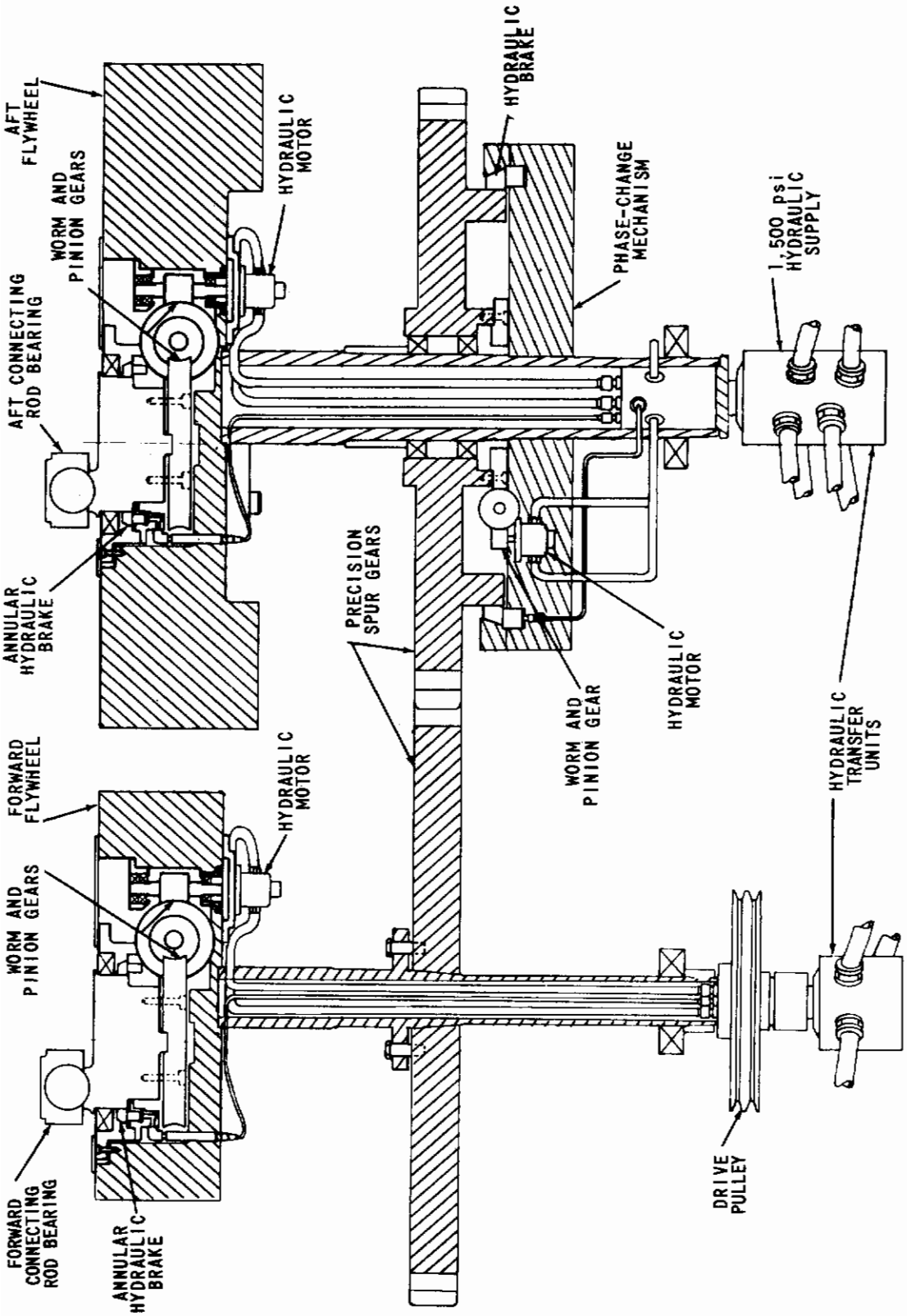

Figure 35 THE MECHANICAL OSCILLATOR DRIVE AND MOTION-CHANGE MECHANISM

Solenoid-actuated, hydraulic control valves are used to operate the brakes and the eccentric drive motors, and to provide a positive shutoff to the hydraulic motor in the phase-control drive. An electrohydraulic servo valve is used to limit the flow in either direction to the phase-control motor. The valves for the brakes are spring-offset (normally open), single-solenoid controlled. Those for the eccentric drive motors are spring-centered (normally closed), double-solenoid controlled. They are all pilot-operated, hydraulic, four-way valves. Additional flow-control valves are used to limit the motion in the so-called "slow speed" lines to the eccentrics.

The sequence of operation is typically to release the brake, then to energize the hydraulic motor in the desired direction and, finally, to reset the brake. This sequence automatically results from selecting and pulsing manually the proper double-pole, double-throw sequencing switch located at the control console.

A schematic of the hydraulic controls for the mechanical oscillator is shown in Figure 36.

The Eccentric Amplitude and Phase Indicators

The phase and amplitudes of the crank positions on the flywheels are measured by means of electronic timers (see Figure 37). A timer is started when a light beam is interrupted by one crank and is stopped by the other crank. By comparing this time interval with the period of oscillation, the phase angle between the cranks can be determined. The radial displacement of each crank is determined from the measurement of the angle that the crank makes with respect to a reference fixed to its flywheel. The timing "gate" for the latter reference is magnetic, whereas the crank "gate" is still optical. One gate starts a timer, the other stops it. The time between the gates is compared with the oscillator period as a measure of the pertinent angle. Figure 38 shows the results of the calibration of this measure of the eccentric amplitude in comparison with the theoretical relationship.

Experience has shown that the elastic deformations of the sting, lever and connecting-rod system during operation are not negligible and that these indicators of the eccentric amplitudes and phase can only be used to set up the approximate motion of the model. Final adjustments must be made on the basis of the model motion as measured by the accelerometers within the model.

The Sting Support and Linkage System

Prime considerations in the designs of the sting, lever and connecting rods were their inertia, fatigue life, and stresses. Calculations on the final designs indicated that the maximum stresses would be under 30,000 psi, which is about one-third the allowable fatigue limit of the heat-treated, precipitation-hardened type stainless steel used in the sting and lever parts.

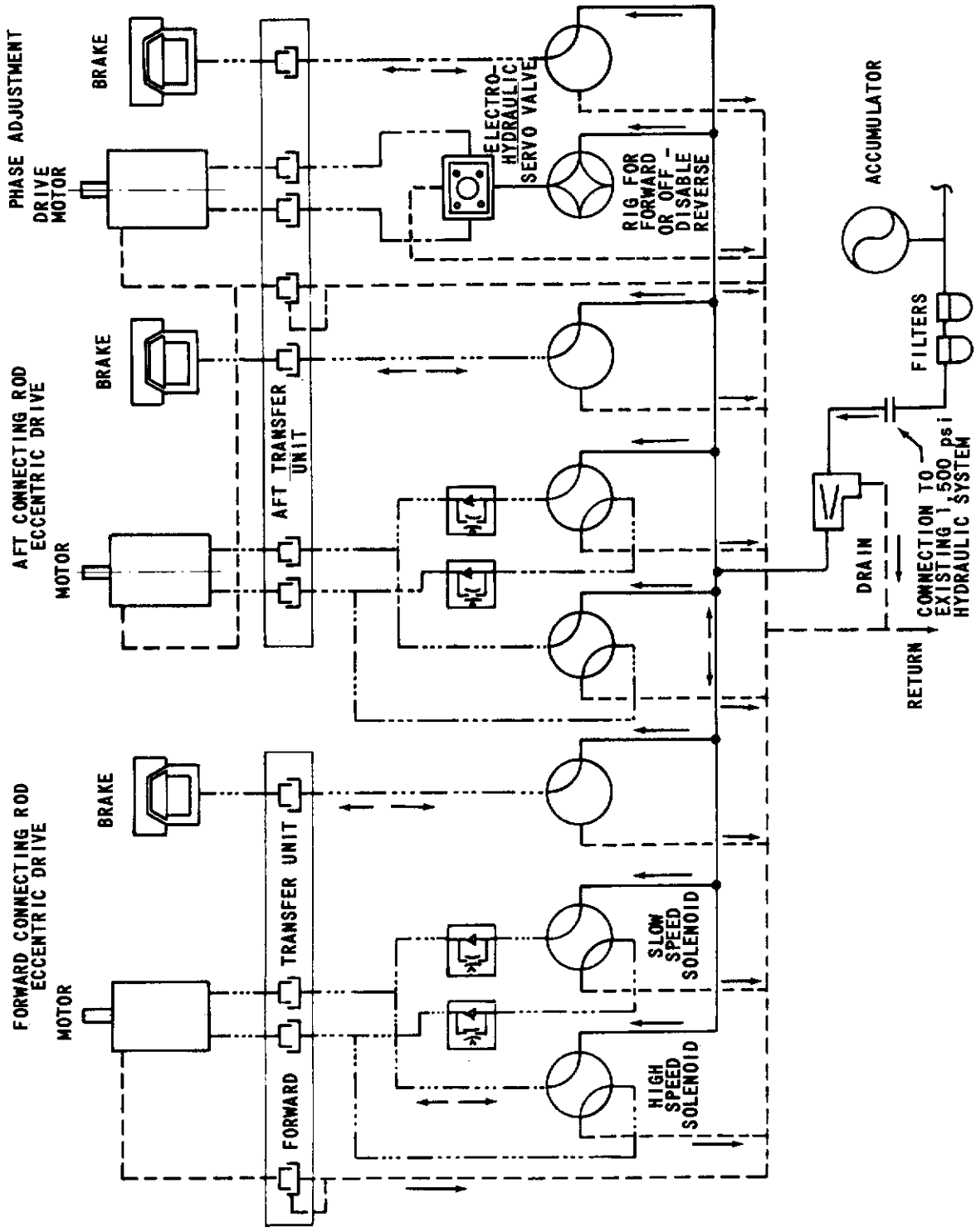

Figure 36 SCHEMATIC OF THE HYDRAULIC CONTROL SYSTEM

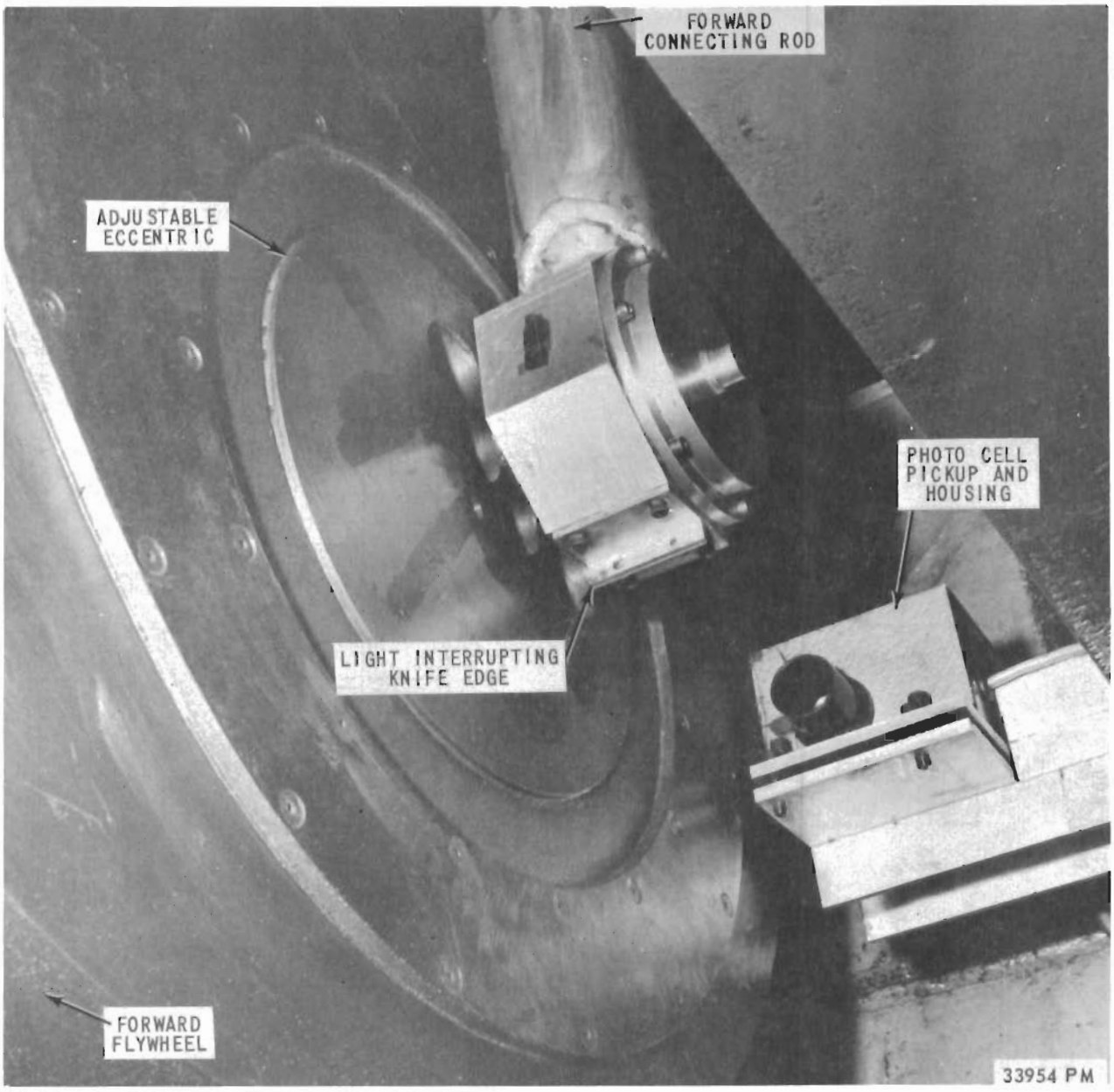

Figure 37 ECCENTRIC MEASUREMENT INSTALLATION

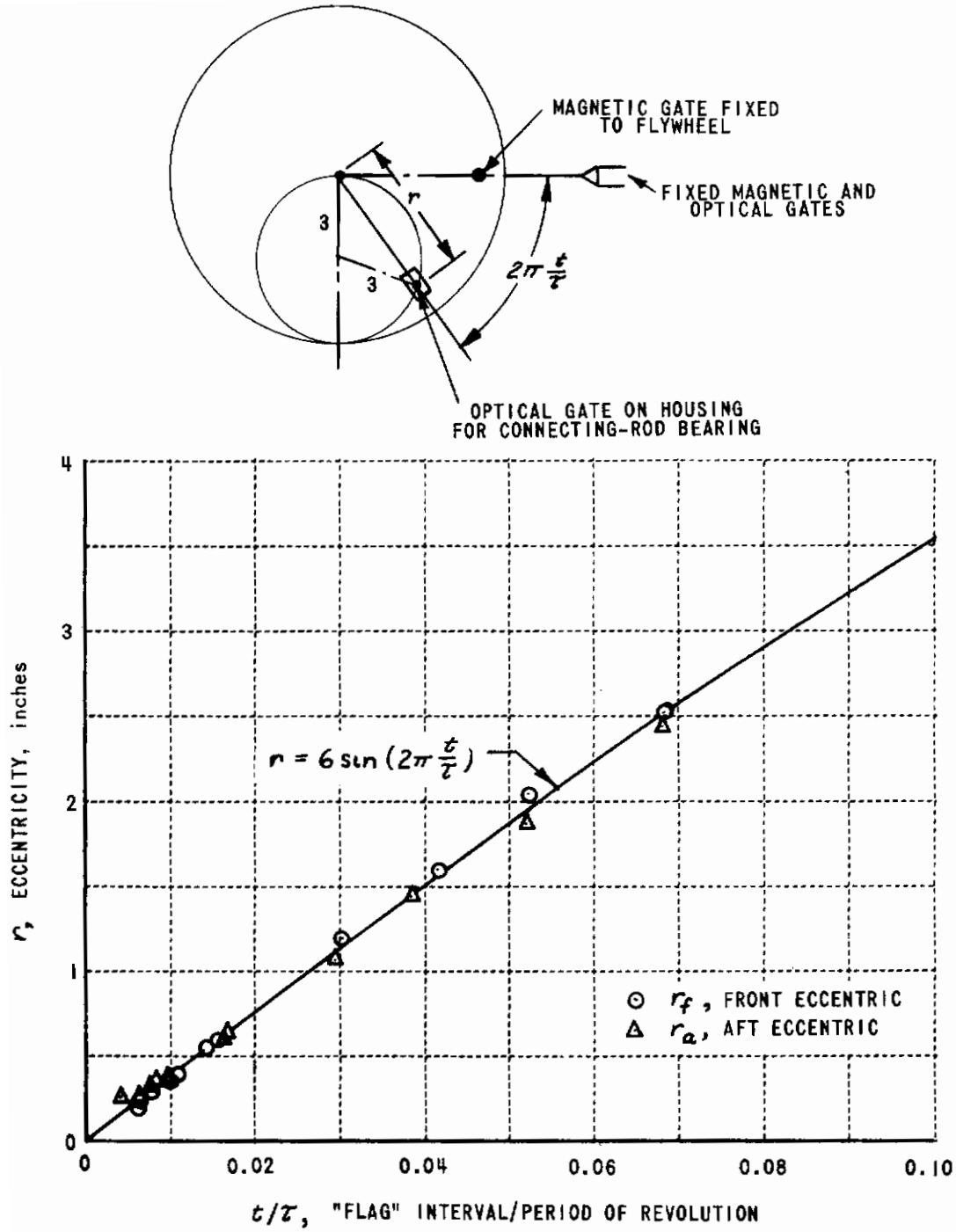

Figure 38 CALIBRATIONS OF THE ECCENTRIC AMPLITUDE INDICATORS

The aft sting and sides of the lever weldments are shown in Figure 39. The weldments were proof tested to full static plus twice dynamic design loads. Stress measurements on the aft lever were within 15% of calculations based on the proof load. The maximum assumed loads in the design of the sting and lever are indicated in the following sketches (see Figure 10).

(1) Vertical Plane

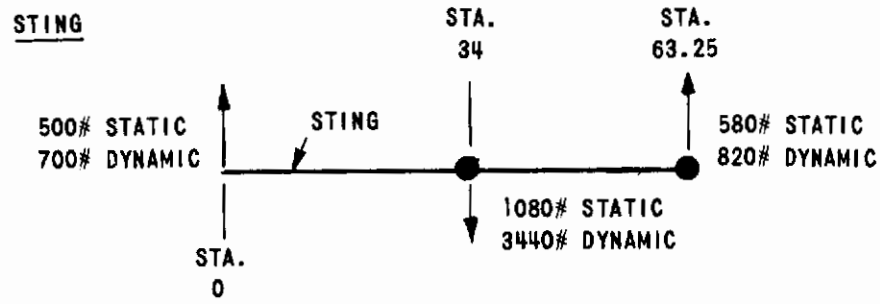

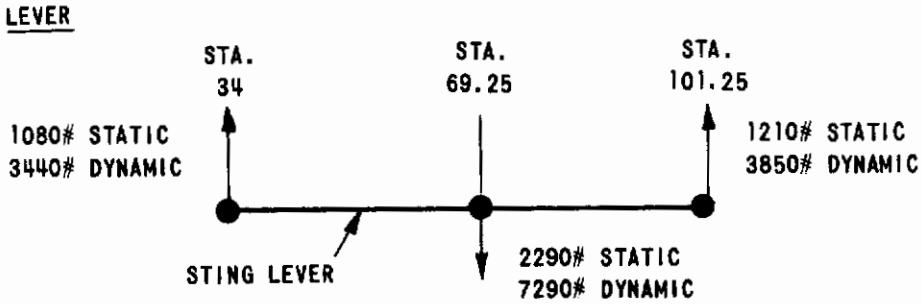

(2) Horizontal Plane

For the case of a model positioned with its wing span vertical, a lift load of 1000 lbs. in the lateral direction was assumed.

The forward sting, which is sketched in Figure 40, was machined from a 4 in. x 5 in. x 46 in. block of nonweldable, precipitation-hardened stainless steel. The front end was milled in the form of an inverted channel to permit the assembly of the sting within the model and the model balance within the sting. The cross section changes from an inverted channel to a tapered tube. Approximately 27 in. from the forward end, it has a minimum diameter of 2.16 in. where it fits through the opening in the aft end of the F-80 model fuselage. The sting has a 4° conical taper for the next 8-1/2 in., then blends into the pivot bearing and mating receptacle for the aft sting. The mating assembly of the fore and aft stings was designed to allow finite (5°) incremental changes of the mean angle of attack of the model.

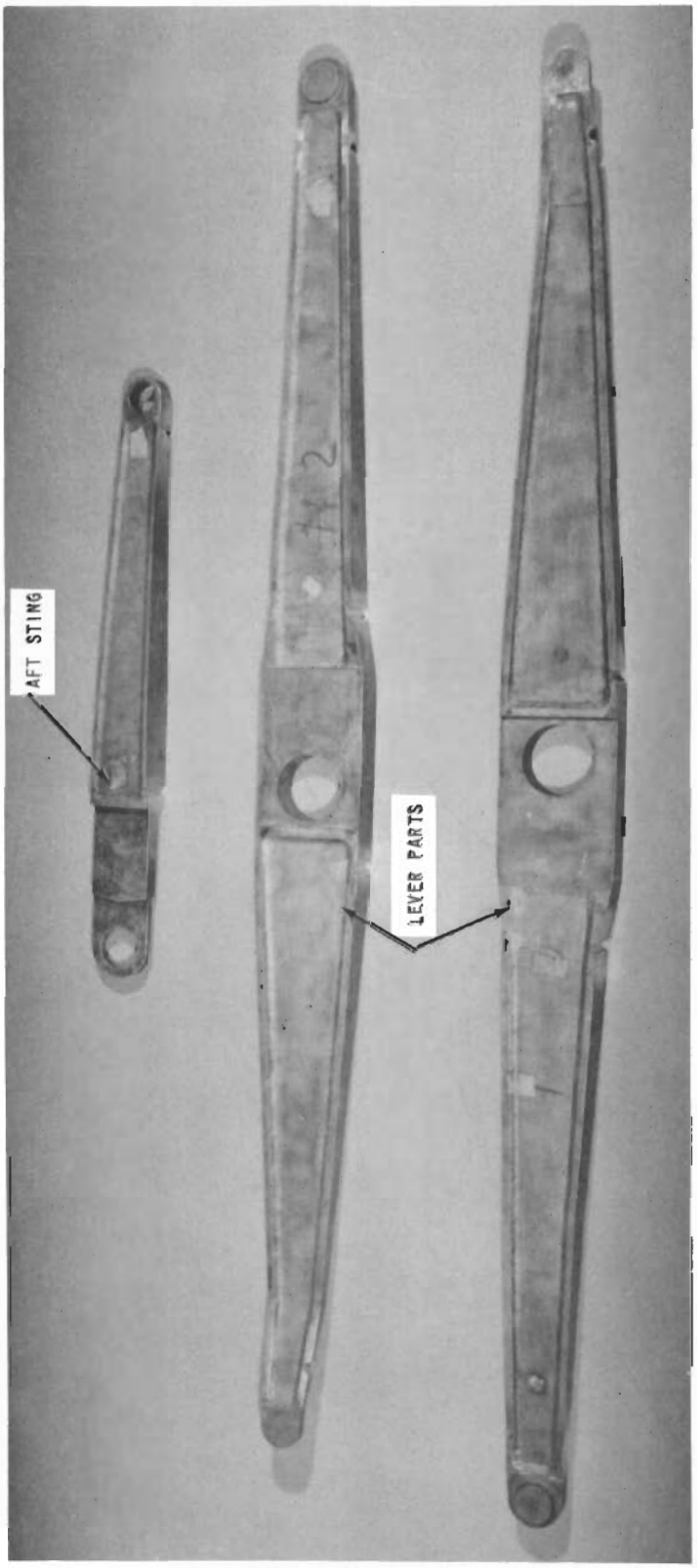

Figure 39 THE AFT STING AND THE LEVER WELDMENTS

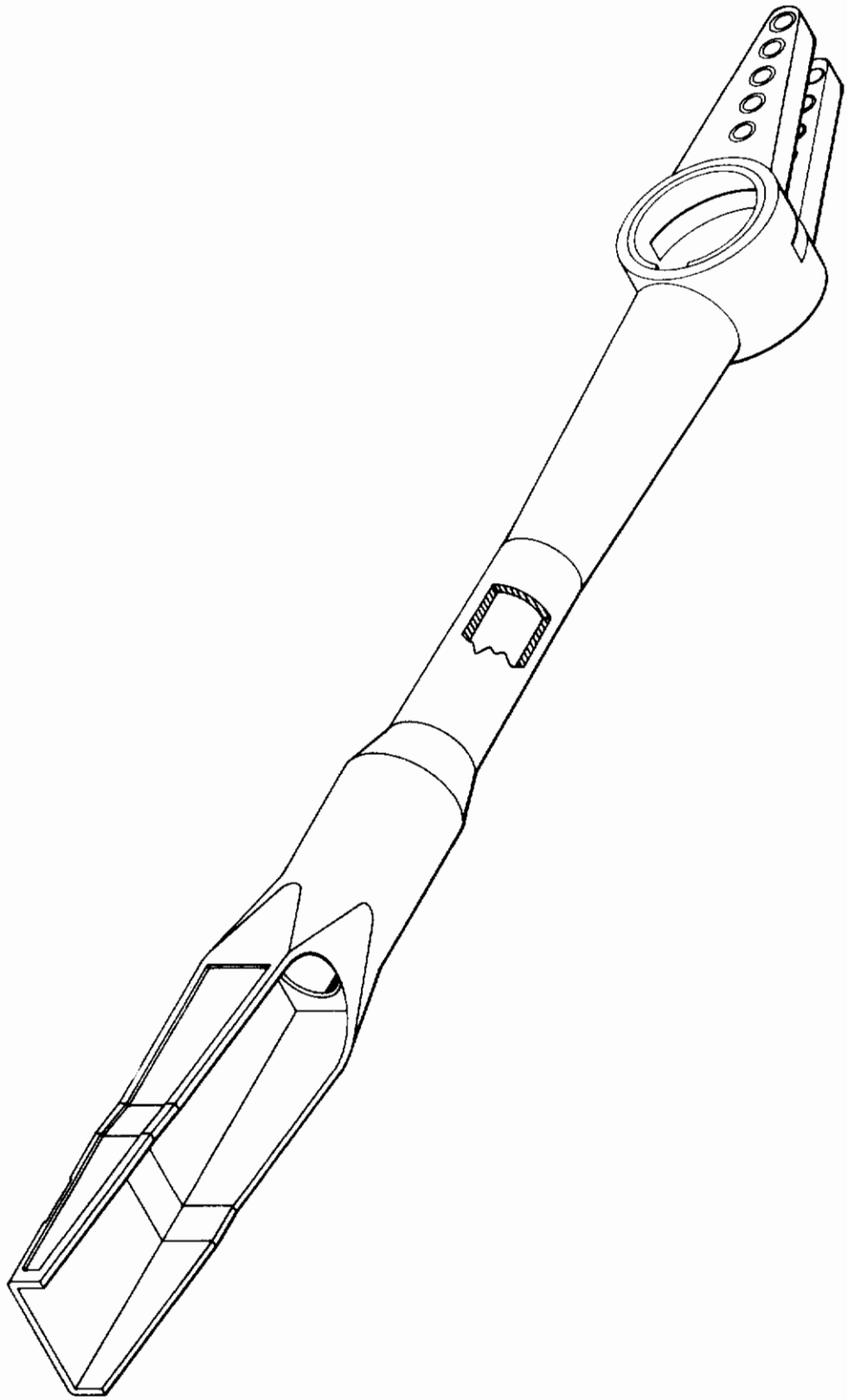

Figure 40 THE FORWARD STING

The forward and aft connecting rods transmit forces directly from the eccentrics to the aft ends of the sting and lever. The connecting rods are loaded primarily in tension and compression and are constructed of aluminum-alloy tubing with machined aluminum-alloy bearing supports welded to the ends. Column stability, fatigue life, stresses and inertia were again prime considerations in their design.

The weights of the components of the sting support and lever linkage system are as follows:

Component	Weight in Lbs.
Sting	52
Lever	124
Forward connecting rod, including bearing housings	9.4
Aft connecting rod, including bearing housings	13.5

Vibration tests were made of the oscillator system with an 18-lb. dummy weight at the model location using both the oscillator itself and an electromagnetic shaker for excitation. Strain gages indicated that the sting and lever stresses during the tests with the oscillator operating were not excessive. Even though the vertical accelerations of the dummy weight exceeded 30 g's, the maximum stress was well under the 30,000 psi design maximum.

The measured fundamental vertical vibration frequency was 17.3 cps with an 18-lb. dummy weight at the location of the model support. Although this natural frequency is sufficiently high with respect to the desired 3-12 cps operating range, it is significantly lower than was predicted during design. The discrepancy is believed to be the result of neglecting a rigid-body rotation of the vertical strut about its base and the deflections of the flywheel axles and connecting rods in the analysis.

The waveform of the model motion has been shown to be quite satisfactory over the operating range of 3-12 cps. The primary distortion of the waveform is attributable to the second-harmonic input due to the kinematics of the crank and connecting rod. As was shown in Figure 12, acceptable-to-good waveforms are achieved over the entire operating range except at discrete frequencies corresponding to the subharmonics of the lowest natural frequency. With the exception of the 1/2-harmonic, these regions of inferior waveform at the subharmonics are very narrow. Another region of poor waveform was encountered at about 11 cps. This probably corresponds to the 1/2-harmonic of the next higher natural frequency of a mode with significant longitudinal motion. Such a mode was indicated during the vibration tests at about 21.5 cps.

A measure of the second-harmonic content of the model motion which was made during pure plunging tests at 15 g's and 7 cps showed a rotational acceleration of 100-150 radians/sec.^{2} and a vertical acceleration of less than 5 g's at 14 cps. These levels are not high enough to introduce errors in the measures at the fundamental frequencies. They indicate a rotational motion of sufficient magnitude and purity, however, to suggest the possibility of measuring the loads due to rotational motion at second-harmonic frequencies while plunging at the fundamental.

The rolling stiffness of the system was indicated during the course of calibrating the crosstalk sensitivity of the angular accelerometer. While plunging at 7 cps and 15 g's, a measure of the rolling acceleration showed less than 0.15 radian/sec.^{2}. It was found to be approximately linear with plunging acceleration and in phase with it. This was considered to be small enough to introduce no significant errors in the longitudinal tests of most configurations.

During the early phases of the development of the mechanical oscillator, the bearings provided one of the more troublesome aspects. The performance of the motion sensors was extremely sensitive to the once-per-revolution transients in the motion resulting from slightly noisy bearings. Two different types of bearing operations are required. The bearings between the connecting rods and the eccentrics are in rotation with steady plus periodic loading. These are pairs of angular-contact, ball bearings which are lightly preloaded. They are periodically lubricated with a high load carrying capacity lubricating grease designated as MIL-G-7118-Am. 2. The other bearings in the sting-lever-connecting-rod system experience only oscillatory motion but also have steady plus periodic loading. The bearings between the connecting rods and the levers are needle bearings which have been hand selected for minimum radial clearance. The fixed pivot of the linkage system at the vertical strut is a tapered roller bearing, as is the pivot bearing between the sting and lever. All these nonrotating bearings are lubricated periodically with a special lubricant designated as MIL-G-25537(USAF)Am. 1. Problems associated with the evaporation of these lubricants during low ambient pressure operation have been minimized by the addition of molybdenum disulphide, a dry film lubricant, to both of the greases. The additive amounts to about 20% by volume of the mixture.

APPENDIX II

THE FORCE AND MOTION SENSORS

The Balance

A balance comprised of a system of four flexures supports the model from the sting, as shown in Figure 16. These flexures were machined from an alloy (NI-SPAN C) which, when properly heat treated after fabrication, has a nearly constant elastic modulus over the operating ambient temperature range of 60° F. - 150° F. The design configuration of the flexures is shown in Figure 41.

The outputs of the strain gages on the two forward beams are summed to provide the measure of the normal force. These are located precisely at the c. g. of the model. The moment-measuring flexure is 6. 5 in. aft of the normal-force-measuring beams. A longitudinally oriented beam is attached between the model and the sting. This flexure does not have strain gages but merely provides restraint in the drag direction without interfering with the sensing flexures.

To obtain a dynamic calibration of the normal-force- and the moment-measuring strain beams in the model, it was oscillated under wind-off conditions with and without a known increment of weight and pitching moment of inertia. (A structural analysis of fuselage strength with the added weight attached indicated a safety factor of about two.) The moment of inertia of the added weight about its own lateral axis was determined experimentally. 15. 2 lbs. of weight were added which produced an increment in the pitching moment of inertia of 0. 39 ft. lb. sec.^{2} (approximately equal to the inertia moment of the F-80 model alone) and was designed to maintain the nominal model c. g.

The normal-force strain beams were calibrated dynamically from measurements of the output signals with and without the known increment of weight while in pure plunging with wind off. The data are presented in Figure 42. For an incremental weight of 15. 2 lbs., the change in the output of the normal-force beams at, say, 10 g's was 2. 63 volts so the sensitivity is 15. 2 x 10/2. 63 = 57. 8 lb/peak volt. Since the excitation voltage was 5. 4 volts and an Epsco amplifier of gain 2000 was used on the output of the strain-gage bridge, the sensitivity of the normal-force strain beams was 1. 7 microvolts/lb/volt of excitation.

The same data of Figure 42 can also be used to check the model weight. At, say, 10 g's, the output signal from the normal-force strain beams for the model alone was 3. 12 volts. When this is multiplied by the sensitivity factor 57. 8 lb/volt and divided by 10 g's, the weight is calculated to be 18 lbs. which checks the static weighing of the model.

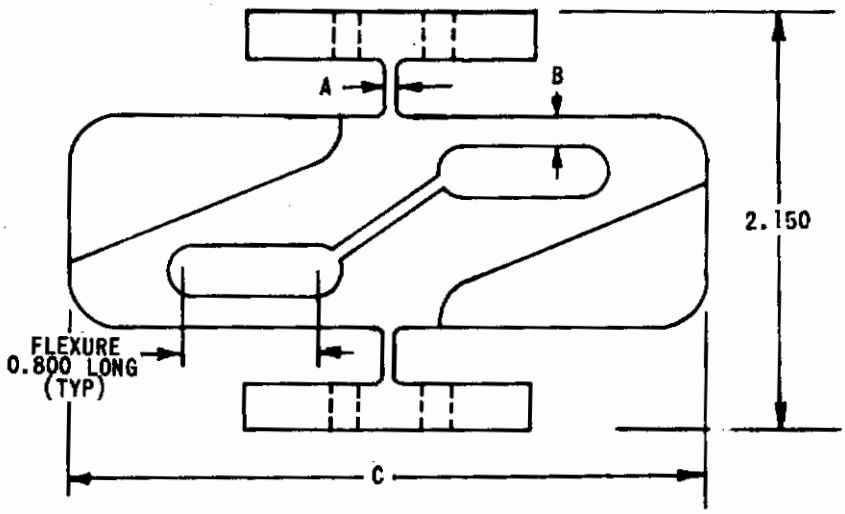

		A	B	C	BEAM DEPTH
AFT BEAM 1 REQUIRED	1	0.025	0.044	2.800	1.000
	*2	0.025	0.054	2.800	1.000
	3	0.025	0.030	2.800	1.000
FORWARD BEAM 2 REQUIRED	4	0.050	0.105	3.300	0.820
	5	0.050	0.130	3.300	0.820
	*6	0.050	0.150	3.300	0.820

*PRESENTLY USED

Figure 41 THE STRAIN-BEAM FLEXURE DESIGN

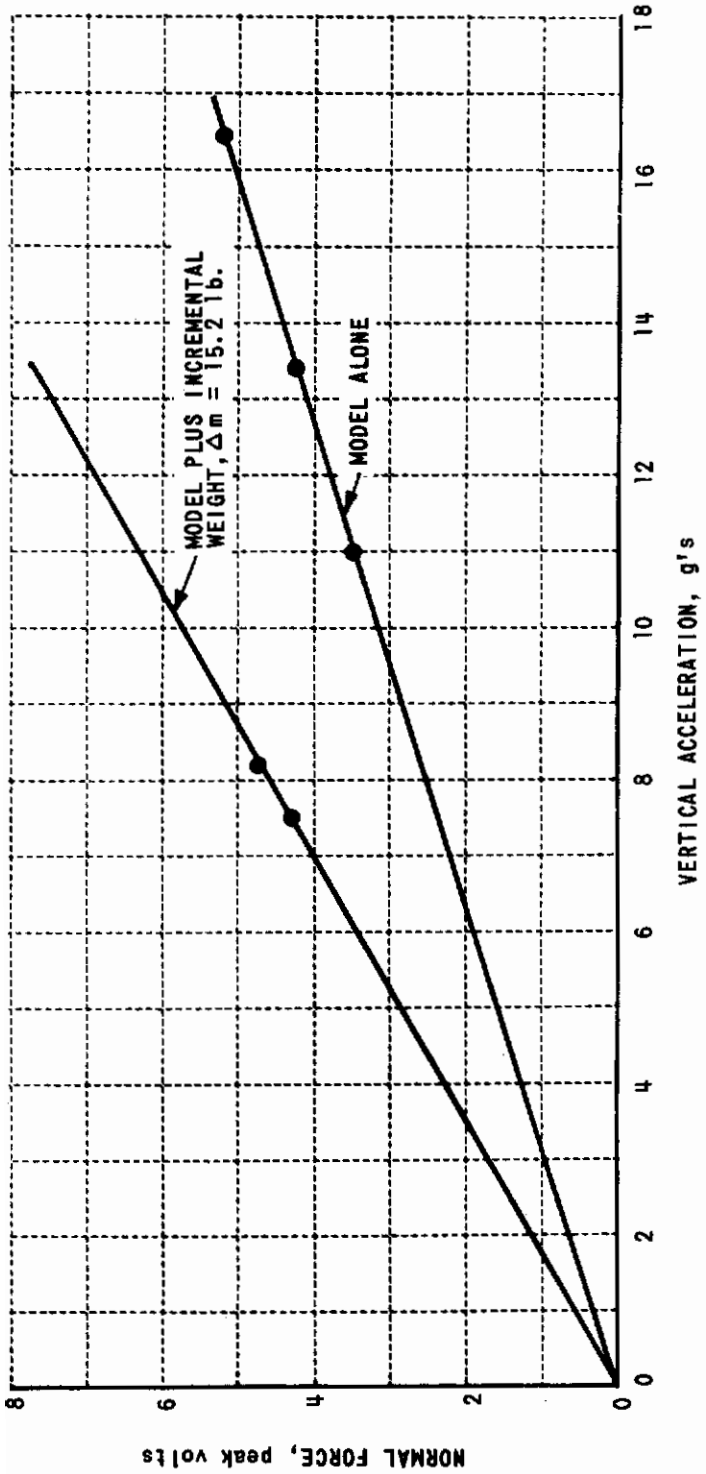

Figure 42 DYNAMIC CALIBRATION OF THE NORMAL-FORCE MEASURING STRAIN BEAMS

Similarly, the moment-measuring strain beam was calibrated dynamically by oscillating the model in pure rotation with and without the known increment of pitching moment of inertia. The data are presented in Figure 43. For an incremental inertia of 0.39 ft.lb. sec.^{2}, the change in the output of the moment beam at, say, 40 radians/sec.^{2} was 7.45 volts so the sensitivity is 0.39 x 40/7.45 = 2.1 ft.lb/peak volt. Taking account of the moment arm to the c.g. of 6.5 in., the 5.4 volts excitation, and the gain of 2000 provided by an Epsco amplifier, the sensitivity of the moment-measuring strain beam is calculated to be 23.8 microvolts/lb/volt of excitation.

The same data of Figure 43 can be used to evaluate the moment of inertia of the F-80 model. At, say, 40 radians/sec.^{2}, the output signal from the moment beam for the model alone was 7.15 volts. When this is multiplied by the sensitivity factor 2.1 ft.lb/volt and divided by 40 radians/sec.^{2}, the inertia is calculated to be 0.375 ft.lb. sec.^{2}.

The sensitivity of the moment balance was also checked statically by loading the moment beam directly and reading its output on a digital voltmeter. The data are presented in Figure 44. The excitation voltage was 5.4 volts and the Epsco amplifier with a gain of 2000 was used. The slope of the straight line through the data points indicates a sensitivity of the moment-measuring strain beam of 23.6 microvolts/lb/volt of excitation. The agreement with the dynamic calibration is well within the experimental accuracy and, so, 2.1 ft.lb/peak volt was subsequently used in reducing the dynamic test data.

To provide good separation of the measurements of the normal force and the moment, it was desired to balance the model so that its center of gravity was, longitudinally, within 0.01 in. of the sensitive axis of the normal-force-measuring strain beams. The following static measurement technique was used to accomplish this. The model was mounted on the sting in the normal manner and was accurately positioned on a true horizontal axis. The entire assembly of model and forward sting could be inverted without disturbing this axis. Repeated model-assembly inversions and model-weight adjustments were accomplished until identical readings of the moment balance were obtained for the model in its upright and inverted positions. Repeatibility of moment readings within 0.01 ft.lb. provided for location of the c.g. within the desired 0.01 in. tolerance.

The Linear Accelerometer

The vertical motion of the model's center of gravity was measured by a specially modified linear accelerometer comprised of a seismic sensor housed in one case and associated electronics in another connected by a 7-ft. long cable. The sensing element itself was small enough to be located between the two forward strain beams (Figure 16). This accelerometer is a servo-balance type employing a pendulous seismic element which is supported by a pivot and jewel bearings. Its servoed error detector is a

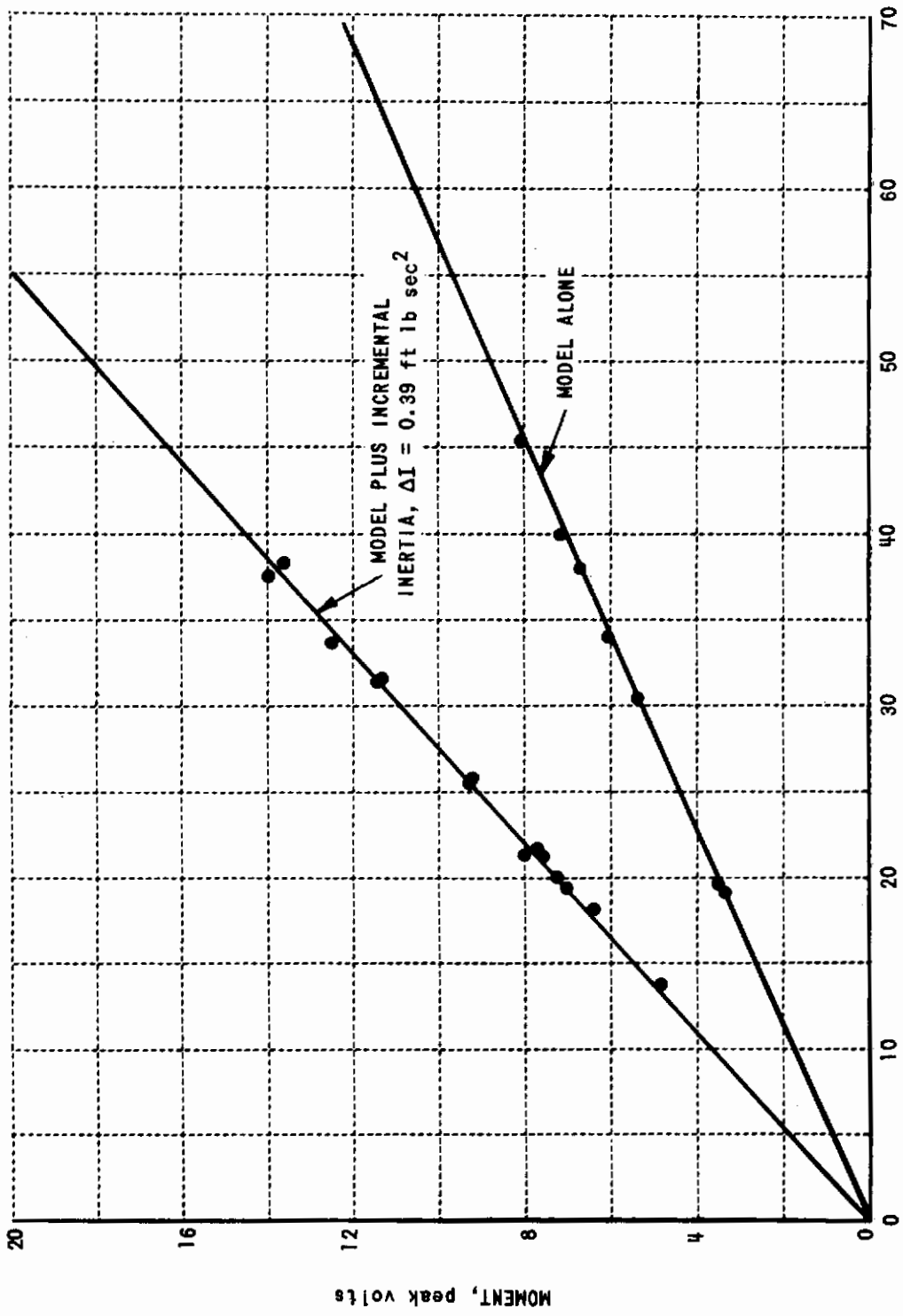

Figure 43 DYNAMIC CALIBRATION OF THE MOMENT-MEASURING STRAIN BEAM

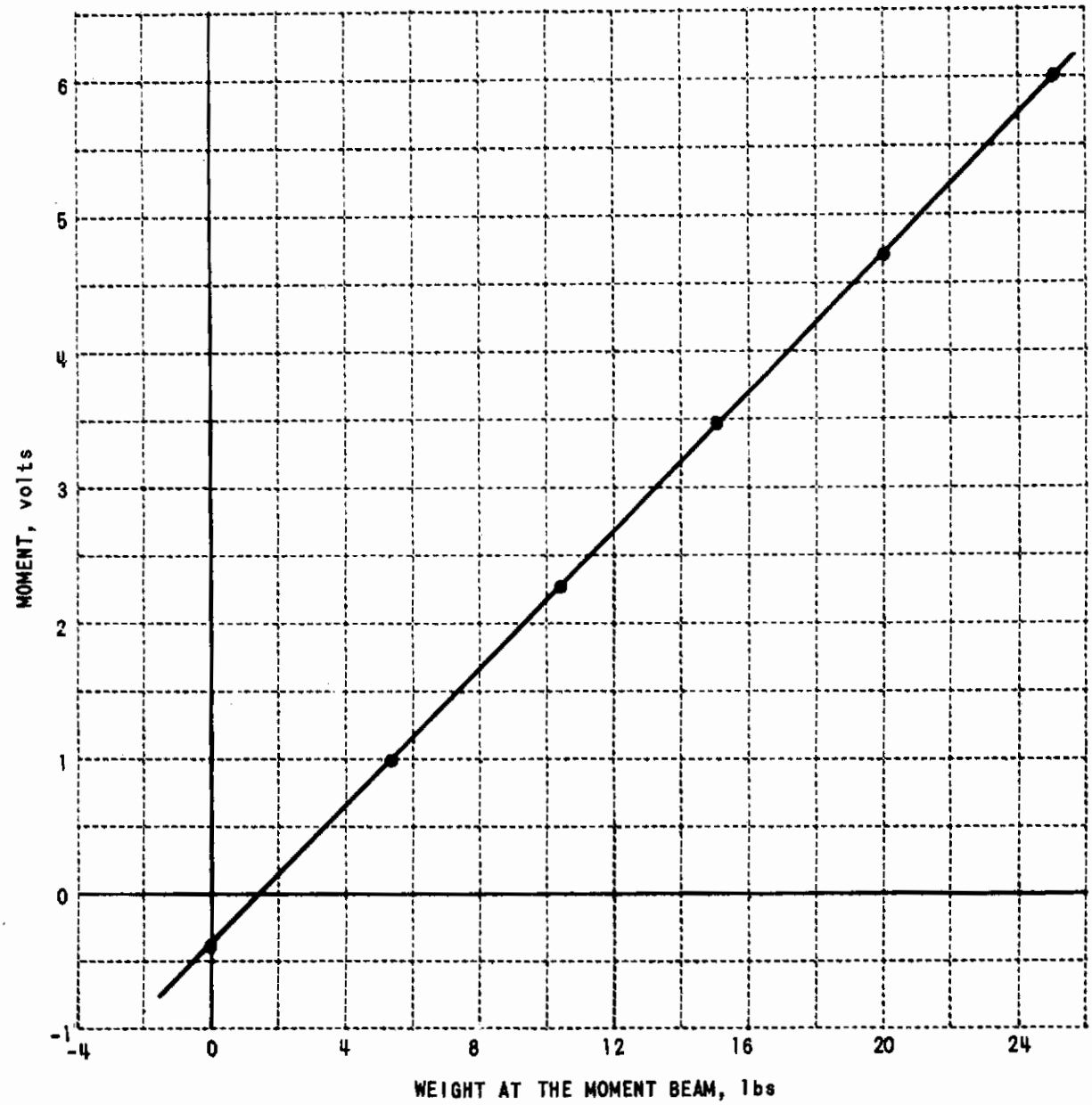

Figure 44 STATIC CALIBRATION OF THE MOMENT-MEASURING STRAIN BEAM

variable reluctance type consisting of a coil excited by a 1.5 megacycle oscillator in the separate electronics package. The seismic element contains a metal "paddle" situated near the face of this coil. A pendulous deflection of the paddle resulting from an acceleration input produces a change in the coil current which is detected by transistorized electronic circuits, amplified, converted to a DC signal, and returned to a force-balancing moving coil attached to the seismic element. This feedback current develops a voltage across a fixed resistor, and this voltage is the output signal of the accelerometer. An outline drawing of the two components of this accelerometer is shown in Figure 45. The operating characteristics of this transducer are presented in the main body of this report in Section 6 - The Force and Motion Sensors.

The linear accelerometer has the capability of measuring accelerations up to 30 times gravity and, for most uses, this device would be calibrated on a centrifuge. But this is a "static" type of calibration, unlike the dynamic input the transducer is intended to measure as used in the dynamic testing system. Consequently, dynamic calibration techniques were used to determine the performance characteristics of the linear accelerometer. The same signal processing system that is used during model tests was also used for these calibrations.

A mechanical oscillator driven by a variable-speed motor was used to provide sinusoidal linear acceleration inputs to the accelerometer in the range from 2-6 g's peak at frequencies from 3-10 cps. The equipment is shown in Figure 46. The main shaft of this oscillator carried a 100-lb. flywheel and an adjustable eccentric cam which provided reciprocating motion to an extended arm. This arm was, in turn, coupled to a small platform to which the accelerometer was attached. This platform was at the upper end of a lever, the lower end of which was bearing mounted. (See Figure 47 and the sketch below.)

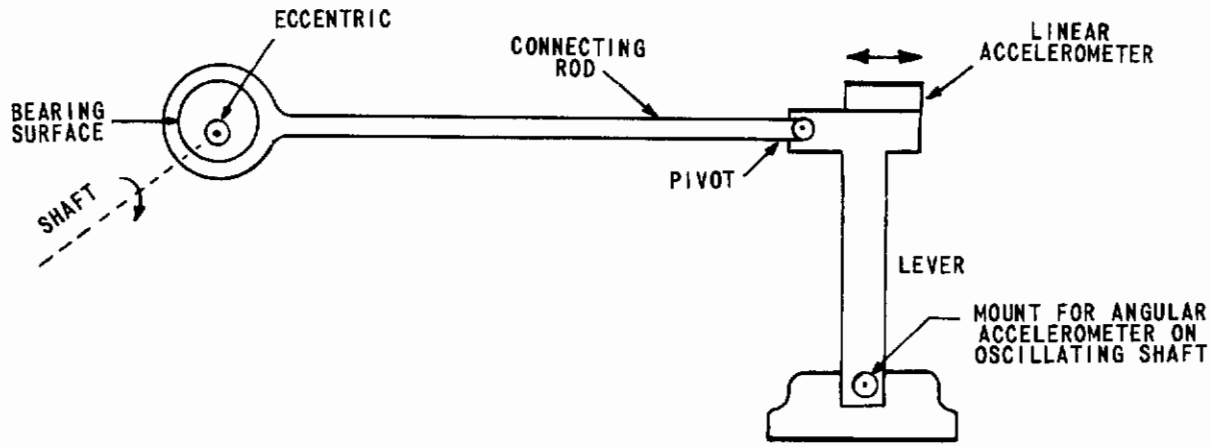

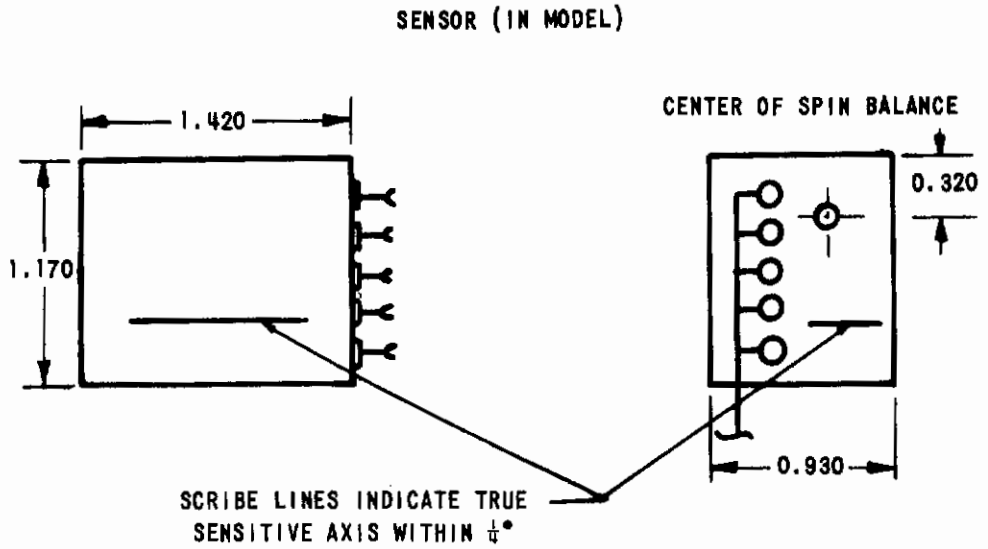

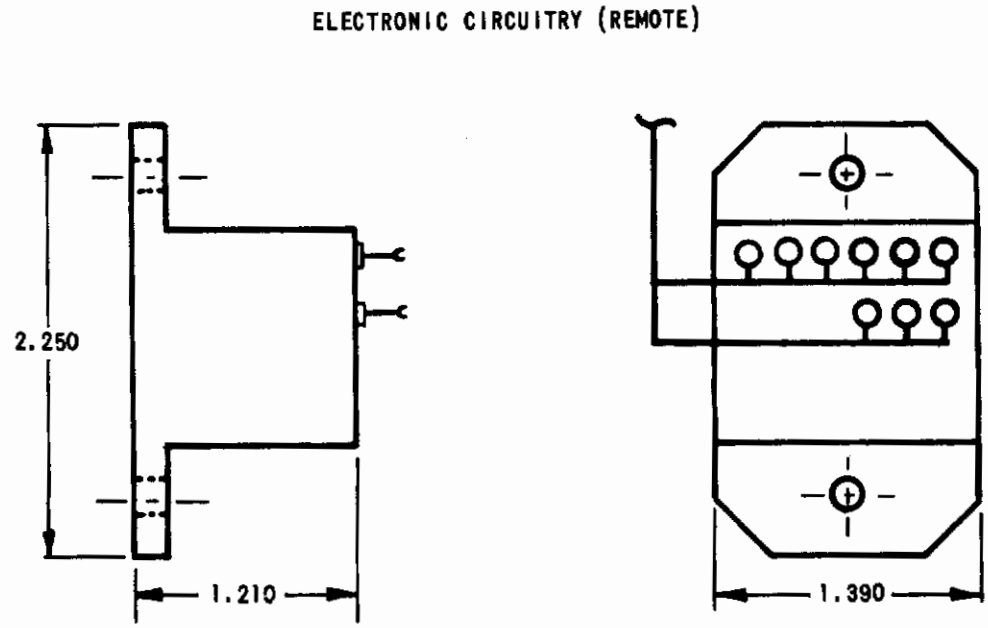

MODIFIED MODEL 4310 WITH SEPARATE SENSOR ±30g

Figure 45 THE LINEAR ACCELEROMETER

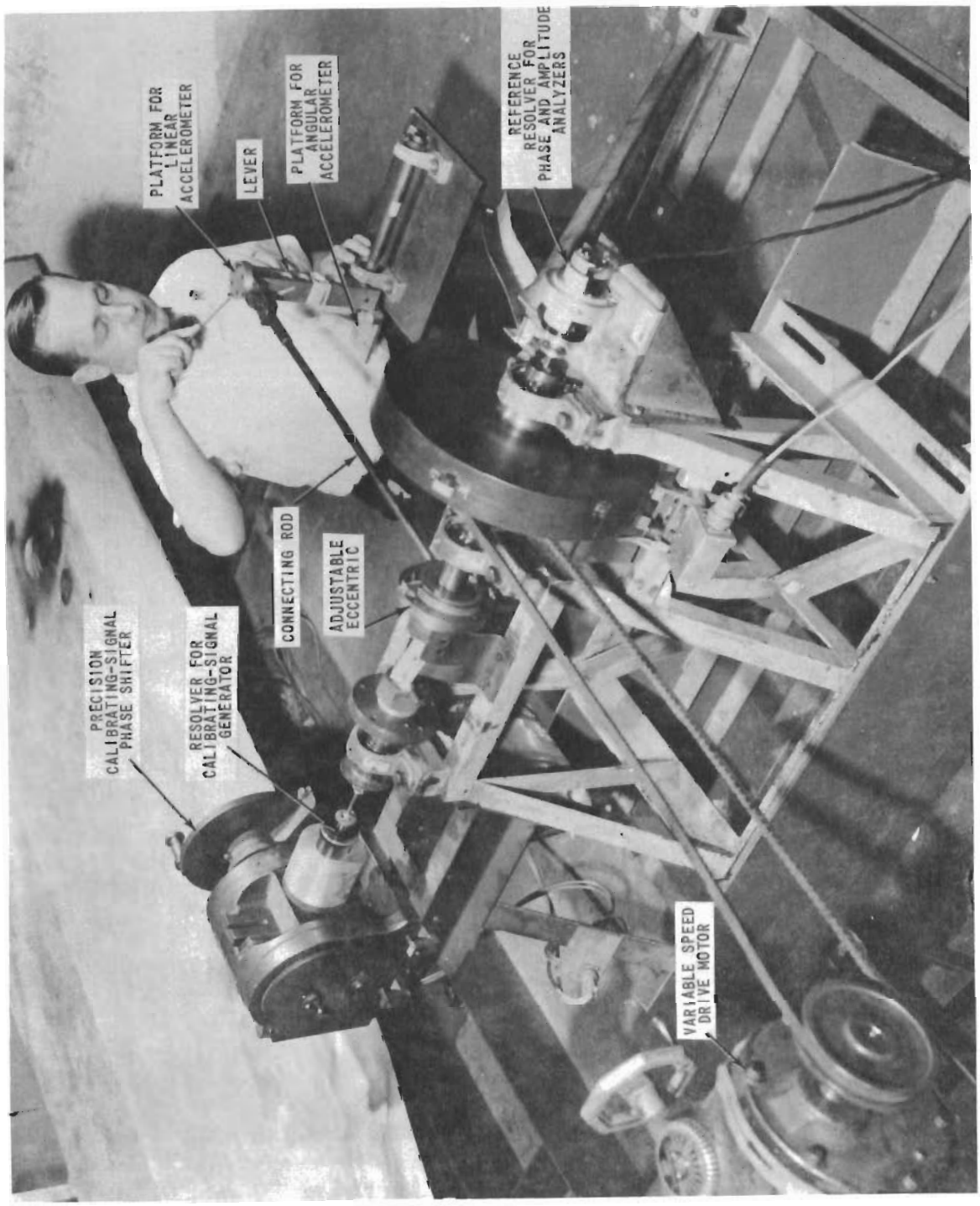

Figure 46 THE OSCILLATOR USED FOR DYNAMIC CALIBRATIONS OF THE LINEAR AND ANGULAR ACCELEROMETERS

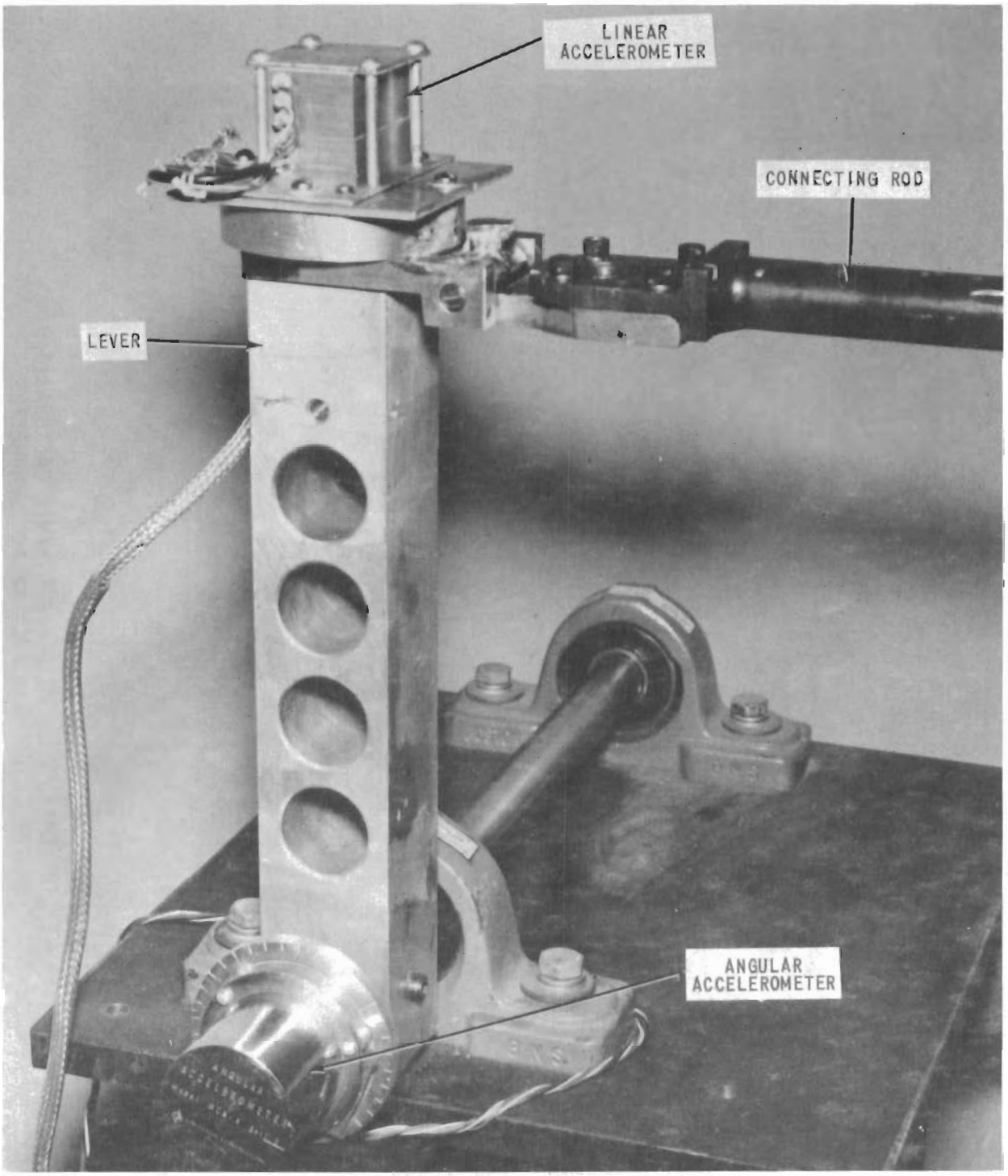

Figure 47 THE MOUNTING OF THE LINEAR AND ANGULAR ACCELEROMETERS DURING CALIBRATION

The main shaft of this machine was also coupled to two resolvers, one of which was used as a calibrating-signal generator and the other as the reference for the synchronizing circuits of the phase and amplitude analyzers. (As described in Appendix III - The Signal Processing System, the amplitude and phase analyzers convert the sinusoidal accelerometer output signal to steady-state DC voltages representing the amplitude and phase which can be easily and accurately measured.)

The calibration was performed as follows:

(1) The shaft eccentric was offset an amount which would produce approximately the desired motion amplitude. The eccentric adjustment was then locked in place.

(2) The shaft was then turned slowly by hand, and the peak-to-peak displacement of the accelerometer platform was measured to an accuracy of $\pm$.0005 in. (1 part in 2000 for a 1-in. double-amplitude displacement) with a micrometer head or dial gage.

(3) The input accelerations were computed for each frequency to be used during the calibration according to the measured fixed amplitude input.

(4) During calibration, the sinusoidal output signal of the accelerometer was fed to one of the phase and amplitude analyzers.

(5) The peak volts of output signal divided by the peak g's at each frequency provided the sensitivity calibration. Information on the phase shift with frequency was directly available.

As indicated above, these calibrations were limited to rather low (6 g) acceleration levels. The peak-to-peak displacement became a less accurate measure of the fundamental amplitude with increasing amplitude of motion simply due to the kinematics of the apparatus. A confirmation of the instrument's calibration for high-g inputs was obtained by using the oscillator of the dynamic testing system itself. The linear accelerometer was attached to a fixture which could be clamped to the rear connecting rod, as shown in Figure 48. Larger displacements could be obtained with this installation so that accelerations as high as 20 g's peak could be attained. No significant effect of level of acceleration on the sensitivity was found. The linear accelerometer's sensitivity and phase shift with frequency are shown in Figure 49.

The linear accelerometer was oriented in the model so as to eliminate all sensitivity to angular accelrations about the pitch axis.

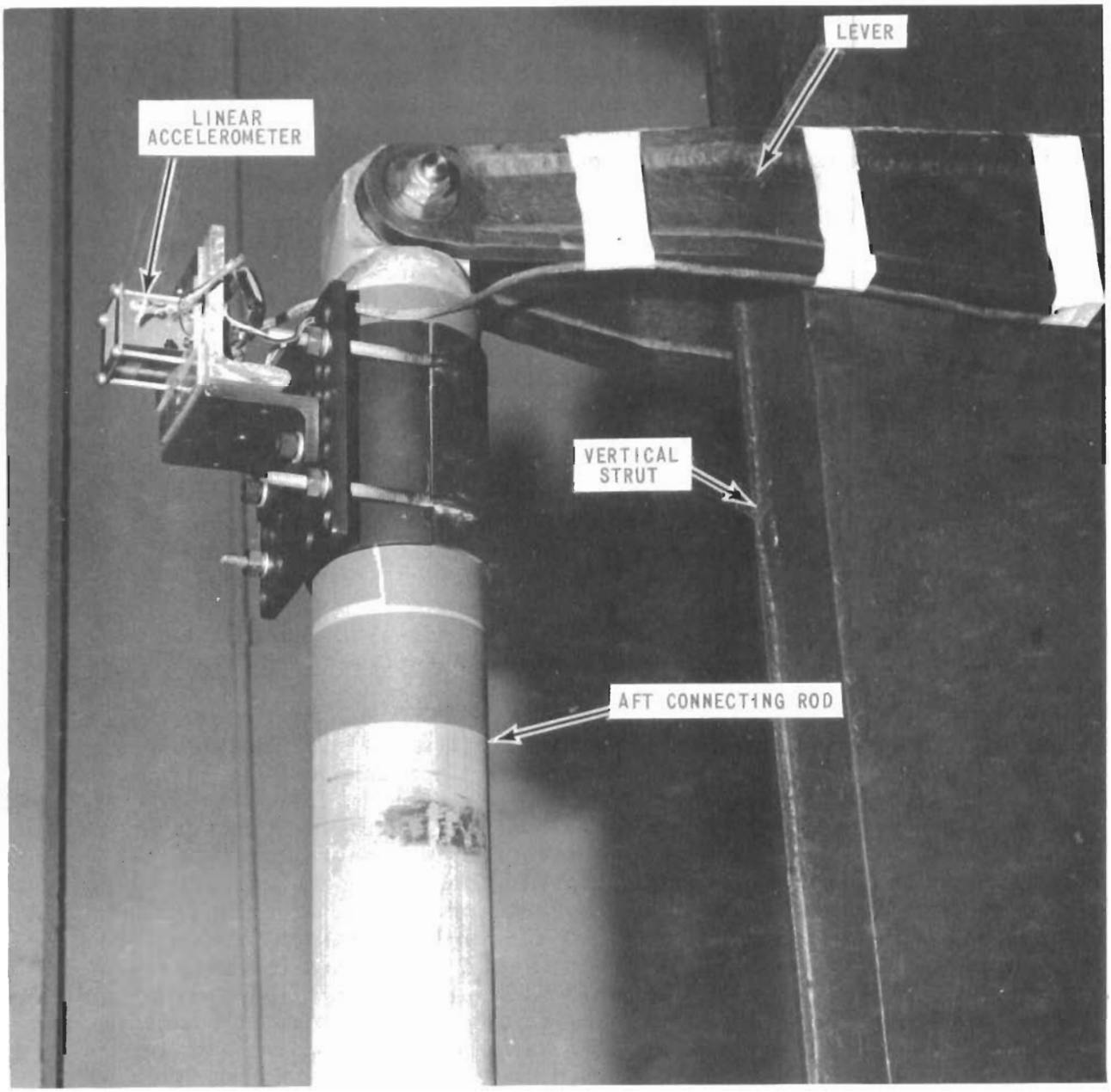

Figure 48 THE MOUNTING OF THE LINEAR ACCELEROMETER ON THE REAR CONNECTING ROD FOR HIGH-g CALIBRATION

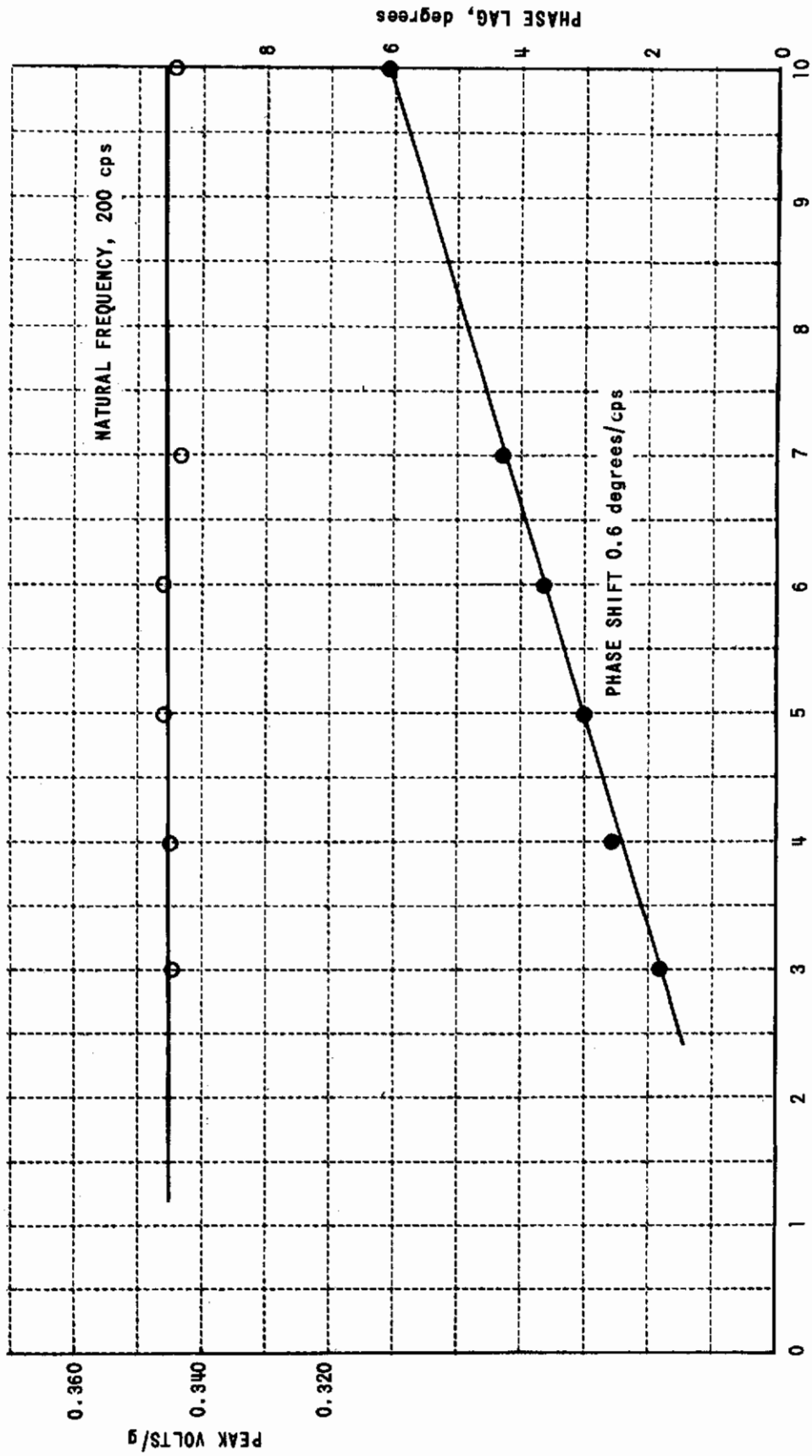

Figure 49 LINEAR ACCELEROMETER CALIBRATION

The Angular Accelerometer

The model's rotary motion about a pitching axis through its c. g. was measured by a unique, specially developed angular accelerometer. This instrument is of the servoed, torque-balanced type and operates as follows:

The angular deflection of the balanced seismic (inertial) element under the influence of the input angular acceleration is detected by an optical sensor whose output is fed back to a torquer coil attached to the seismic element. Due to servo action, the seismic deflection is arrested when the opposing torque equals the torque produced by the product of the input angular acceleration and the inertia of the seismic element. The torque developed by the torquer coil is accurately linear with respect to input current and this current (or a voltage proportional to it) constitutes the output signal of the instrument. The heart of the accelerometer's DC servo system is its optical sensor which provides a high energy output and, therefore, permits high loop-gain operation without the use of amplifiers. The high effective internal gain insures that the seismic deflection will be small and contributes to the instrument's high fidelity performance. The optical sensor is made up of a pair of photo-conductive cells which characteristically change electrical resistance when illuminated by a light source. In the circuitry of the accelerometer, the two cells form the two active resistive arms of a bridge circuit; the other two arms of the bridge are formed by a center-tapped DC supply which powers the instrument. The output of the two photo-active arms of the bridge is sufficient to supply the necessary torquer feedback current without any auxiliary transistor circuitry. While the servo system is comprised of a bridge circuit, the instrument's sensitivity is not affected by power supply variations. In this instrument, feedback constants set gain in a manner similar to methods used in establishing gain of DC operational amplifiers with feedback.

An outline drawing of the angular accelerometer and its installation in the model are shown in Figures 16(a) and (b). Its operating characteristics are presented in the main body of this report in Section 6 - The Force and Motion Sensors.

The angular accelerometer was calibrated on the same machine used to calibrate the linear accelerometer (see Figures 46 and 47). The sketch and photographs presented previously showed that the driven lever is pivoted in a bearing at its lower end. The angular accelerometer was attached at this location where only sinusoidal rotation takes place when the machine is in operation. Sinusoidal angular accelerations up to and in excess of 100 radians/sec.^{2} peak were available. The actual values employed at calibrating points were computed from the angle variation (measured to within ± 3 arc-minutes) and the frequency. The output of the angular accelerometer, like that of the linear accelerometer, was a sinusoidal signal which was converted to DC in the signal analyzer and read out on a digital voltmeter.

Calibration data of the angular accelerometer were taken over the frequency range of 4-10 cps and with acceleration inputs of 17-100 radians/sec.^{2} peak. A mean sensitivity curve was established from these data. The sensitivity is a function of frequency varying from 0.0560 volts/radian/sec.^{2} at 4 cps to 0.0365 volts/radian/sec.^{2} at 10 cps. (Eighty percent of the data points were within $\pm$0.2% of the mean curve and 64% were within $\pm$0.1%.)

With this apparatus for calibrating the linear and angular accelerometers simultaneously, the phase difference between these two transducers as a function of frequency was established over the frequency range of 3-10 cps.

Typical results of these calibrations are presented in Figure 50.

As indicated previously in this report, a most important consideration in the calibration of the angular accelerometer was the measurement of its crosstalk sensitivity. A procedure was developed which used the dynamic testing oscillator and the angular accelerometer itself to produce and measure the motion of this transducer.

The measure of the sensitivity of the angular accelerometer to vertical accelerations was obtained in the following manner. The linear and angular accelerometers were mounted on the forward sting and positioned as they are normally in the model, as shown in Figure 51. At the desired testing frequency, the oscillator motion was set so that the linear accelerometer indicated, say, about 15 g's and the angular accelerometer indicated approximately 1 radian/sec.^{2}. The signal from the angular accelerometer then consists of the vector sum representing the true (but unknown) angular acceleration and the spurious (also, as yet, unknown) output due to the 15 g vertical acceleration. The amplitude and phase of this output signal was recorded. The accelerometer was then rotated precisely 180^o about a vertical axis without changing the oscillator controls, and the signal was again recorded. (A special rotatable platform which was designed for this calibration is shown in Figure 51.) The component of the output signal, which is due to the true angular acceleration, changes its directional sense whereas the crosstalk component, which is due to the mass unbalance, does not. Consequently, the vector sum of these two measurements is equal to twice the output signal due to linear acceleration, i.e., the crosstalk sensitivity. If this output was too large, the orientation of the angular accelerometer about its input axis was changed within its own support bracket. The objective was to orient an imaginary line drawn from the (unknown) center of the seismic mass to the input axis so that it is parallel to the direction of the linear acceleration. After several adjustments, the sensitivity to linear acceleration was reduced to 0.02 radian/sec.^{2}/g, i.e., a 1 g vertical acceleration would cause a signal output from the angular accelerometer equivalent to 0.02 radian/sec.^{2} of angular acceleration input. Repeatibility checks of this sensitivity over a period of several days indicated that a value of 0.02 $\pm$0.02 radian/sec.^{2}/g could be accepted with a high degree of confidence.

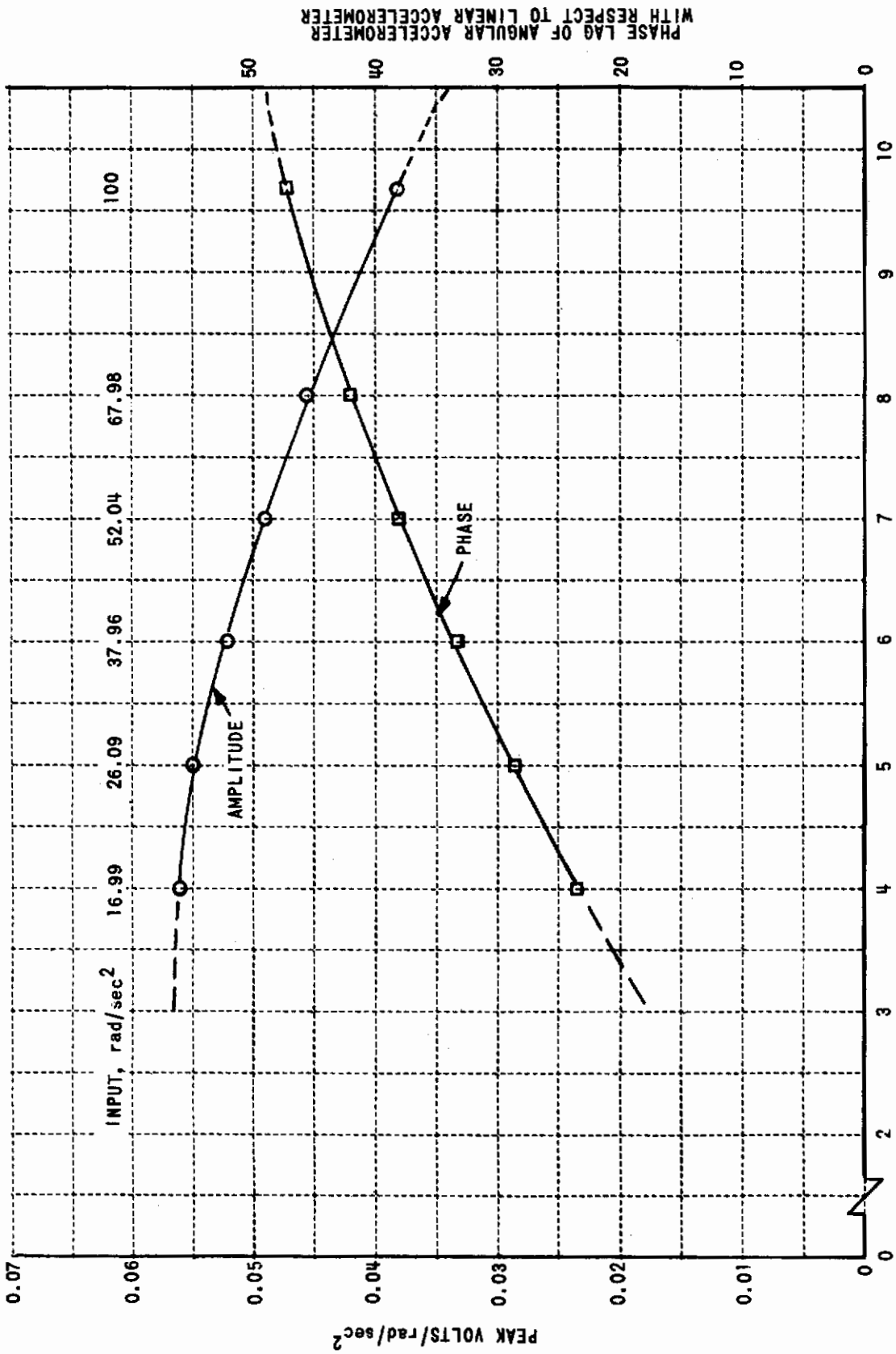

Figure 50 ANGULAR ACCELEROMETER CALIBRATION

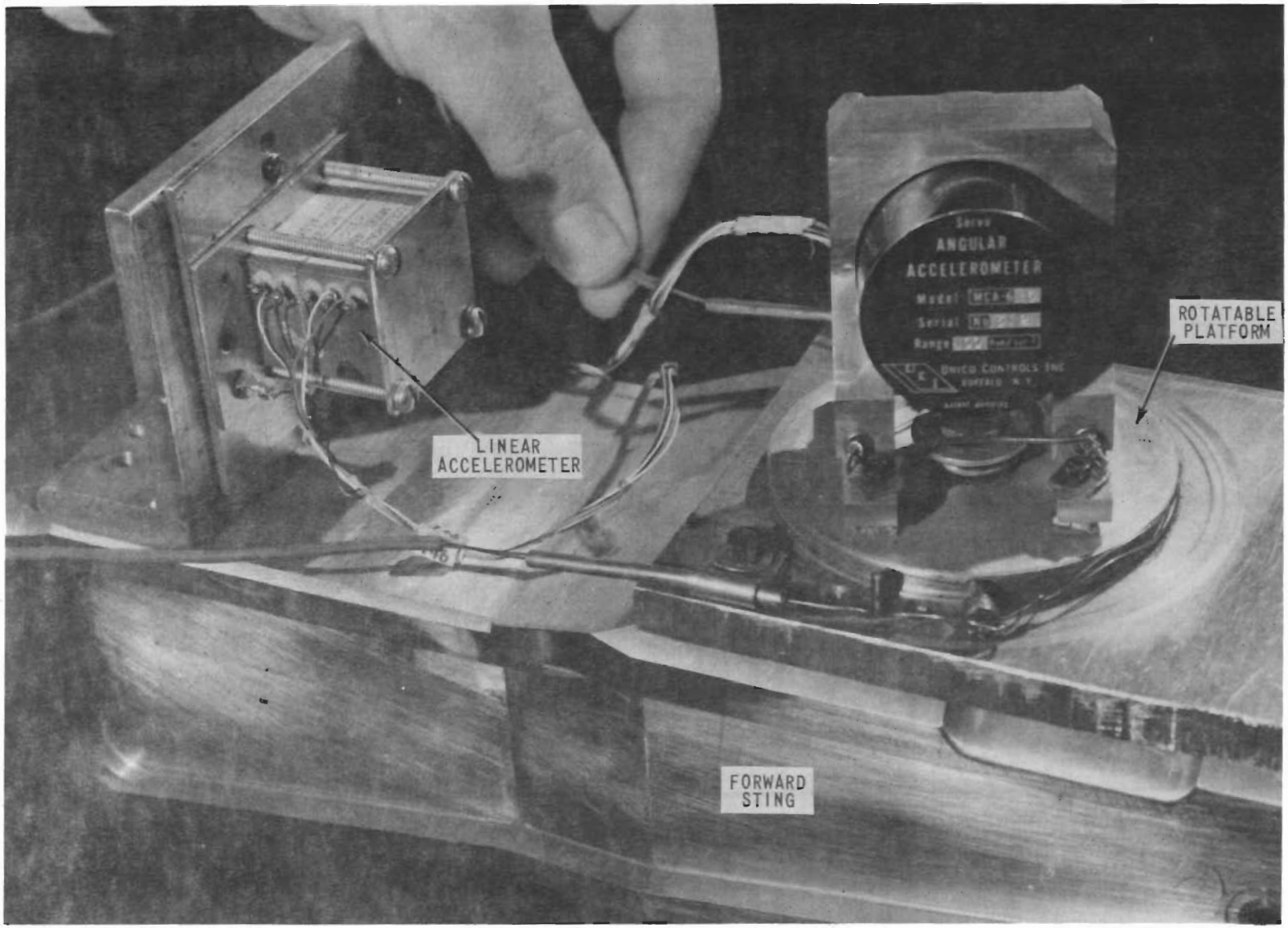

Figure 51 ARRANGEMENT FOR CROSSTALK CALIBRATION OF THE ANGULAR ACCELEROMETER

APPENDIX III

THE SIGNAL PROCESSING SYSTEM*

Introduction

Signal processing is based on a direct analog instrumentation system. An examination of the amplifier and recording system required to process the signals from the transducers discloses that a carrier-type system would not take full advantage of the basic characteristics of the force and motion sensors. For example, the accelerometers develop a direct analog voltage at a 10-volt level. To use this signal in a carrier system would require that the signal be converted to a modulated carrier and then multiplied by a signal derived from the resolver driven by the oscillator shaft. Both of these operations subject the signal to potential noise injection and distortion. Advances in the development of stable DC amplifiers led to the postulation of a direct analog instrumentation system which would preserve the fidelity obtained in the transducers. DC amplifiers of a commercial design were available that would meet the requirements of low noise, low drift, and adequate gain stability. The use of DC amplifiers removed the stringent requirements of carrier phase coherence throughout the system. Signal mixing is readily accomplished by use of operational amplifiers comparable with those regularly employed in analog computer systems.

The signal processing system accepts, simultaneously, the four transducer outputs originating in the model at a particular frequency within the range of 3-12 cps, combines them in prescribed manner, extracts the fundamental signals in the presence of random noise and harmonics, and automatically derives from these signals their phase angles and individual magnitudes. This information is displayed visually and is printed out and punched on IBM cards. A block diagram of the signal processing system is shown in Figure 52. The major subassemblies of this system are (1) the signal mixing unit, (2) the second-harmonic generator, (3) the phase and amplitude analyzers, (4) the signal matching units, and (5) the test signal generator and peak reader.

The Signal Mixing Unit

The signal mixing unit accepts the four signals from the transducers in the model which are related to normal-force, pitching moment, normal acceleration and angular acceleration. The mixing unit contains DC

---

* The authors wish to acknowledge the special contributions to this aspect of the dynamic testing system of Mr. Leland F. Pemberton, currently a Research Instrumentation Engineer in CAL's Computer Research Department. In particular, Mr. Pemberton was responsible for the development of the test signal generator and the peak reader.

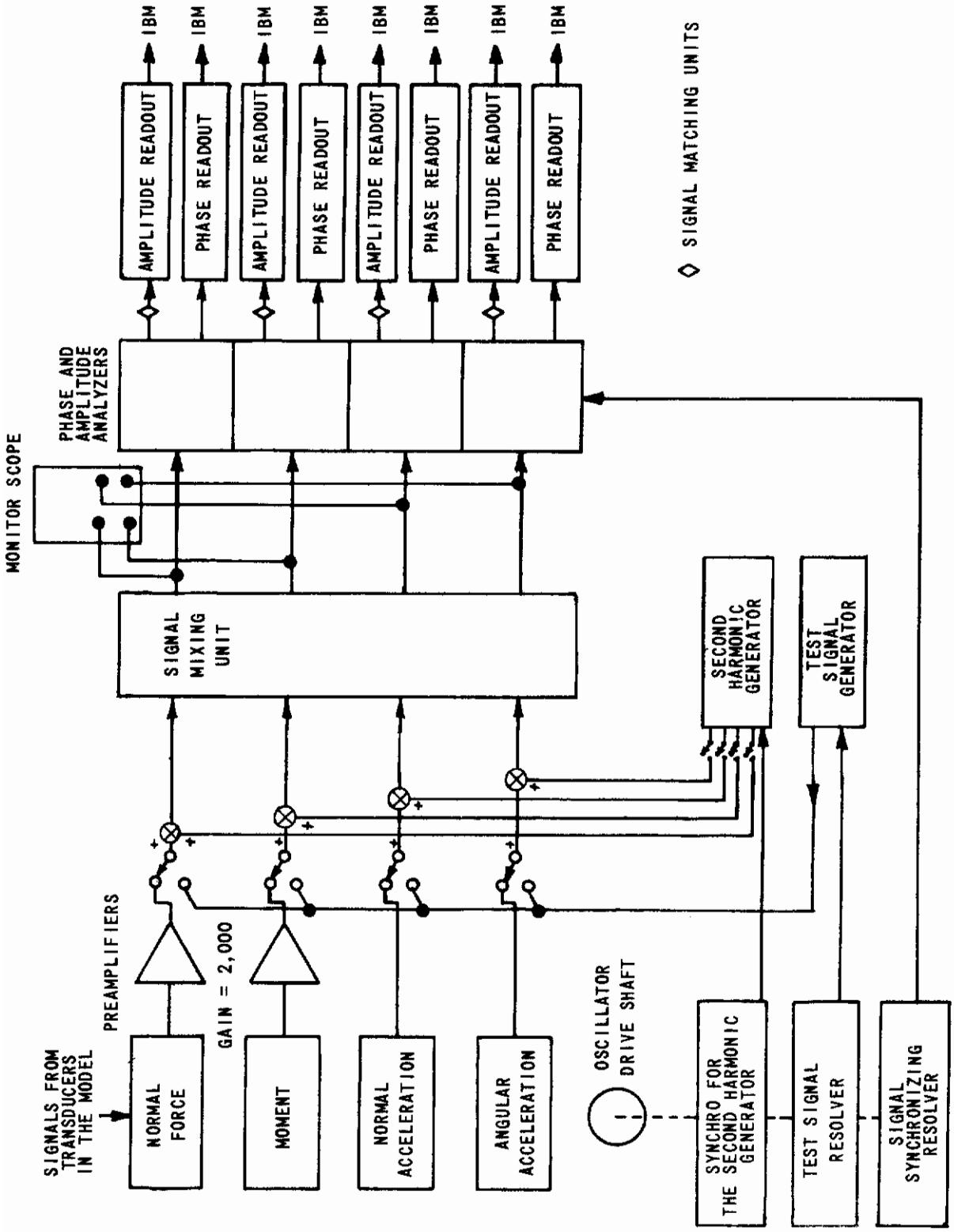

Figure 52 THE BLOCK DIAGRAM OF THE SIGNAL-PROCESSING SYSTEM

amplifiers with gain controls on all four channels to permit suitable scaling of the individual transducer outputs for a given test condition. Phase compensation controls are provided in three of the channels (namely, normal force, moment and linear acceleration) to permit phase equalization so that the signals can be combined as desired. The most important function of the mixing unit is to enable the combining of certain signals in order to allow accurate extraction of desired data signals during wind-tunnel testing conditions. The operations performed in the signal mixing unit are indicated in Figure 19, and the control panel for the unit is indicated in the photograph of the dynamic testing control room in Figure 7. A schematic diagram of the signal mixing unit showing how these operations are mechanized is presented in Figure 53. The signal from the normal-force strain beams can be combined with signals from the linear accelerometer and the moment beam; the signal from the pitching-moment strain beam can be combined with signals from the linear accelerometer and the angular accelerometer. The procedures for setting up the gains, the phase compensations, and the combinations of signals were described in the main text of this report in Section 9, titled "System Evaluation Tests".

The Second-Harmonic Generator

It was indicated previously in this report that the primary distortion of the waveform of the model motion is attributable to the second-harmonic input due to the kinematics of the crank-connecting rod. This second-harmonic content of the model motion becomes particularly troublesome during pure plunging at high g levels when it is required to minimize the rotational motion at the fundamental frequency. Under these circumstances, the kinematics of the cart oscillator are such that the second-harmonic rotational signal can be two or more orders of magnitude larger than the fundamental component. Although the phase and amplitude analyzers are extremely insensitive to signals outside the fundamental frequency, they cannot contend with the ratio that exists when the fundamental must be minimized. Such extremely low signal-to-noise ratios exceed the capability of these analyzers. When such conditions prevail, the character of the signals as monitored on the oscilloscope is obscured, and the phase and amplitude analyzers exhibit a random, small amplitude variation in their outputs when operating in the "high-gain" mode.

To overcome this problem, a means was developed for canceling the second-harmonic components of the signals at the output of the model transducers. The signal mixing unit is designed to accept adjustable signals into all four channels from a source of pure second-harmonic signal. A summing junction at the input of each of the four mixer channels makes it possible to introduce, at these points, a second-harmonic signal which can be independently adjusted in magnitude and phase for each channel.

The second-harmonic signal used for canceling is generated by a synchrotransmitter on the cart which is geared to turn at two times the oscillator driveshaft speed. The voltage output of this synchrotransmitter

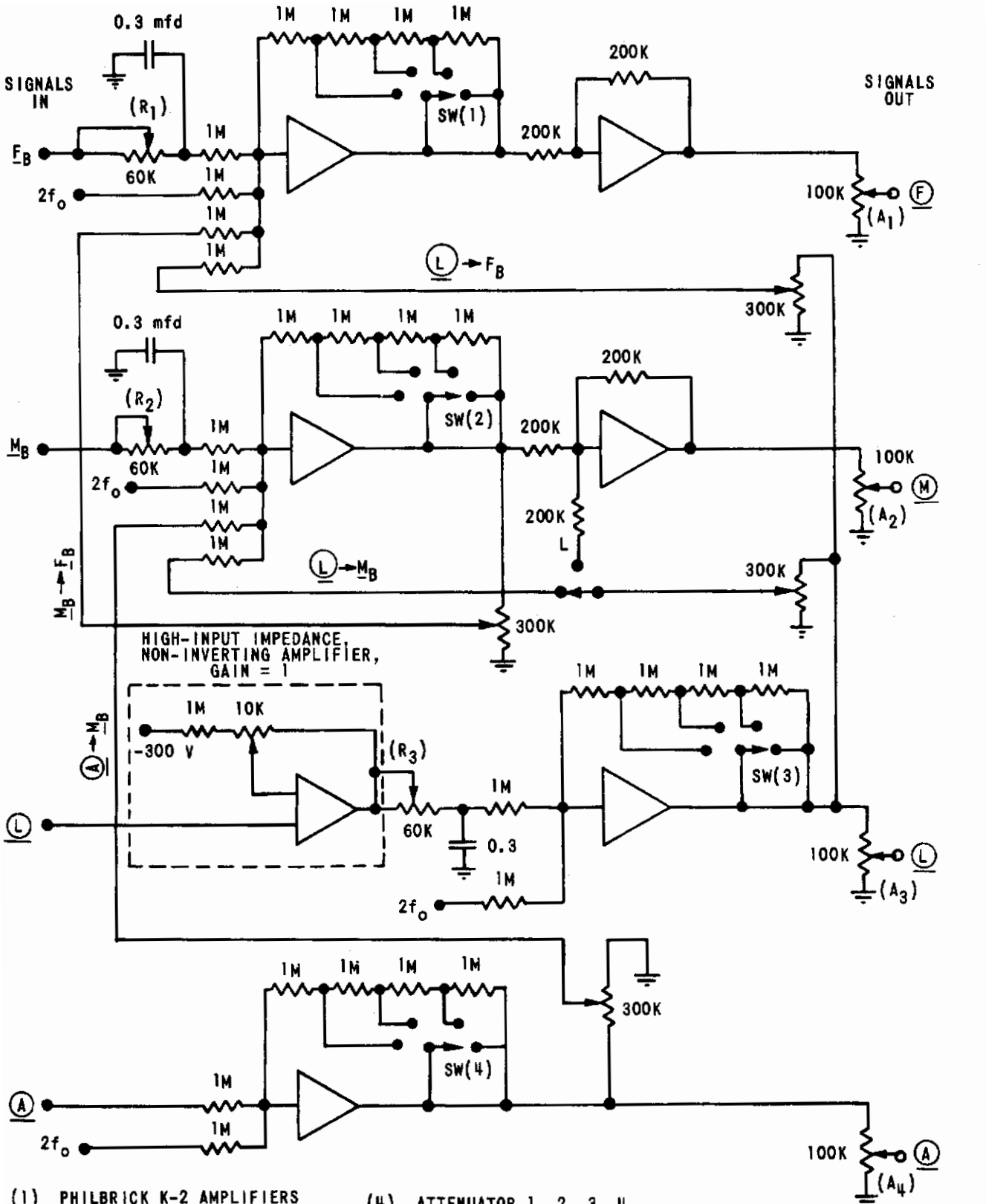

(1) PHILBRICK K-2 AMPLIFIERS
(2) $2f_o$ = SECOND HARMONIC
(3) SWITCH 1, 2, 3, 4 COARSE GAIN
(4) ATTENUATOR 1, 2, 3, 4 FINE GAIN
(5) RESISTOR 1, 2, 3 PHASE LAG CONTROL

Figure 53 SCHEMATIC DIAGRAM OF THE SIGNAL MIXING UNIT

is fed through cables to the control room where it connects to a chassis containing four synchros used as phase shifters, four amplitude controls, and associated demodulators and low-pass filters. This chassis provides, therefore, four sources of second-harmonic signal controllable in their phases and amplitudes which, in turn, are mixed with sensor signals coming from the model. The schematic for the second-harmonic signal generator is shown in Figure 54.

The Phase and Amplitude Analyzers

From the signal mixing unit, the four signals are fed to the phase and amplitude analyzers. These units constitute the heart of the signal processing system, since they provide the capability to measure in real time the amplitude and phase of only that component of each signal which is at the reference frequency.

The problem of extracting the desired information from the noisy signals generated by the transducers is considerably more difficult in dynamic wind-tunnel tests than it is in static. In either case, the signal-to-noise ratio is generally low because of the high-level vibration environment to which a model is subjected during wind-tunnel testing. Examination of this problem in the early phases of the program indicated that the noise could be expected to have a broad spectrum of random frequencies at high-energy levels which could not be filtered by conventional techniques during dynamic tests. During static wind-tunnel tests, a low-pass signal filter with sufficiently low cutoff frequency is all that is needed to permit the reading of the DC component of the signal. During dynamic wind-tunnel tests, on the other hand, it becomes necessary to read the amplitude and phase angle of the particular component of the signal at the oscillator driveshaft frequency. Furthermore, it is necessary that this be accomplished with equal accuracy for any reference frequency over the entire operating range of 3-12 cps.

In recognition of the very special requirements which dynamic testing imposes on the signal processing system, CAL initiated the development of the "phase and amplitude analyzers". Four channels of these units have been provided by CAL for use with the dynamic testing system.

These units are indicated in the photograph of the dynamic testing control room presented in Figure 7. A block diagram of one channel of this signal analyzer system is presented in Figure 55. This diagram aids in the explanation of the operation of the unit and, for the sake of clarity, various signal amplifiers, power supplies, and standardizing circuits are not shown.

The reference oscillator shown in the diagram of Figure 55 is common to all four channels. Its output is a 4,000 cps signal derived from a temperature-controlled quartz resonator. The output from the reference oscillator is the excitation voltage of the synchronizing resolver (also common to all four channels) and of a servo-controlled phase resolver

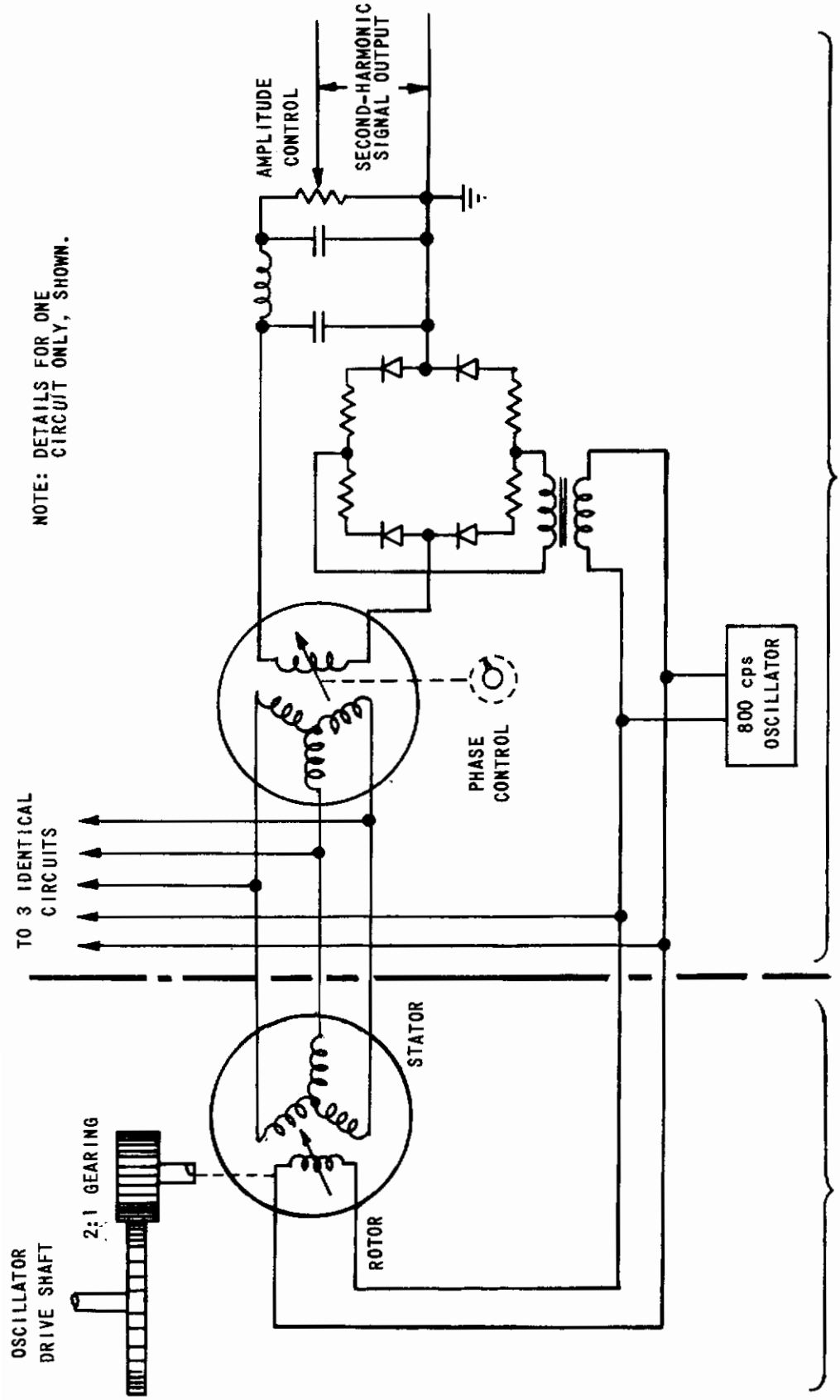

Figure 54 SCHEMATIC DIAGRAM OF THE SECOND-HARMONIC SIGNAL GENERATOR

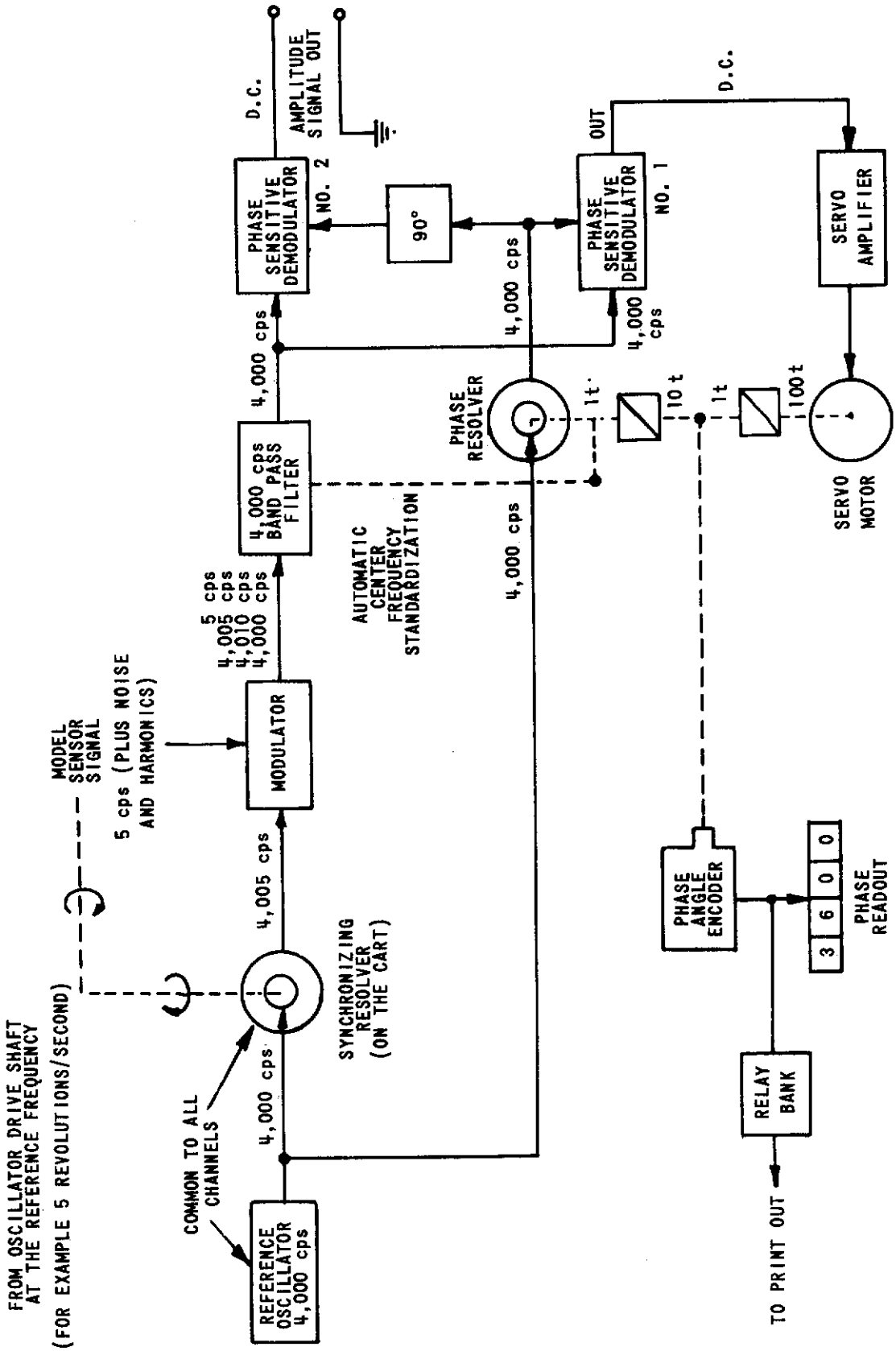

Figure 55 THE BLOCK DIAGRAM OF ONE CHANNEL OF PHASE AND AMPLITUDE ANALYZERS

contained in each channel. The synchronizing resolver is located on the cart, and its shaft is driven by one of the powered shafts on the model drive mechanical oscillator. This resolver operates as a continuous phase shifter. As it rotates, it adds 360° of phase to its 4, 000 cps excitation signal for every revolution it makes. Therefore, if, for example, it is turned at a speed of 5 rps, the resolver adds to the 4, 000 cps voltage five complete cycles for each second it is turning. The output of the resolver under these conditions is therefore 4, 005 cps. Under these conditions, the output signals from the model sensors must also be predominantly at 5 cps, since both the synchronizing resolver and the model are directly driven by the mechanical oscillator.

The signal from the model sensor consisting of components at 5 cps plus noise and harmonics and the 4, 005 cps signal from the synchronizing resolver are inputs to a precision feedback modulator. The output of this modulator is a composite signal comprised of, primarily, each of the input frequencies plus their sum and difference frequencies. In the example case shown in Figure 55, the components are at frequencies of 5 cps, 4, 005 cps, 4, 010 cps, 4, 000 cps, and 4, 005 cps plus or minus the frequencies of noise and harmonics. This composite signal is the input to a narrow band-pass, high-"Q", quartz-crystal filter whose center frequency is maintained precisely the same as that of the reference oscillator (4, 000 cps). Due to its very high selectivity, this filter passes only the 4, 000 cps component and rejects all the other components of the composite input signal. The amplitude of this 4, 000 cps component is accurately linear with respect to the magnitude of the 5 cps signal from the model sensor by virtue of the linearity of the modulator. The phase angle of this 4, 000 cps component with respect to the 4, 000 cps voltage from the reference oscillator is the same as the phase angle difference that exists between the model input motion and the 5 cps component of the model sensor output signal.

The pure 4, 000 cps signal from the band-pass filter is the input to two phase-sensitive demodulators. The 4, 000 cps output signal from the servo-controlled phase resolver is the phase reference for demodulator #1. The 4, 000 cps output of the phase resolver, shifted in phase by precisely 90°, is the phase reference for demodulator #2. When the phase angle of the input signal to demodulator #1 is not precisely 90° with respect to the phase resolver signal, a DC voltage exists at the output of this demodulator. This DC voltage is the input to a servo amplifier which drives a servo motor geared to the phase resolver. The directional sensing in the servo system is arranged to cause the servo to drive the phase resolver until its output phase is 90° from the input signal. When this angle is reached, the demodulator output drops to zero and the servo comes to a stop. The servo also drives a brush-contact-type, shaft-angle encoder which has a resolution of 0. 1°. Through transistor logic circuits, this encoder operates an illuminated readout display and relay banks which serve as the interface between the phase information and the IBM printout and cardpunch. When the servo is at rest, the phase readout display indicates the phase angle that exists between the oscillator driveshaft motion and the output of the model sensor at the reference frequency.

Under the conditions of phase servo balance, the voltage output from the phase resolver is precisely 90° from the input signal to the demodulator #1. It therefore cannot produce an output at demodulator #2, which is the signal amplitude demodulator. To correct this, a fixed 90° phase-shift network is introduced in the reference voltage circuit of demodulator #2. This network returns the reference to zero phase with respect to the input signal for this demodulator, and the result is a DC output voltage proportional to the 5 cps component of the signal from the model sensor. This output voltage is fed to the signal matching unit which makes it compatible with the standard CAL wind-tunnel data readout system.

It is worth reiterating the unusual filtering capabilities provided by these phase and amplitude analyzers. From Figure 56, which shows the filtering characteristic of these analyzers, it can be seen that the response to a frequency 2.5 cps away from the reference frequency is attenuated by 1,000 times (or 60 db) more than the response to the center pass frequency. This filtering characteristic is constant and independent of the reference frequency. That is, it is synchronous to the fundamental frequency in the sense that the center pass frequency is always the same as the frequency of the component of interest. This unique filter feature is also required for a proper operation of the amplitude and phase measuring techniques employed in the analyzers.

An indication of the effect of these phase and amplitude analyzers in the operation of the total signal processing system can be obtained by examining the records presented in Figure 57. These are oscillograph records of the "raw" signals produced at the outputs of the signal mixing unit and are typical of the four signals to the analyzers which were obtained during the wind-tunnel tests using the F-80 model. The conditions were pure pitching motion of the F-80 model at a fundamental frequency of 5 cps and Mach number of 0.8. Cancellation of the second-harmonic components in the signal mixing unit was not used in this example. In trace #1 at the top (normal force), note that the fundamental frequency component can be seen but its amplitude is obscured by distortion caused by a second-harmonic component. Trace #2 is the aerodynamic moment signal. The inertial component has been canceled in the mixing unit. Trace #3 is the signal from the linear accelerometer which has considerable second-harmonic content and higher frequency noise. Trace #4 is the output of the angular accelerometer and, in this case, the fundamental component is practically invisible in the noise and second-harmonic frequencies.

The components at the fundamental frequencies extracted from these signals were indicated by the phase and amplitude analyzers to be the following:

(1) aerodynamic normal force, 16 lbs. at 212.7°,

(2) aerodynamic pitching moment, 2.5 ft. lbs. at 218.6°,

(3) linear acceleration, 12 g's at 215.8°,

(4) angular acceleration, 13.5 radians/sec.^{2} at 305.4°.

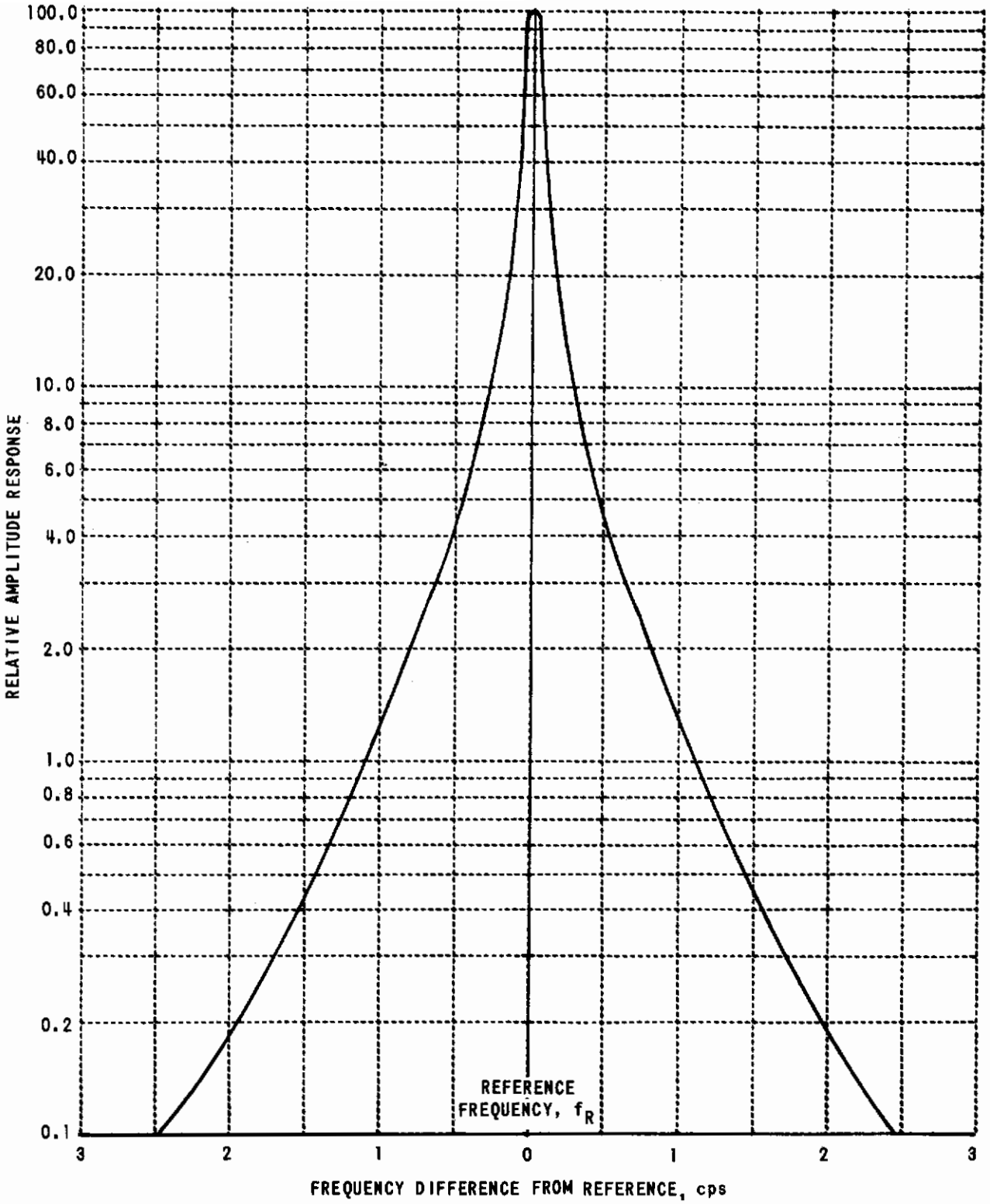

Figure 56 BAND-PASS CHARACTERISTICS OF THE PHASE AND AMPLITUDE ANALYZERS

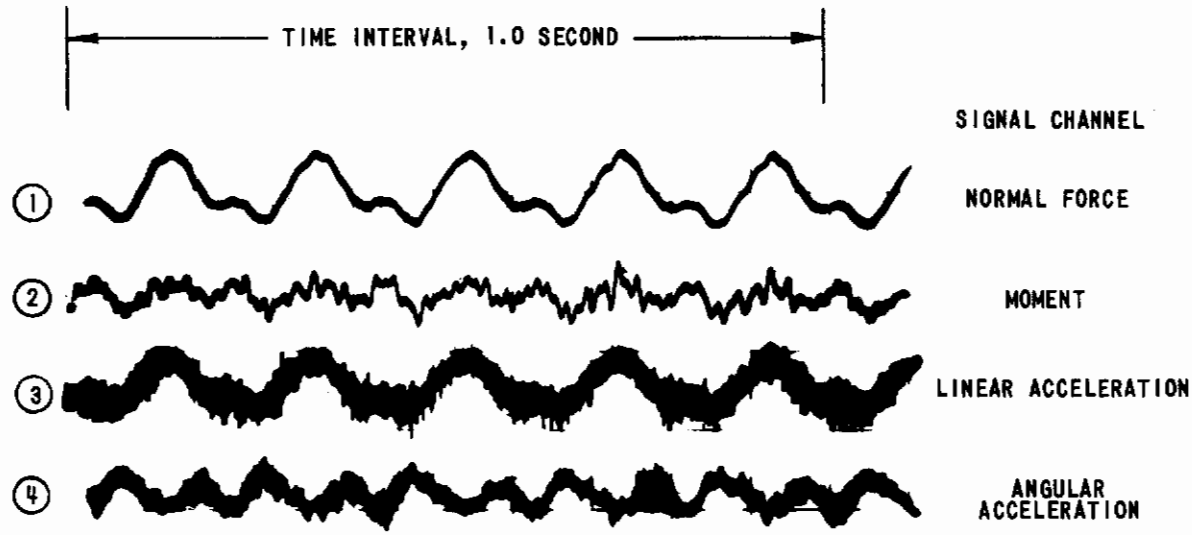

NOTE:
NO SECOND HARMONIC CANCELLATION
NO INERTIA CANCELLATION IN NORMAL FORCE

Figure 57 TYPICAL SIGNALS AT THE INPUTS TO THE PHASE AND AMPLITUDE ANALYZERS F-80 MODEL, PURE PITCH, 5 cps, M = 0.8

A measure of the overall stability of the system, as well as the noise rejection capability of the phase and amplitude analyzers, is given by the variations in the readouts about these indicated values. This was typically about $\pm 1\%$ in amplitude and $\pm 0.5^{\circ}$ in phase.

The Signal Matching Unit

This unit contains the circuitry necessary to make the output circuits of the phase and amplitude analyzers compatible with the requirements of the available CAL wind-tunnel data readouts (digital voltmeters).

One output of each analyzer channel is a DC voltage referenced to ground which rises to 20 volts for a full-scale signal input (approximately 10-volt peak) and is proportional to the amplitude of this input signal. The CAL wind-tunnel readouts require a differential voltage input, both terminals of which must be held approximately 60 volts above ground. The signal matching unit contains the necessary bias supplies and voltage-divider networks to convert the ground-referenced analyzer signals into the differential, above-ground signals required by the CAL wind-tunnel readouts. A circuit diagram of one of the four identical matching units is shown in Figure 58.

The Test Signal Generator and Peak Reader

The gain of each of the four signal processing channels can be varied to suit the conditions of a particular test. The gain is generally selected to give near full-scale readout for the maximum transducer signal expected to exist during that test.

The gain of the signal processing channel refers to the instrumentation transfer gain between the peak value of a low-frequency (3-12 cps) sine-wave input signal to the signal processing system and the resultant readout which is steady-state and displayed on a digital voltmeter. The gain calibration is made by introducing at the input to each signal processing channel a low-frequency sinusoid (whose peak amplitude can be measured with high precision) and observing the steady-state output displayed on the readouts. The calibrating equipment described herein was developed during this program by CAL. Test equipment capable of measuring the amplitudes of such low-frequency sine waves to the required accuracy of 0.1% or better was nonexistent.

The test signal generator is composed of two major parts — (1) a pure sine-wave signal source, and (2) a precision measuring circuit called a "peak reader" which accurately determines the magnitude of the test signal sine wave.

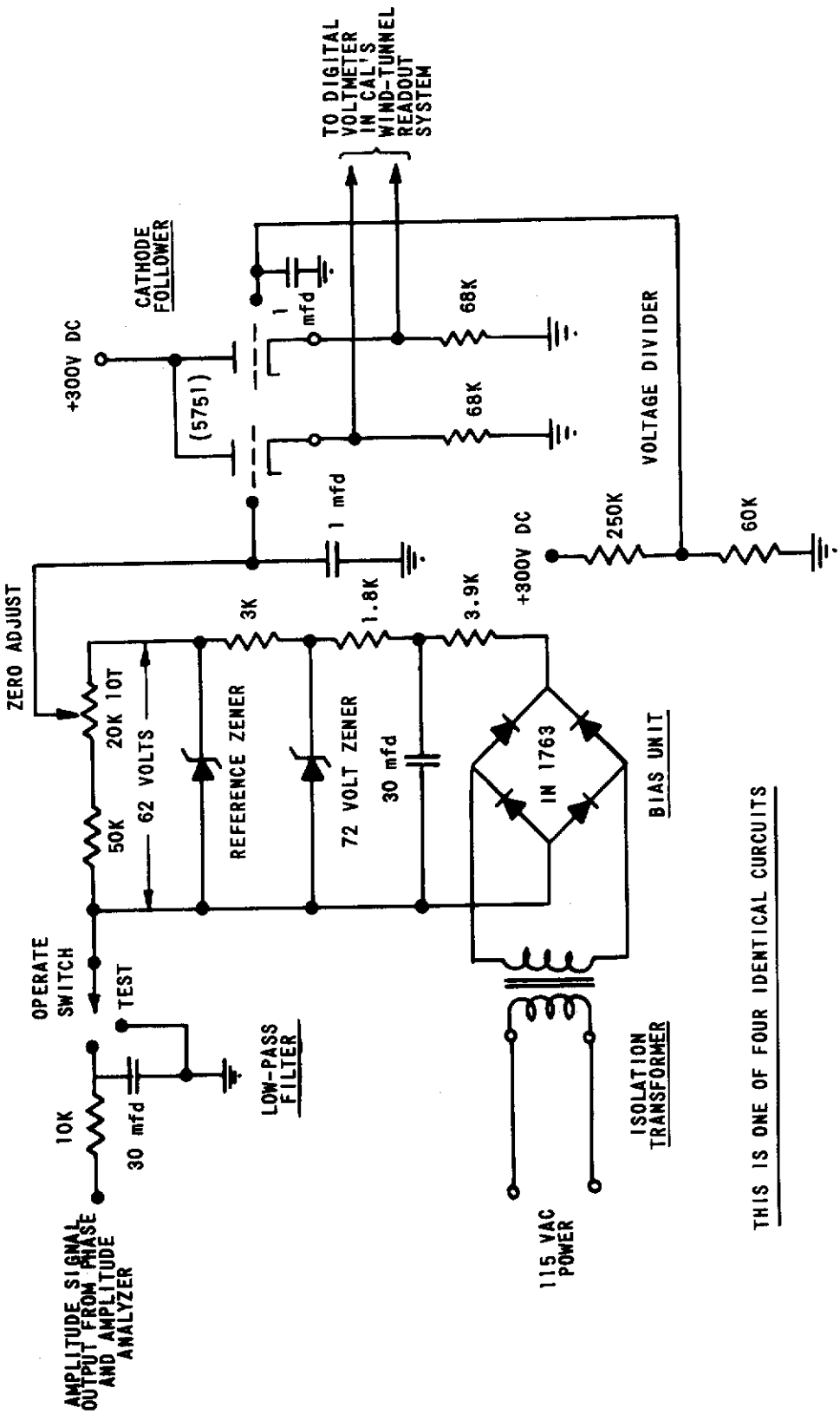

Figure 58 SCHEMATIC DIAGRAM OF THE MATCHING UNIT FOR AMPLITUDE READOUT FROM ONE CHANNEL

The sine-wave test signal is derived from a rotating resolver which is turned by a shaft connected to the oscillator driving system. The test signal so derived is therefore at the same frequency (between 3-12 cps) as the model oscillating frequency. The stator of this resolver is excited by a 2000 cps oscillator. A resolver can be likened to a transformer having a movable secondary winding (rotor) with respect to a fixed primary winding (stator). When the shaft is turned, the mutual coupling between these windings changes and, as a result, a voltage is induced in the rotor winding which varies in magnitude as the sine of the rotor's angular position. Thus, as the rotor turns, the voltage at the output winding of the resolver is a 2000 cps signal which is amplitude-modulated at the rotor-turning frequency. This voltage is amplified and fed to a coherent demodulator and a low-pass filter which removes the 2000 cps carrier frequency and leaves the low-frequency sinusoid. This signal is then fed to an active filter, a high-resolution variable amplitude control and, finally, to an output amplifier having a low output impedance. A block diagram of the system is shown in Figure 59.

The test signal so generated possesses a high degree of symmetry and very low distortion (less than 0.1%). This high degree of waveform purity is not a requisite of the signal processing channels, since they have the designed-in ability to discriminate against waveform distortion components. It is the requirement on the measurement of the amplitude of the calibrating signal that demands it to be distortion free. In order to be able to use this test signal for calibration of the signal processing system, its magnitude must be adjustable and measurable to a high degree of accuracy. Circuitry of the so-called peak reader provides this function, and its accuracy diminishes if the fundamental waveform is distorted by harmonic frequencies.

The peak reader is capable of accurately measuring the peak value of the calibrating test signal. The heart of this measuring circuit is a voltage comparator which can indicate when the peak value of a pure sine-wave signal is equal to a DC voltage that can be accurately measured on a digital voltmeter. The comparator uses a direct-coupled, high-gain, analog-computer-type operational amplifier whose feedback loop is closed through resistor and biased-diode networks. (A schematic of the peak reader is shown in Figure 60.) The input summing junction of the comparator amplifier accepts three voltages — a negative DC 30-millivolt bias, a low-frequency (3-12 cps) sine-wave test signal which is adjustable, and a DC reference voltage of measurable value. The output of the comparator is monitored on an oscilloscope. In operation, the DC reference voltage is set to equal the desired test signal peak voltage to be used in the calibration of the signal processing system. (During the F-80 model tests, the gains of the various channels were such that 3.5 volts was an optimum value to use for the test signal. In this case, therefore, the DC reference was set to 3.5 volts DC as measured by a digital voltmeter.)

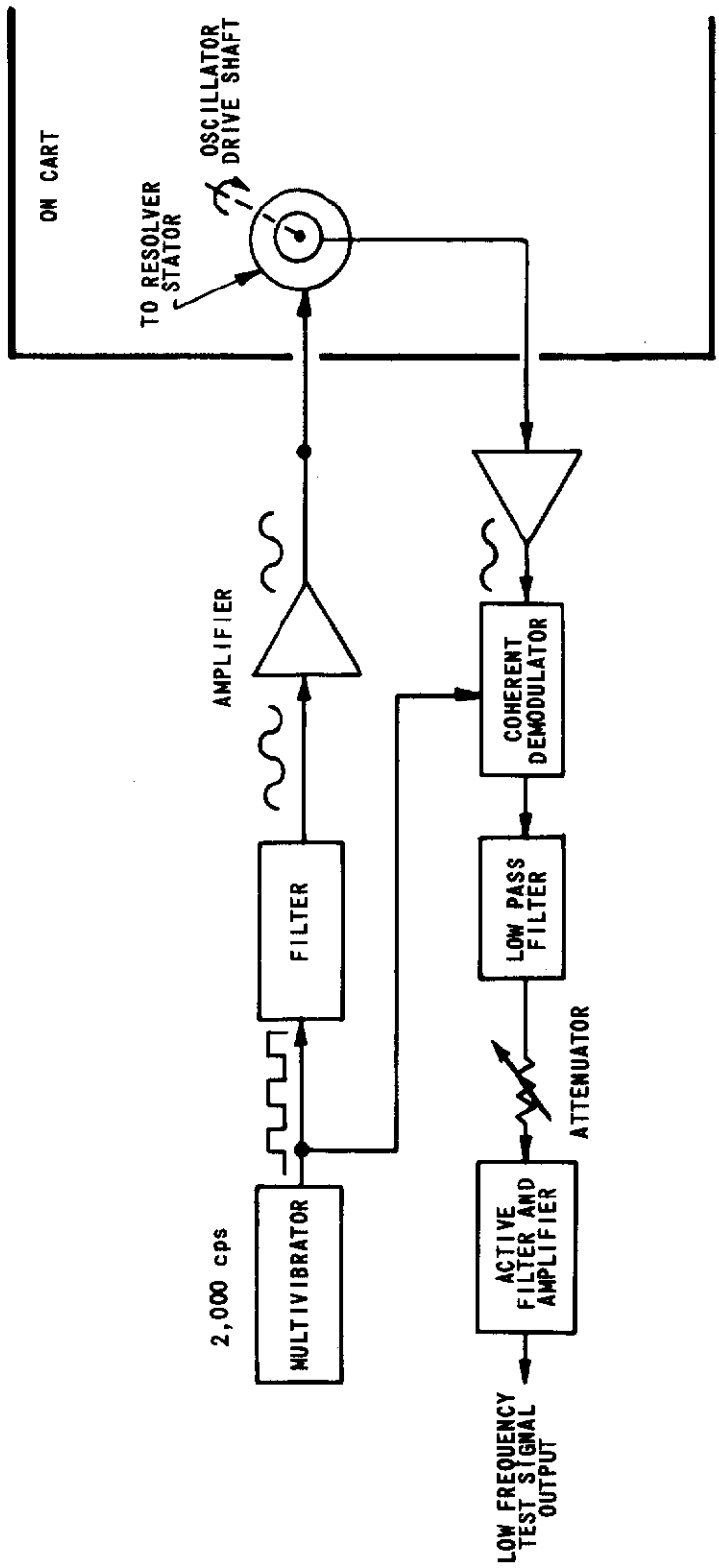

Figure 59 THE BLOCK DIAGRAM OF THE TEST SIGNAL GENERATOR

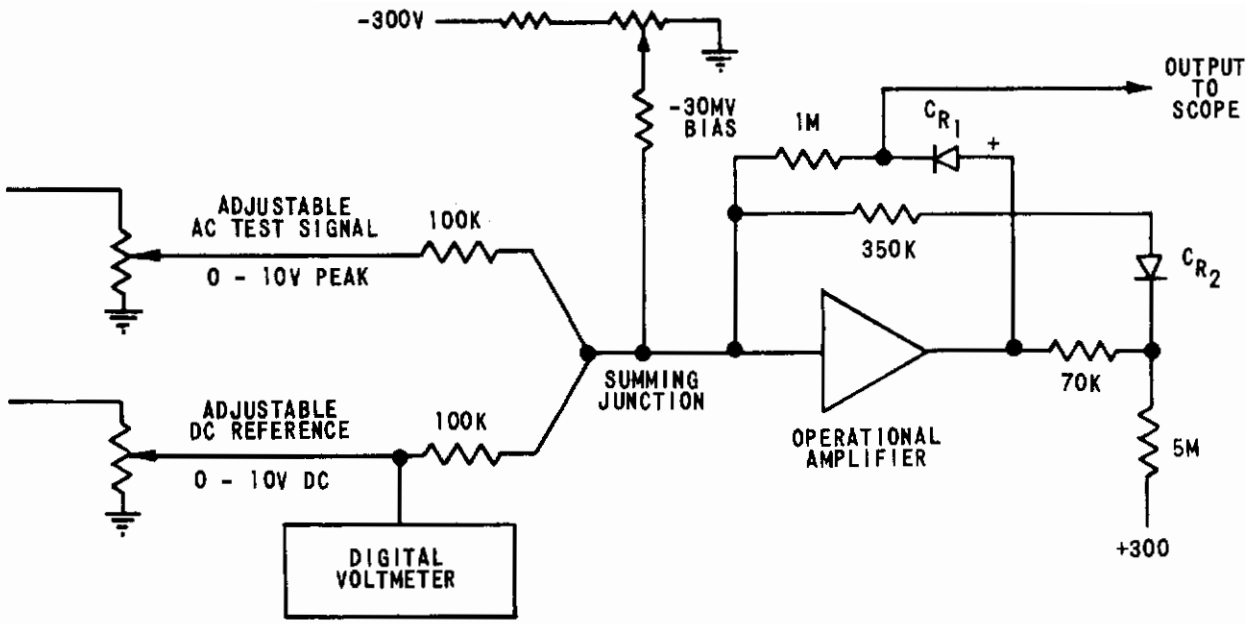

Figure 60 SCHEMATIC DIAGRAM OF THE PEAK READER

The portion of the positive half of the sine wave above the base line set by the DC reference voltage appears at the output of the comparator and is observed on an oscilloscope. The test signal voltage is then varied until the scope indicates an output value that peaks above the reference by 30 millivolts. Under these conditions, the peak value of the test signal is equal to the accurately established DC reference voltage. The 30 millivolt surplus used to indicate when equality is reached is automatically subtracted from the real value of the test signal by the fixed 30 millivolt DC bias applied to the input of the comparator. With a vertical scope sensitivity set to 0.01 volts/cm, a test signal of the order of 5 volts peak can be measured to within $\pm$4 millivolts.

APPENDIX IV

SYSTEM ACCURACY REQUIREMENTS

Reference 16 reports the results of a study which was concerned with the probable accuracies to be expected in the aerodynamic derivatives as measured by dynamic tests in a wind tunnel. This study was undertaken to point out important sources of errors, as well as to indicate the feasibility of measuring the separate parts of the rotary damping derivatives. Numerical accuracy studies were carried out using the parameters of the F-80 model.

After reviewing various techniques, it was concluded that the system of dynamic testing which promised the greatest likelihood of success and utility uses a sting-mounted, internal strain-gage balance system which measures total forces and moments acting on a model that can be inexorably forced at various reduced frequencies. A further requirement is that the motion of the model itself be measured directly with greatest accuracy.

Subsequently, a study was made of how errors in the individual measurements and the failure to operate exactly at desired test conditions affect the overall accuracy with which dynamic stability derivatives can be measured by such a system. Expressions were derived for the probable errors in derivative determination resulting from basic measurement errors. These were applied to a particular case in order to indicate the relative importance of errors in the various measurements. The case considered was the measurement of the rotary damping derivatives of the F-80 model at a Mach number of 0.7 and a reduced frequency of $\omega c/2U = 0.02$. Results of this study were used to establish the accuracy and performance requirements prior to design of the present dynamic testing system.

Instrumentation and Oscillator-Control Requirements

There are two ways in which the actual dynamic tests in the wind tunnel might deviate from the ideal test technique. First, the motions imparted to the model by the oscillator might differ somewhat from the desired test condition. Second, there might be errors in the measurements of the model motions and of the forces applied to the model.

A study was made of the requirements which must be placed on the instrumentation accuracy and on the mechanism for adjusting the oscillator to desired test conditions. A first step in establishing criteria for the required accuracies in the basic test data was to select acceptable tolerances in the measured derivatives. These tolerances were arbitrarily set as follows:

The error in C_{L_α} shall be less than 10% of C_{L_α}.

The error in C_{m_α} shall be less than 10% of C_{m_α}.

The error in $C_{m_{\dot\alpha}} + C_{m_{\dot\theta}}$ shall be less than 10% of $C_{m_{\dot\alpha}} + C_{m_{\dot\theta}}$.

The error in $C_{m_{\dot\alpha}}$ shall be less than 10% of $C_{m_{\dot\alpha}} + C_{m_{\dot\theta}}$.

The error in $C_{m_{\dot\theta}}$ shall be less than 10% of $C_{m_{\dot\alpha}} + C_{m_{\dot\theta}}$.

The measurement accuracies of the static lift derivative, the static moment derivative, and the total rotary damping derivative, $C_{m_{\dot\alpha}} + C_{m_{\dot\theta}}$, were expected to be well within the 10% error indicated. However, when using them to determine the requirements for the measurement of the separate components, $C_{m_{\dot\alpha}}$ and $C_{m_{\dot\theta}}$, it was assumed that these quantities were known only to within 10%.

The acceptable errors in the measurement of $C_{m_{\dot\alpha}}$ and $C_{m_{\dot\theta}}$ were specified as a percentage of the total rotary damping derivative. The rationale was that, if either of these components is a small percentage of the total damping derivative, it will have a comparatively small affect on stability characteristics and the accurate measurement of such a derivative would be less important.

CAL's previous experience in instrumentation techniques applied to the measurement of derivatives in the dynamic testing equipment [14, 15] indicated that the principal problem was one of separating useful signals from wide-band noise induced by tunnel turbulence and mechanical vibration. Efforts in the mechanical design of the balance system were, therefore, directed at increased signal-to-noise ratios by tailoring each transducer to its separate measurement. This was accomplished, in part, by separating the force and moment measurements. If the forward balance beams were located precisely at the c. g. of the model, then the aft balance beam signal would be due only to the moment applied about the c. g., thereby reducing the probable errors in moment measurement. Similar considerations indicated the need for a separate angular accelerometer which featured high damping and was not sensitive to linear acceleration. The establishment of reasonable instrumentation requirements was based, therefore, on a measurement of angular acceleration by an angular accelerometer insensitive to plunging acceleration, rather than by the difference between the outputs of two linear accelerometers. It was also assumed that the forward balance beams were located very close to the model c. g. The normal forces on the model then have a negligible influence on the loads in the beam displaced from the c. g., and the signals from the aft beam are proportional to the moment about the c. g.

An error analysis of the measurement accuracy of $C_{m_{\dot\alpha}}$ from plunging tests was based on the assumptions that

(1) the tunnel velocity is known to $\pm$1%,

(2) the fundamental oscillation frequency is known to $\pm$1%,

(3) the magnitude of the plunging acceleration is known to $\pm 2\%$,

(4) the magnitude of the balance moment is known to $\pm 2\%$,

(5) the phase angle between the balance moment and the plunging acceleration is known to $\pm 1^{\circ}$,

(6) the geometry, mass, and inertia of the model are known exactly, and

(7) C_{m_α}, and $C_{m_{\dot\alpha}} + C_{m_{\dot\theta}}$ are known to $\pm 10\%$.

The assumed errors in the tunnel velocity, the oscillation frequency, the value of C_{m_α}, and the value of $C_{m_{\dot\alpha}} + C_{m_{\dot\theta}}$ were not large enough to appreciably influence the determination of $C_{m_{\dot\alpha}}$ and, yet, these accuracies are easily obtainable with CAL equipment. The error in the measurement of $C_{m_{\dot\alpha}}$ due to the combined effect of assumed errors in all these quantities was less than 2% of $C_{m_{\dot\alpha}} + C_{m_{\dot\theta}}$. This result pertains when the oscillator has been adjusted to give a nominal plunging condition within the limits given in the following discussion.

Errors in the measurement of the magnitude and phase of the extraneous rotational motion constitute the primary sources of error in the measurement of $C_{m_{\dot\alpha}}$ during plunging tests. The physical explanation for the large effect of this residual rotational motion is that only a very small rotational acceleration can cause a moment due to inertial reaction which is large compared with the moment associated with $C_{m_{\dot\alpha}}$ and the translational acceleration.

If the angular accelerometer is used as a null-reading device in conjunction with adjustments to the oscillator to eliminate unwanted rotational motion in plunging tests, then the magnitude of the angular acceleration can be reduced to the magnitude of the error in angular acceleration measurement. Even if the most unfavorable phase relationship between rotation and translation existed in the resultant motion, the error in $C_{m_{\dot\alpha}}$ due to the residual rotation would be only about 4% of $C_{m_{\dot\alpha}} + C_{m_{\dot\theta}}$ if the magnitude of the angular acceleration is reduced to 0.4 radian/sec.^{2}.

The measurement of the extraneous rotational acceleration is also the principal source of error in the measurement of C_{m_α} in plunging tests. Consequently, it is again useful to minimize this error by adjusting the oscillator until the rotational acceleration is the magnitude of the error in its measurement. The error analysis showed that the instrumentation requirements for the measurement of $C_{m_{\dot\alpha}}$ are also satisfactory for the determination of C_{m_α}. The maximum allowed error in the magnitude of the plunging acceleration is established by the requirements for measuring C_{m_α} in plunging tests.

In the error analysis of the measurement accuracy of $C_{m_{\dot{\theta}}}$ from pitching tests, the assumed accuracies used were

(1) the tunnel velocity is known to $\pm 1\%$,

(2) the oscillation frequency is known to $\pm 1\%$,

(3) the magnitude of the plunging acceleration is known to $\pm 5\%$,

(4) the magnitude of the balance moment is known to $\pm 2\%$,

(5) the magnitude of the rotational acceleration is known to ± 0.8 radian/sec.^{2},

(6) the geometry, mass, and inertia of the model are known exactly, and

(7) C_{m_α} and $C_{m_{\dot{\alpha}}} + C_{m_{\dot{\theta}}}$ are known to $\pm 10\%$.

In carrying out the analysis, it was assumed that the plunging amplitude was adjusted within $\pm 5\%$ of the value required for perfect pitching test. Calculations were made under the assumption that the nominal phase angle of the plunging acceleration relative to the rotational acceleration was 90° as required for a perfect pitching motion. Calculations were also made assuming nominal plunging phase angles of 85° and 95°; i.e., deviations of $\pm 5^\circ$ from the perfect motion. The errors indicated for the tunnel velocity, the oscillation frequency, C_{m_α} and $C_{m_{\dot{\alpha}}} + C_{m_{\dot{\theta}}}$ again did not appreciably influence the results. The 2% error assumed in the magnitude of the balance moment produces an error in $C_{m_{\dot{\theta}}}$ equal to about 2-1/2% of the total damping derivative. The 0.8 radian/sec.^{2} error in the magnitude of the rotational acceleration produces a corresponding error of 2% in $C_{m_{\dot{\theta}}}$. If the phase angle of the plunging acceleration relative to the rotational acceleration is measured within $\pm 1^\circ$ and the nominal plunging phase angle is set between 89° and 91°, the resulting error in $C_{m_{\dot{\theta}}}$ is only 1.4% of the total damping derivative. Analysis showed that $\pm 1^\circ$ errors in the measurement of the phase of plunging relative to the rotational accelerations still result in only a 1.4% error in $C_{m_{\dot{\theta}}}$ when the nominal plunging phase angles were assumed to be 85° or 95°, provided the incorrect phase angle is accounted for in the reduction of the data. It was found that the critical error when there is no inertia cancellation is the measurement of the phase of the balance moment relative to the motion. If this measurement is made within $\pm 1^\circ$, the corresponding error in $C_{m_{\dot{\theta}}}$ is 8.7% of the total damping derivative. The effects of all the errors were combined by taking the square root of the sum of the squares of the individual errors. This procedure resulted in an overall error in $C_{m_{\dot{\theta}}}$ equal to 9.5% of the total damping derivative when the inertial component of the measured moment is not canceled ahead of readout.

During a pure pitching test, the moment-measuring balance has a very large component which is in phase with rotational acceleration. This component is largely due to the inertial reaction. In the determination of $C_{m_{\dot{\theta}}}$, it is necessary to know the moments which are out of phase with the rotational acceleration. Since the real component of the balance moment is a very large quantity, the phase angle must be measured very accurately in order to obtain an accurate measure of the out-of-phase component of the moment. The readout accuracy requirements on the phase angle would be greatly relieved if the real component of the moment signal were reduced in magnitude. This reduction in the real component of the indicated balance moment can be accomplished by canceling the part of the moment signal due to the inertial load. Only the out-of-phase moment is used in computing $C_{m_{\dot{\theta}}}$ and this component is unaffected by the use of inertia cancellation. If the magnitude of the real component of the moment were reduced to one-third by inertia cancellation, it would be possible to relax the permissible error in the indicated phase of the moment to $\pm 3^{\circ}$. It should be emphasized that this reduction in required accuracy pertains to the readout of the phase of the moment and not to its measurement at the transducer.

In studying the effects of errors in rotation tests, a nominal rotational angle of $\pm 2^{\circ}$ was used and it was assumed that the oscillator was adjusted to reduce the undesired plunging motion to less than two-thirds of a g. It was found that the rotation tests did not introduce any additional requirements on instrumentation accuracy. The most critical item in the determination of $C_{m_{\dot{\alpha}}} + C_{m_{\dot{\theta}}}$ is the measurement of the phase angle of the balance moment relative to the rotational acceleration. It is again possible to use inertia cancellation to reduce the required accuracy of this readout as discussed in the measurement of $C_{m_{\dot{\theta}}}$ during pitching tests. If inertia cancellation were not used, $C_{m_{\dot{\alpha}}} + C_{m_{\dot{\theta}}}$ could still be measured to within $\pm 8\%$ using instrumentation meeting the specifications required for the measurement of the other derivatives.

In summary, instrumentation accuracy and oscillator-control requirements were selected on the basis of assuring satisfactory measurement of the derivatives of the F-80 model at M = 0.7 and at 7 cps with no subsequent corrections during data reduction. Throughout the analysis, it was assumed that the tunnel velocity and oscillation frequency were both known to $\pm 1\%$ which is well within the accuracy of the CAL test equipment. Since errors of this magnitude were not found to have an important effect on the derivatives, more exacting specifications were not required for the measurement of speed and frequency. The table on the following page summarizes the requirements on oscillator control.

TABLE III

Oscillator Control Requirements

Quantity Controlled	Required Adjustment	The Test Determining the Control Requirement
Rotational Acceleration	$\pm$0.4 radian/sec.^{2}	Measurement of $C_{m_{\dot{\alpha}}}$ in plunging tests with no consideration of the phase of the residual rotational motion.
Plunging Acceleration	$\pm$0.7 g	Measurement of $C_{m_{\dot{\alpha}}} + C_{m_{\dot{\theta}}}$ in rotation tests.
Phase Angle Between Rotational & Plunging Motions	$\pm 1^\circ$	Measurement of $C_{m_{\dot{\theta}}}$ in pitching tests.

The table below summarizes the basic measurement accuracies required to measure the stability derivatives of the F-80 model with acceptable errors.

TABLE IV

Measurement Accuracy Requirements

Quantity	Maximum Permissible Measurement Error	Derivative Whose Measurement Requirements Determine Permissible Error
Magnitude of Balance Moment	$\pm$2% of the oscillating moment	C_{m_α}, $C_{m_{\dot{\theta}}}$, and $C_{m_{\dot{\alpha}}} + C_{m_{\dot{\theta}}}$
Phase of the Balance Moment Relative to Rotational Acceleration	$\pm 3^\circ$ (with inertia cancellation)	$C_{m_{\dot{\theta}}}$
Magnitude of Plunging Acceleration	$\pm$2%	C_{m_α}
Phase Angle Between Plunging and Rotational Acceleration	$\pm 1^\circ$	$C_{m_{\dot{\theta}}}$
Magnitude of Rotational Acceleration	$\pm$0.4 radian/sec.^{2}	$C_{m_{\dot{\alpha}}}$

On the basis of these accuracy studies, it was concluded that it was feasible to measure the separate parts of the total rotary damping derivative, $C_{m_{\dot{\alpha}}} + C_{m_{\dot{\theta}}}$, to acceptable accuracies.

An error analysis was also made using parameters typical of fighters which fly in the low-supersonic speed range. Damping derivative separation was found to be possible with the apparatus meeting the requirements previously established for tests of the F-80 model at Mach number 0.7. This analysis assumed that the tests at higher Mach numbers would be made at the same dynamic pressure as at M = 0.7 and that the model used would be so constructed as to have inertia and weight properties approximately equal to those of the F-80. Some difficulty might be experienced with configurations whose trim conditions vary substantially over the Mach number range of the tests. The resultant bias load on the moment balance can limit the accuracy of measurement of the oscillatory moment unless, of course, some stabilizer adjustment is possible.

APPENDIX V

NOISE PROBLEMS ENCOUNTERED IN THE DEVELOPMENT OF THE DYNAMIC TESTING SYSTEM

An unusual noise problem was encountered in the course of performing exploratory wind-tunnel tests during the early phase of the system's development. With the F-80 model in a rotational mode, wind-tunnel testing was initiated at a Mach number of 0.5 and 1 atmosphere. At this test condition, unexpected and severe high-frequency "noise signals" were overriding the ordinarily observable model-motion signals. An attempt was made to alleviate this condition by reducing the tunnel density to 1/2 atmosphere. The high-frequency signals were attenuated sufficiently so that several data points could be taken, but they again became intolerable at higher Mach numbers. The noise level became so large that the signal readouts displayed excessive variations even though they were highly filtered. The test was terminated.

In a subsequent series of wind-tunnel tests with a completely different configuration (a gust probe), there was an opportunity for a limited investigation of the unusual noise problem which had been encountered previously. During dynamic wind-tunnel tests of the gust probe, a noise problem was again encountered which was similar, in most respects, to the one that had caused suspension of the previous F-80 wind-tunnel test program. While a thorough investigation of the problem was not possible at that time, some valuable information was derived.

The plan was to perform dynamic tests of the gust probe at Mach numbers of 0.4, 0.5 and 0.6 at 4,000 ft. pressure altitude and at 0.7, 0.8 and 0.95 at 22,000 ft. No difficulty was encountered in obtaining data at 0.4 Mach number and 4,000 ft. or at 0.7, 0.8 and 0.95 at 22,000 ft. Difficulty was first encountered as the Mach number was increasing from 0.4 to 0.5 at 4,000 ft. Somewhere between these two conditions, excessive noise was first encountered. Both the linear and angular accelerometers indicated very high amplitudes of noise at frequencies of about 280 to 300 cps. During a later test at the same condition, another (different) linear accelerometer (which was strapped on the outside of the probe at the location of the internal linear and angular accelerometers) also indicated a very high noise level at the same time, again, at about 300 cps. Pressure altitude was then increased to 22,000 ft. and, while holding the Mach number at 0.6, the altitude was gradually reduced in 2,000-ft. increments while monitoring the signal outputs on an oscilloscope. While there was no clear-cut quantitative criterion, it was generally agreed by the observers that the noise became excessive at about 14,000 ft. pressure altitude. The same test was repeated at a Mach number of 0.5 and here it was found that the noise appeared to be excessive at about 9-10,000 ft. pressure altitude. Data were actually taken at a Mach number of 0.6 and an altitude of 16,000 ft., and a Mach number of 0.5 and an altitude of 11,000 ft. It is interesting to note these points on

the constant-altitude operating map of CAL's 8-Ft. Transonic Wind Tunnel, as shown in Figure 61. The points at which data were taken during the gust-probe tests are indicated by the open circles. One particular point on the boundary between excessive and satisfactory noise levels seems to be well established. This is at the intersection of about 1 atmosphere and 4,000 ft. pressure altitude for a Mach number between 0.4 and 0.5. For example, during the gust-probe tests, we found we could obtain data at 4,000 ft. at Mach number 0.4 (as indicated by the open circle) but could not obtain data at 4,000 ft. at Mach number 0.5 (as indicated by the solid circle). Further, during the previous wind-tunnel test program using the F-80 model, data had been obtained at a Mach number of 0.4 at 1 atmosphere (as indicated by the flagged open circle), but data could not be obtained at Mach number 0.5 at 1 atmosphere (as indicated by the flagged solid circle). The dashed line on Figure 61 starts at this boundary point and is drawn parallel to the maximum clear-tunnel capability curve. The distribution of the satisfactory (open circles) test conditions and the unsatisfactory (solid circles) test conditions relative to this curve appears to be significant. This is, perhaps, not surprising when this line is recognized as one of nearly constant energy being introduced into the system by the wind-tunnel fans. These conditions of noise were independent of whether the oscillator was running or not. In a subsequent wind-tunnel test, discussed below, the oscillator flywheels were, in fact, clamped. An exceptional point of the data appears to be at Mach number 0.95. It should be noted, however, that, although data were taken at this condition, the noise level was generally agreed to be somewhat higher than desirable.

Upon conclusion of the dynamic tests of the gust probe, another series of tests was performed for further investigation of the noise problem. These tests were conducted with the normal F-80 model setup, except that the oscillator was stationary. In addition to the usual linear and angular accelerometers in the model, various other velocity and acceleration pickups (as well as a microphone) were monitored during the tests. The objectives of these tests were: (1) to attempt to obtain an indication of the nebulous boundary between "satisfactory" and "unsatisfactory" noise levels using the F-80 model and to compare it with the boundary obtained for the gust probe, and (2) to see whether this "noise boundary" could be changed significantly by introducing various additional isolators and dampers between the dynamic testing cart and the wind-tunnel structure. The second objective was completely unsuccessful, although many things were tried. With regard to the first objective, a few rather tentative conclusions could be reached. The sharp increase in noise level between 0.4 and 0.5 Mach number at 4,000 ft. altitude observed with the gust probe was confirmed in these static tests with the F-80 model. In general, it was noted that, as the tunnel conditions went from the high-altitude, low-Mach-number region toward the hypothetical boundary indicated by the dashed line, the noise level increased. Except at the condition between 0.4 and 0.5 Mach number at low altitude, however, the cases investigated showed a rather gradual increase in noise and a definitive boundary could not be established. For example, a test was run starting at 24,000 ft. altitude and 0.7 Mach number, and the altitude was gradually reduced by 2,000-ft. increments until the noise level for the linear and

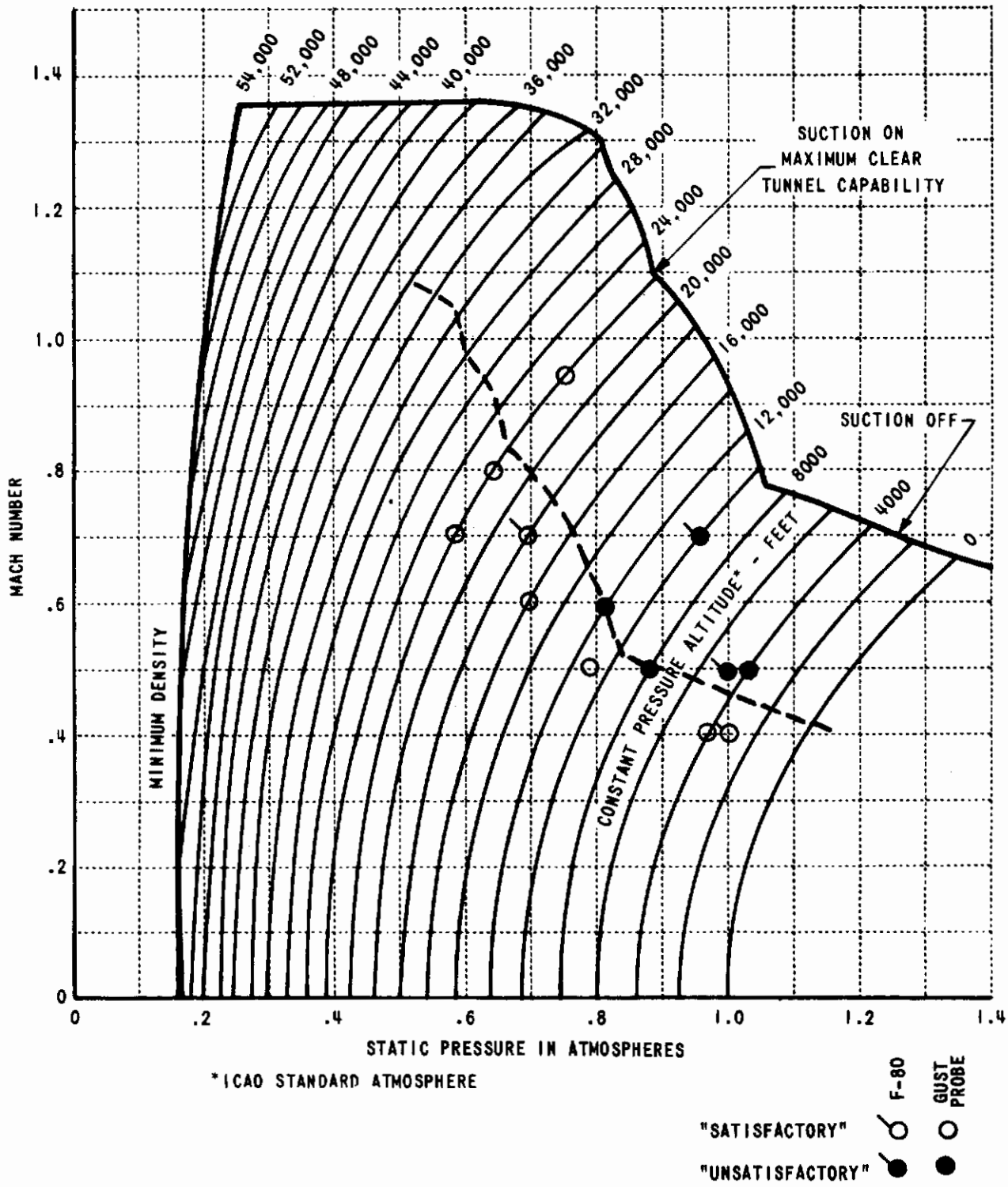

Figure 61 NOISE BOUNDARY ON TUNNEL OPERATING MAP

angular accelerometers as viewed on the oscilloscope was deemed to be excessive. This latter point was found to occur at 10,000-ft. altitude, as indicated on Figure 61. After completion of the tests, however, upon questioning the observers and reviewing the oscillograph records, it appeared that the noise attained unsatisfactory levels somewhere between 14,000 and 12,000 ft. altitude.

On the basis of all of the available data obtained during the dynamic F-80 model tests, the dynamic gust-probe tests, and the subsequent static F-80 model tests, the following conclusions were reached:

(1) The noise level boundary between satisfactory and unsatisfactory conditions appeared to be relatively independent of the model configuration, although the frequencies involved were quite different.

(2) No significant improvement could be realized by introducing additional mechanical isolation between the wind-tunnel structure and the dynamic testing cart.

(3) Both the linear and angular accelerometers became velocity proportional devices for inputs above their natural frequencies. Simple RC filters on the outputs of both of these transducers were warranted to provide prefiltering before entering the phase and amplitude analyzers.

(4) Although the operational domain of the dynamic testing system (comprised of the transonic tunnel, the mechanical oscillator, the model, and the transducers) was constrained by this noise boundary, the limitation did not appear to be so great as to prevent testing throughout a practical range of test conditions.

(5) Good blade balance and track and a tight blade-pitching mechanism and lock on the wind-tunnel fan were deemed essential for successful dynamic tests.

As a result of these investigations, prefiltering was added to the outputs of the linear and angular accelerometers to attenuate their velocity sensitivities at high frequencies. In addition, improvements in the routine maintenance of the transonic tunnel were instituted which includes a very careful check of the pitching mechanism on the blades.

The wind-tunnel test conditions for the final evaluation tests of the F-80 model were well below the hypothetical "noise boundary" indicated in Figure 61. There was no evidence of noise levels at any test condition which could not be adequately handled by the filtering capability of the amplitude and phase analyzers. The raw signals monitored on an oscilloscope never indicated excessive noise levels, and the digitized readouts were very stable.

APPENDIX VI

DATA REDUCTION PROCEDURES*

The results of the wind-tunnel tests as presented in printed and punched-card form are not directly usable in the evaluation of the aerodynamic lift and moment derivatives. The data reduction process converts the recorded signals to their corresponding physical measurements that can be plotted in vector form.

A typical test print-out, rotation, 7 cycles per second (cps), is shown in Table V. Column 1 is the run number and Column 2 is the point number used for identification. Column 5 is dynamic pressure, q, in pounds per square foot (psf) and Column 6 is the velocity, U, in feet per second (fps). In Columns 7, 9, 11 and 13, the last three digits give the amplitudes in counts on the DVM's of normal force $|\underline{Ⓕ}|$, pitching moment $|\underline{Ⓜ}|$, linear acceleration $|\underline{Ⓛ}|$, and angular acceleration $|\underline{Ⓐ}|$. Columns 8, 10, 12 and 14 are the corresponding phase angles $\phi_{Ⓕ}$, $\phi_{Ⓜ}$, $\phi_{Ⓛ}$ and $\phi_{Ⓐ}$ in tenths of degrees.

Column 17 is a code designation of the gain settings on the four channels of the amplitude and phase analyzers. A list of the codes for all possible combinations of low- and high-gain settings is given in Table VI. The maximum possible number of counts for a given signal is desirable in Columns 7, 9, 11 and 13 for maximum readout accuracy. The normal (or low) gain setting is designated "1" and corresponds to the counts per volt when a test signal of 3.5 volts is introduced in that channel. If the number of counts on any channel becomes too low during the tests, that channel can be switched to "10" which designates the high gain used with a test signal of 0.35 volts. A gain code of 51 corresponds to the gains in counts per volt indicated when a 3.5 volt test signal is applied to all four channels, and a gain code of 66 corresponds to the gains when a 0.35 volt test signal is applied on all channels.

Column 19 is the oscillation period, τ, in tenths of milliseconds. The frequency, f, in cycles per second equals $1/\tau$.

Column 21 is clock time of day.

Column 24 is the nominal Mach number.

The rest of the columns are not used in reducing the data.

---

* Much credit for the development of the data reduction procedures and for the preparation of this appendix is due Mrs. Miriam Watson, Senior Computer in the Applied Mechanics Department of CAL.

TABLE V

TYPICAL DATA PRINT-OUT (RUN 2, ROTATION, 7 cps)

ORIGINAL

FORM 161 (REV. 2-58)

CORNELL AERONAUTICAL LABORATORY, INC.

8 FOOT TRANSONIC WIND TUNNEL

9921

DATE	RUN
7 — 29 — 65	2

Tunnel Pressure: $\simeq \frac{1}{2}$ St'd Atms. Operations Engr. Model F-80 Configuration ROTATION - 7 cps

1	2	3	4	5	6	7	8	9	10	11	12	13	14	15	16	17	18	19	20	21	22	23	24
RUN	PT	ΔP_V	P_1	q	U	X_1 / (F)	X_2 / $\phi_{(F)}$	X_3 / (M)	X_4 / $\phi_{(M)}$	X_5 / (L)	X_6 / $\phi_{(L)}$	X_7 / (A)	X_8 / $\phi_{(A)}$	X_9 /	/	G.C. /	/	τ /	TC	TIME	T_o	M CODE	MACH. NO.
2	1		1044			173	1693	126	1671	348	3437	611	3046			51		1429		1916	542		
2	2		1051			174	1695	77	1678	258	3434	415	3046			66		1429		1917	542		
2	3		1037			372	183	380	161	11	1233	500	1949			57		1429		1921	542		
2	4		1041			29	513	20	2942	11	1292	501	1950			62		1429		1922	542		
2	5	165	883	155	550	54	152	406	1524	20	450	530	1950			59		1429		1928	536	1	500
2	6	309	799	275	767	109	164	99	1557	25	246	556	1951			54		1429		1938	540	2	700
2	7	348	771	310	824	122	169	112	1579	10	221	558	1953			54		1429		1941	542	3	750
2	8	389	747	330	882	108	154	102	1490	11	2647	552	1952			54		1429		1942	544	4	800
2	9		1032			27	452	18	3087	20	1013	502	1950			62		1430		1946	540		
2	10		1030			382	187	383	161	18	1000	503	1949			57		1429		1947	540		
2	11		1030			173	1696	127	1675	346	3432	612	3045			51		1428		1949	542		
2	12		1031			175	1699	77	1680	257	3428	415	3044			66		1429		1950	542		

Table VI

GAIN CODES FOR THE
AMPLITUDE AND PHASE ANALYZER CHANNELS

CHANNELS				CODE
1 (F)	2 (M)	3 (L)	4 (A)	
1	1	1	1	51
10	1	1	1	52
1	10	1	1	53
1	1	10	1	54
1	1	1	10	55
10	10	1	1	56
10	1	10	1	57
10	1	1	10	58
1	10	10	1	59
1	1	10	10	60
1	10	1	10	61
10	10	10	1	62
10	10	1	10	63
10	1	10	10	64
1	10	10	10	65
10	10	10	10	66

The first step in the data reduction is to convert the print-out information to the form required for polar plots. As an example, for "Run 2", which was the rotation case at 7 cps presented in Table V, points 1 and 11 are the low-gain test signals (code 51). A 3.5 volt signal at 7 cps was introduced into all four channels. Points 2 and 12 are at high gain (code 66) with 0.35 volts on all the channels. The number of counts of $|\underline{Ⓕ}|$, $|\underline{Ⓜ}|$, $|\underline{Ⓛ}|$ and $|\underline{Ⓐ}|$ in tests 1 and 11 are divided by 3.5 to determine the counts/peak volts at low gain and in tests 2 and 12 by 0.35 to obtain counts/peak volts at high gain for each channel. To account for a possible drift during the test, an average value for the counts/peak volts is found for both low and high gain for each amplitude channel from test signals taken before and after each series of points.

The sensitivities of the force and motion sensors themselves in terms of volts per unit measured were determined during the calibrations of the transducers (see discussion in Appendix II). The inverses of these are listed here in Table VII for convenience of discussion of their use in the data reduction procedure.

TABLE VII

Transducer Sensitivities

FREQUENCY, CPS / TRANSDUCER	5	7	10
Normal-Force Beams in lbs/peak volts	57.8	57.8	57.8
Moment Beam in ft. lbs/peak volts	2.10	2.10	2.10
Linear Accelerometer in g's/peak volts	2.90	2.90	2.90
Angular Accelerometer in rad/sec^2/peak volts	18.9	20.4	26.0

The conversion factors for high and low gains in terms of lbs/count, ft. lb/count, g's/count and rad/sec.^{2}/count are found by multiplying these transducer sensitivities by the corresponding counts/peak volts for the appropriate channel. Multiplication of the counts of $|\underline{Ⓕ}|$, $|\underline{Ⓜ}|$, $|\underline{Ⓛ}|$ and $|\underline{Ⓐ}|$ from the data sheets by the appropriate conversion factors taking account of the proper gain as indicated by the "Gain Code" gives $|\underline{Ⓕ}|$ in lbs., $|\underline{Ⓜ}|$ in ft. lbs., $|\underline{Ⓛ}|$ in g's, and $|\underline{Ⓐ}|$ in rad/sec.^{2}. Using the transducer sensitivities tabulated in Table VII and the following equations, the counts from Columns 7, 9, 11 and 13 can be converted to lbs., ft. lbs., g's, and rad/sec.^{2}.

$$|\underline{F}| \text{ lbs.} = \frac{\text{transducer sensitivity, lbs/peak volt}}{\text{avg. test signal gain, counts/peak volt}} \times |\underline{F}| \text{ counts}$$

$$|\underline{M}| \text{ ft. lbs.} = \frac{\text{transducer sensitivity, ft. lbs/peak volt}}{\text{avg. test signal gain, counts/peak volt}} \times |\underline{M}| \text{ counts}$$

$$|\underline{L}| \text{ g's} = \frac{\text{transducer sensitivity, g's/peak volt}}{\text{avg. test signal gain, counts/peak volt}} \times |\underline{L}| \text{counts}$$

$$|\underline{A}| \text{ rad/sec.}^2 = \frac{\text{transducer sensitivity, rad/sec.}^2\text{/peak volt}}{\text{avg. test signal gain, counts/peak volt}} \times |\underline{A}| \text{counts}$$

The conversions of the amplitudes in the example of Table V are presented in Table VIII. Points 3, 4, 9 and 10 were wind-off tests (M = 0) and 5, 6, 7 and 8 were the wind-on tests for M = 0.5, 0.7, 0.75 and 0.8.* In the example of Table V, point 3 has a gain code of 57. From Table VI, code 57 is seen to mean that $\underline{F}$ and $\underline{L}$ were at high gain, $\underline{M}$ and $\underline{A}$ were at low gain. Therefore, the counts/peak volts as determined from the high-gain test signal are used in the above relations to convert $|\underline{F}|$ and $|\underline{L}|$ to pounds and g's, and the counts/peak volts as determined from the low-gain test signal are used to convert $|\underline{M}|$ and $|\underline{A}|$ to foot pounds and radians per second squared. The amplitudes for all test points are evaluated in this way.

The angles of the vectors can be read directly from the print-out. Any zero shift in phase during the test is accounted for by adding algebraically one-half the difference between the indicated phases of the first and the last test signal taking into account the appropriate gain codes for each test point. The values for Run 2 are shown in Table IX. The final step is to evaluate the vectors $\underline{L}/U$ and $\tau\underline{A}/2\pi j$ which relate directly to the rate of change of angle of attack. These vectors corresponding to Run 2 are presented in Table X. The multiplication by $1/j$ rotates the vector by $-\pi/2$ degrees.

The data have now been reduced to the desired dimensional form and can be presented in polar plots. The phase angle convention is indicated

---

* Inertia cancellation was used during points 4 and 9 and in all wind-on tests. It was not used in the repeats of the wind-off tests — points 3 and 10.

Table VIII

REDUCTION OF THE AMPLITUDE DATA FOR RUN 2

PT	G.C.	(F) CHANNEL		(M) CHANNEL		(L) CHANNEL		(A) CHANNEL		
		COUNTS	COUNTS / PV	COUNTS	COUNTS / PV	COUNTS	COUNTS / PV	COUNTS	COUNTS / PV	
1	51	173	57.667	126	42.0	348	116.0	611	203.7	TEST SIGNAL GAINS
2	66	174	580.0	77	256.67	258	860.0	415	1383.3	
11	51	173	57.667	127	42.333	346	115.3	612	204.0	
12	66	175	583.33	77	256.67	257	856.7	415	1383.3	
			COUNTS / PV		COUNTS / PV		COUNTS / PV		COUNTS / PV	
1 & 11	51		57.667		42.167		115.67		203.85	AVERAGE TEST SIGNAL GAINS
2 & 12	66		581.67		256.67		858.35		1383.3	
			LBS / COUNT		FT. LBS / COUNT		"g" / COUNT		RAD/SEC^2 / COUNT	
1 & 11	51		1.0023		0.04980		0.02507		0.10005	AVERAGE TRANSDUCER GAINS
2 & 12	66		0.09936		0.0081817		0.0033771		0.014747	
			LBS		FT-LBS		"g"		RAD/SEC^2	
3	57		36.96		18.92		0.03715		50.03	TEST DATA
4	62		2.88		0.1636		0.03715		50.13	
5	59		54.12		3.322		0.06754		53.03	
6	54		109.3		4.930		0.08443		55.63	
7	54		122.2		5.578		0.03377		55.83	
8	54		108.2		5.080		0.03715		55.23	
9	62		2.68		0.1473		0.06754		50.23	
10	57		37.96		19.07		0.06079		50.33	

Table IX

CORRECTED PHASE ANGLES FOR RUN 2

PT	G.C.	$\phi_{(F)}$ CHANNEL DEG	$\phi_{(M)}$ CHANNEL DEG	$\phi_{(L)}$ CHANNEL DEG	$\phi_{(A)}$ CHANNEL DEG	
1-11	51	-0.3	-0.4	+0.5	+0.1	AVERAGE TEST SIGNAL
2-12	66	-0.4	-0.2	+0.6	+0.2	PHASE SHIFT
3	57	18.1	15.9	123.6	195.0	
4	62	51.1	294.1	129.5	195.1	
5	59	15.0	152.3	45.3	195.1	
6	54	16.2	155.5	24.9	195.2	TEST DATA
7	54	16.7	157.7	22.4	195.4	
8	54	15.2	148.8	265.0	195.3	
9	62	45.0	308.6	101.6	195.1	
10	57	18.5	15.9	100.3	195.0	

Table X

MOTION VECTORS FOR RUN 2

PT	U FT/SEC	$\frac{\lvert(L)\rvert}{U}$ 1/SEC	$\phi_{(L)}$ DEG	$\frac{\lvert(A)\rvert\tau}{2\pi}$ 1/SEC	$\phi_{(A)}+\frac{\pi}{2}$ DEG
3	0	—	123.6	1.138	285.0
4	0	—	129.5	1.140	285.1
5	550	0.003951	45.3	1.206	285.1
6	767	0.003541	24.9	1.265	285.2
7	824	0.001319	22.4	1.270	285.4
8	882	0.001355	265.0	1.256	285.3
9	0	—	101.6	1.143	285.1
10	0	—	100.3	1.145	285.0

in the following sketch where vector II leads vector I.

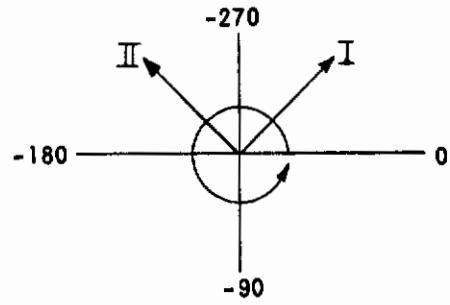

The phase readouts are in degrees of lag and so, consistent with the indicated sign convention, $|\underline{F}|$ is plotted at the angle $-\phi_{F}$, $|\underline{M}|$ at the angle $-\phi_{M}$, $\frac{|\underline{L}|}{U}$ at the angle $-\phi_{L}$ and $\frac{\tau|\underline{A}|}{2\pi}$ at the angle $(-\phi_{A}-\frac{\pi}{2})$.

From the vector plots of $\underline{M}$ and $\underline{F}$ measured in rotation as shown in Figures 22 and 25, the values of the aerodynamic lift and moment can be found using the following equations:

$$\underline{F} = \left\{ F_{\alpha}\left(\frac{\tau}{2\pi j}\right) + \left(F_{\dot{\alpha}} + F_{\dot{\theta}}\right)\right\}\frac{\tau\underline{A}}{2\pi j}$$

$$\underline{M} = \left\{ M_{\alpha}\left(\frac{\tau}{2\pi j}\right) + \left(M_{\dot{\alpha}} + M_{\dot{\theta}}\right)\right\}\frac{\tau\underline{A}}{2\pi j}$$

The nondimensional aerodynamic lift derivatives are then given as follows:

$(C_{L_{\dot{\alpha}}} + C_{L_{\dot{\theta}}})$ is the magnitude of the component of $\underline{F}$ in the direction of $\frac{\tau\underline{A}}{2\pi j}$ divided by $qS\left(\frac{c}{2U}\right)\left(\frac{\tau|\underline{A}|}{2\pi}\right)$ and

$C_{L_{\alpha}}$ is the magnitude of the component of $\underline{F}$ normal to $\frac{\tau\underline{A}}{2\pi j}$ divided by $qS\left(\frac{\tau}{2\pi}\right)\left(\frac{\tau|\underline{A}|}{2\pi}\right)$.

For all nondimensionalizing factors

q = dynamic pressure, lb/ft.^{2}

S = wing area (2.37 sq. ft. for the F-80 model)

c = mean aerodynamic chord (0.672 ft. for the F-80 model)

U = velocity in ft/sec.

For rotation, components along the direction of $\frac{\tau\underline{\textcircled{A}}}{2\pi j}$ are positive if in phase with $\tau\underline{\textcircled{A}}/2\pi j$. Components normal to $\tau\underline{\textcircled{A}}/2\pi j$ are positive if they lag $\tau\underline{\textcircled{A}}/2\pi j$.

Similarly, the components of $\underline{\textcircled{M}}$ in the direction of and normal to $\tau\underline{\textcircled{A}}/2\pi j$ give the nondimensional aerodynamic pitching-moment derivatives $(C_{m_{\dot\alpha}} + C_{m_{\dot\theta}})$ and C_{m_α}.

Figures 23 and 26 are the vector plots for pure plunge at 7 cps. In pure plunge,

$$\underline{\textcircled{F}} = \left\{ F_{\dot\alpha} + F_\alpha \left(\frac{\tau}{2\pi j} \right) \right\} \frac{\underline{\textcircled{L}}}{U}$$

$$\underline{\textcircled{M}} = \left\{ M_{\dot\alpha} + M_\alpha \left(\frac{\tau}{2\pi j} \right) \right\} \frac{\underline{\textcircled{L}}}{U}$$

The magnitude of the component of $\underline{\textcircled{F}}$ in the direction of $\underline{\textcircled{L}}/U$ divided by $qS\left(\frac{c}{2U}\right)\frac{|\underline{\textcircled{L}}|}{U}$ provides $C_{L_{\dot\alpha}}$.

The magnitude of the component of $\underline{\textcircled{F}}$ normal to $\underline{\textcircled{L}}/U$ divided by $qS\left(\frac{\tau}{2\pi}\right)\frac{|\underline{\textcircled{L}}|}{U}$ gives C_{L_α} .

Similarly, for the moment derivative, the component of $\underline{\textcircled{M}}$ in the direction of $\underline{\textcircled{L}}/U$ gives $C_{m_{\dot\alpha}}$, and the component normal to $\underline{\textcircled{L}}/U$ yields C_{m_α} .

For pure plunge, components in phase with $\underline{\textcircled{L}}/U$ are negative. Components normal to $\underline{\textcircled{L}}/U$ are positive if they lag $\underline{\textcircled{L}}/U$.

In pure pitch, shown in Figures 24 and 27,

$$\underline{\textcircled{F}} \cong \left\{ F_{\dot\theta} \right\} \frac{\tau\underline{\textcircled{A}}}{2\pi j}$$

$$\underline{\textcircled{M}} \cong \left\{ M_{\dot\theta} \right\} \frac{\tau\underline{\textcircled{A}}}{2\pi j}$$

The components of $\underline{\textcircled{F}}$ and $\underline{\textcircled{M}}$ normal to $\tau\underline{\textcircled{A}}/2\pi j$ should be zero. The magnitudes of the components of these vectors in the direction of $\tau\underline{\textcircled{A}}/2\pi j$ divided, respectively, by $qS(c/2U)(\tau|\underline{\textcircled{A}}|/2\pi)$ and by $qSc(c/2U)(\tau|\underline{\textcircled{A}}|/2\pi)$ are measures of the derivatives $C_{L_{\dot\theta}}$ and $C_{m_{\dot\theta}}$. For pitch motion, the components in phase with $\tau\underline{\textcircled{A}}/2\pi j$ are positive.

REFERENCES

1. Chalk, C. R., Additional Flight Evaluations of Various Longitudinal Handling Qualities in a Variable-Stability Jet Fighter, Cornell Aeronautical Laboratory Reports TB-1141-F-1 and TB-1141-F-2 (also WADC TR-57-719), March 1958.

2. Durand, W. F., Aerodynamic Theory, Vol. V, Division N - Dynamics of the Airplane, Dover Publications, New York, 1963. (first published by Julius Springer in 1935)

3. Valensi, J., "A Review of the Techniques of Measuring Oscillatory Aerodynamic Forces and Moments on Models Oscillating in Wind Tunnels in use on the Continent", AGARD paper presented at the Fifth Meeting of the Wind Tunnel and Model Testing Panel, 3-7 May 1954.

4. Arnold, L., "Dynamic Measurements in Wind Tunnels", AGARDograph 11, August 1955.

5. Beam, B. H., A Wind-Tunnel Test Technique for Measuring the Dynamic Rotary Stability Derivatives at Subsonic and Supersonic Speeds, NACA Report 1258, 1956.

6. Welsh, C. J. and Clemens, P. L., A Small-Scale Force-Oscillation Dynamic Balance System, AEDC TN-58-12, ASTIA Document No. AD-157143, July 1958.

7. Orlik-Ruckemann, K., Methods for Measurement of Aircraft Dynamic Stability Derivatives, National Research Council of Canada, Aeronautical Report LR-254, July 1959.

8. Scherer, M. and Mathe, P., "Measurement of Aerodynamic Derivatives in the Wind Tunnel and in Flight" (in French), Paper presented at AGARD Meeting, April 1961.

9. Scherer, M., Mesure des Derivees Aerodynamiques en Ecoulement Transsonique et Supersonique, Office National d'Etudes et de Recherches Aerospatiales Publication 104, 1962.

10. Braslow, A. L., Wiley, H. G. and Lee, C. Q., A Rigidly Forced Oscillation System for Measuring Dynamic Stability Parameters in Transonic and Supersonic Wind Tunnels, NASA Technical Note D-1231, March 1962.

11. Vaucheret, X., Determination of the Dynamic Stability Derivatives by the Method of Free Oscillations, Office National d'Etudes et de Recherches Aerospatiales Publication 20, 1963.

REFERENCES (Cont'd)

12. Reed, W. H., III and Abbott, F. J., Jr., "A New 'Free-Flight' Mount System for High-Speed Wind-Tunnel Flutter Models", Proceedings of Symposium on Aeroelastic and Dynamic Modeling Technology, RTD-TDR-63-4197, Part I, March 1964.

13. Hill, J. A. and Gikas, X. A., "Application of Aeroelastic Modeling Techniques to the Determination of Structural Loads and Stability and Control Dynamic Characteristics", Proceedings of Symposium on Aeroelastic and Dynamic Modeling Technology, RTD-TDR-63-4197, Part I, March 1964.

14. Tufts, O. B., Duryea, G. R., Jr., MacArthur, R. C., Zimmerman, A. H., Longitudinal Airplane Dynamics Wind-Tunnel Testing Equipment WADC TR-55-184, July 1955.

15. Tufts, O. B. and MacArthur, R. C., Measurement of Dynamic Stability Derivatives in the Wind Tunnel — Part I: Development Testing of the Apparatus, WADC TR-57-274, Part I, ASTIA Document No. AD-118258, April 1957.

16. Daughaday, H., DuWaldt, F. and Statler, I., Measurement of Dynamic Stability Derivatives in the Wind Tunnel — Part II: Evaluation of Testing Techniques, WADC TR-57-274, Part II, ASTIA Document No. AD-118258, May 1957.

17. Kidder, R. C., Dynamic Longitudinal Stability Flight Tests of an F-80A Airplane by the Forced Oscillation and Step Function Response Methods Including Measured Horizontal Tail Loads, Cornell Aeronautical Laboratory Report TB-495-F-11, 10 February 1950.

18. Cleary, J. W. and Gray, L. J., High-Speed Wind-Tunnel Tests of a Model Pursuit Airplane and Correlation with Flight Test Results NACA RM A7I16, 21 January 1948.

19. Statler, I. C., The Development and Evaluation of the CAL/Air Force Dynamic Wind-Tunnel Testing System, Part II - Dynamic Tests of an F-104 Model, AFFDL TR 66-153, Part II (to be published)

20. Landahl, M., Unsteady Transonic Flow, Pergamon Press, New York, N. Y., 1960.

UNCLASSIFIED
Security Classification

DOCUMENT CONTROL DATA - R&D
(Security classification of title, body of abstract and indexing annotation must be entered when the overall report is classified)

1. ORIGINATING ACTIVITY *(Corporate author)*
Cornell Aeronautical Laboratory, Inc.
Buffalo, New York 14221

2a. REPORT SECURITY CLASSIFICATION
UNCLASSIFIED

2b GROUP

3. REPORT TITLE
The Development and Evaluation of the CAL/Air Force Dynamic Wind-Tunnel Testing System, Part I - Description and Dynamic Tests of an F-80 Model

4. DESCRIPTIVE NOTES *(Type of report and inclusive dates)*
Final Report, March 1961 - August 1966

5. AUTHOR(S) *(Last name, first name, initial)*
Statler, Irving C.
Tufts, Orren B.
Hirtreiter, Walter J.

6. REPORT DATE	7a. TOTAL NO. OF PAGES	7b. NO. OF REFS
February 1967	152	20

8a. CONTRACT OR GRANT NO.	9a. ORIGINATOR'S REPORT NUMBER(S)
Contract AF 33(616)-8034 b. PROJECT NO. 8219, Task No. 821902	
c.	9b. OTHER REPORT NO(S) *(Any other numbers that may be assigned this report)*
d.	AFFDL-TR-66-153, Part I

10. AVAILABILITY/LIMITATION NOTICES
Distribution of this document is unlimited.

11. SUPPLEMENTARY NOTES	12. SPONSORING MILITARY ACTIVITY
Part II of this report discusses dynamic tests of an F-104 model.	Air Force Flight Dynamics Laboratory Research and Technology Division Wright-Patterson Air Force Base, Ohio

13. ABSTRACT

This report reviews the development and evaluation of a new capability for dynamic testing in wind tunnels. The Cornell Aeronautical Laboratory (CAL) system provides a unique mounting through which a model can be forced precisely in any desired planar sinusoidal motion.

The versatility and overall accuracy of the CAL/Air Force dynamic testing system was demonstrated during a series of wind-tunnel tests. These tests permitted, for the first time, a measurement of the separate components of the rotary damping moment. The moment due to rate of change of angle of attack was measured by oscillating the model in pure plunging motion. The moment due to pitch rate was measured during pitching motion. The sum of these is compared with the total rotary damping moment as measured in rotation. Comparisons of data taken at two frequencies and four Mach numbers indicate that the components are accurate to within plus or minus ten percent of the total rotary damping moment. The results are compared with theory, flight test data, and other wind-tunnel measurements on the same and similar models.

Future applications of this equipment are reviewed, particularly with regard to its use as a research tool to support basic investigations for the development of theoretical or semiempirical methods for predicting dynamic stability characteristics of aircraft at transonic speeds. Recommendations for modifications and improvements to the system are presented and discussed.

DD FORM 1 JAN 64 1473

UNCLASSIFIED
Security Classification

14. KEY WORDS	LINK A		LINK B		LINK C	
	ROLE	WT	ROLE	WT	ROLE	WT
Dynamic Wind-Tunnel Testing Wind-Tunnel Testing Dynamic Stability Rotary Damping Derivatives Forced Oscillation Tests F-80						

INSTRUCTIONS

1. ORIGINATING ACTIVITY: Enter the name and address of the contractor, subcontractor, grantee, Department of Defense activity or other organization *(corporate author)* issuing the report.

2a. REPORT SECURITY CLASSIFICATION: Enter the overall security classification of the report. Indicate whether "Restricted Data" is included. Marking is to be in accordance with appropriate security regulations.

2b. GROUP: Automatic downgrading is specified in DoD Directive 5200.10 and Armed Forces Industrial Manual. Enter the group number. Also, when applicable, show that optional markings have been used for Group 3 and Group 4 as authorized.

3. REPORT TITLE: Enter the complete report title in all capital letters. Titles in all cases should be unclassified. If a meaningful title cannot be selected without classification, show title classification in all capitals in parenthesis immediately following the title.

4. DESCRIPTIVE NOTES: If appropriate, enter the type of report, e.g., interim, progress, summary, annual, or final. Give the inclusive dates when a specific reporting period is covered.

5. AUTHOR(S): Enter the name(s) of author(s) as shown on or in the report. Enter last name, first name, middle initial. If military, show rank and branch of service. The name of the principal author is an absolute minimum requirement.

6. REPORT DATE: Enter the date of the report as day, month, year; or month, year. If more than one date appears on the report, use date of publication.

7a. TOTAL NUMBER OF PAGES: The total page count should follow normal pagination procedures, i.e., enter the number of pages containing information.

7b. NUMBER OF REFERENCES: Enter the total number of references cited in the report.

8a. CONTRACT OR GRANT NUMBER: If appropriate, enter the applicable number of the contract or grant under which the report was written.

8b, 8c, & 8d. PROJECT NUMBER: Enter the appropriate military department identification, such as project number, subproject number, system numbers, task number, etc.

9a. ORIGINATOR'S REPORT NUMBER(S): Enter the official report number by which the document will be identified and controlled by the originating activity. This number must be unique to this report.

9b. OTHER REPORT NUMBER(S): If the report has been assigned any other report numbers *(either by the originator or by the sponsor)*, also enter this number(s).

10. AVAILABILITY/LIMITATION NOTICES: Enter any limitations on further dissemination of the report, other than those imposed by security classification, using standard statements such as:

(1) "Qualified requesters may obtain copies of this report from DDC."

(2) "Foreign announcement and dissemination of this report by DDC is not authorized."

(3) "U. S. Government agencies may obtain copies of this report directly from DDC. Other qualified DDC users shall request through

_____."

(4) "U. S. military agencies may obtain copies of this report directly from DDC. Other qualified users shall request through

_____."

(5) "All distribution of this report is controlled. Qualified DDC users shall request through

_____."

If the report has been furnished to the Office of Technical Services, Department of Commerce, for sale to the public, indicate this fact and enter the price, if known.

11. SUPPLEMENTARY NOTES: Use for additional explanatory notes.

12. SPONSORING MILITARY ACTIVITY: Enter the name of the departmental project office or laboratory sponsoring *(paying for)* the research and development. Include address.

13. ABSTRACT: Enter an abstract giving a brief and factual summary of the document indicative of the report, even though it may also appear elsewhere in the body of the technical report. If additional space is required, a continuation sheet shall be attached.

It is highly desirable that the abstract of classified reports be unclassified. Each paragraph of the abstract shall end with an indication of the military security classification of the information in the paragraph, represented as *(TS)*, *(S)*, *(C)*, or *(U)*.

There is no limitation on the length of the abstract. However, the suggested length is from 150 to 225 words.

14. KEY WORDS: Key words are technically meaningful terms or short phrases that characterize a report and may be used as index entries for cataloging the report. Key words must be selected so that no security classification is required. Identifiers, such as equipment model designation, trade name, military project code name, geographic location, may be used as key words but will be followed by an indication of technical context. The assignment of links, rules, and weights is optional.